Materials Science and Tehcnology PhD School
Kerpely Antal

Leader: Prof. Dr. András Roósz, DSc, full member of the Hungarian Academy of Sciences

Foam evolution and stability at various gravity conditions

PhD Thesis

Béla Márton Somosvári
physicist-astronomer

Consultant:
Prof. Dr. Pál Bárczy
professor emeritus

University of Miskolc
Faculty of Materials Science
Department of Polymer Engineering
Miskolc, 2012

Abstract

The following PhD thesis deals with the evolution and the stability of particle stabilised aqueous foams under different gravity conditions. Motivations and an introduction into the general properties and industrial importance of foams is given in the first two chapters. After describing the state of the art in foam research and some highlighted points in particle stabilisation and microgravity studies, experiments and their results are detailed. The role of particles' contact angle in foamability is discussed through experimental results using PVC-water-ethanol solution as a foam precursor. The effect of increased and decreased gravity levels were both investigated using a suspension of 2wt% of SiO_2 particles in aqueous solution of 0.05% SDS. Foam volumes and foam stability in the function of different gravity levels and foaming directions are experimentally revealed and discussed.

Acknowledgements

First of all I would to thank the excellent possibility to deal with such an interesting topic in materials science to my supervisor, Prof. Dr. Pál Bárczy. Many thanks to the whole ADMATIS TEAM — without them I could never finish this work: Tamás Bárczy, Zsolt Bárczy, Zsolt Kovács, Mr. and Mrs. Zoltán Márkus, Róbert Oláh, Zoltán Pintér, Ágnes Solczi, László Szegedi, Péter Szirovicza and János Szőke, inventor and project manager of FOCUS experiment. I will allways remember the long and inspiring discussions and the hard work we did during FOCUS times. Also many thanks to the present and former collegaues at the University of Miskolc, Department of Polymer Engineering. Special thanks to Prof. Dr. George Kaptay for the many fruiful discussions we made and to Dr. László Kuzsella for helping me since the very beginning.

I would also like to acknowledge the help and supervision of Dr.-Ing. Martin Meier at the Brandenburgische Universität Cottbus back in 2004. A great thanks to the Helmholtz-Zentrum Berlin für Materialien und Energie GmbH — to Prof. Dr. John Banhart, Dr. Manas Mukherjee, Dr. Francisco Garcia-Moreno, and for the excellent supervision of Dr. Norbert Babcsán. Also many thanks for helping me to Dr.-Ing. Axel Griesche, Almuth Berthold and Prof. Dr. Reinhard Miller at TU Berlin. A huge thanks to Clara Stattegger who taught me how to 'survive' in X-berg.

I will never forget the kind support of FOCUS Experiment Staff: Dr. Raimondo Fortezza, Neil Melville, Dr. Sebastien Vincent-Bonnieu, Pranav Trivedi, Claudio Moratto, John Meehan, Sabine Carriére-Ansel, Zeholy Pronk, Kim Vijle, Arif Arshad, Kagan Kayal, Uwe Müllerschkowski, Céline Schöne, Kevin Doherty ... (the list is not complete).

Experiments on PVC-water-ethanol foams were supported by ESA project ID: AO-99-075, contract no: 98009, ADMATIS and LEONARDO DA VINCI II MOBILITY PROGRAMME. Increased gravity experiments in 2006 were supported by the Hungarian Space Office (project no. MŰI TP-212). ADMATIS would like to acknowledge the excellent support of the European Space Agency (ESA), Hungarian Space Office (HSO) and all our subcontractors during FOCUS project. FOCUS is part of the SURE (International Space Station: a Unique Research Infrastructure) project, financed by ESA, ID: SURE AO-019/PECS 98045, and co-funded by the EC project SURE, contract no: RITA-CT-2006-026069.)

I am very grateful to my loving wife for the constant encouragement and for being always next to me, and to my little son who delights me every day! I am also grateful to my parents and all family members for supporting me all the time. God bless you all!

Contents

List of Figures

(Those figures where there is no reference in the text belong to the author.)

List of Tables

Chapter 1

Introduction

1.1 Background

Foams are dispersion of gas in a liquid or solid phase. These materials play an essential role in nature and in our artificial world as well. They can act as structural or functional materials in industry - food, construction, furniture, transport, aerospace - and in our everyday life.

Engineers constantly try to find the best method to achieve well controllable manufacturing of foams with homogeneous cell structure, good stability and tailorable functionality, or, on the contrary, want to completely get rid of the unwanted foams in several processes (e.g. paper industry). Understanding the evolution and stability of foam structures is therefore indispensable and always a truly interdisciplinary field where chemistry, physics, mathematics and materials science all have a significant role [1, 2].

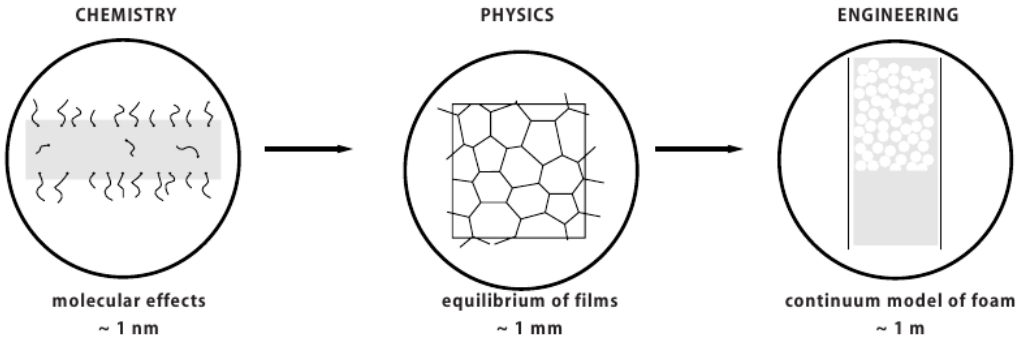

Figure 1.1: Foam research at different length scales - from chemistry to engineering [1].

The call for microgravity and to study gravity-related effects on foams is obvious: gravity has a key role in the life of foams. The liquid due to gravity and capillary forces drains out of the foam resulting cell wall thinning and finally rupture.

Gas diffusion through the cell walls leads to coarsening - the bubbles become larger with time. Bubble coalescence, coarsening due to diffusion, or film rupturing all depend on foam liquid fraction and they are interconnected through the gravity-driven drainage. These key effects can be separated by the elimination of gravity which is very important from the scientific point of view [3–5].

ADMATIS Ltd.[1] in Hungary started to research aluminium foams back in 2003 in the frame of the ESA project called 'Advanced Foams under Microgravity'[2], as a co-investigator and facility supplier. Aluminium foams are stabilised solely by solid particles. Particle stabilisation of foams or emulsions is also a hot topic due to the good potential for aluminium foams in transportation industry, and a vast amount of applications for aqueous systems in food and pharmaceutical industry. ADMATIS initiated a project called 'FOCUS - Foam Casting and Utilisation in Space'[3] in 2006 to investigate foaming and stability of particle stabilised aqueous foams using a new type of foam generator (henceforth FG) that can create foams at various gravity conditions. Main experiment objective was a technological demonstration that the new technology is capable of producing particle stabilised foams under microgravity. In parallel, a project for increased gravity measurements was running with the support of the Hungarian Space Office[4].

The above activities ensured an ideal background for me as a PhD student at the University of Miskolc and as an employee at ADMATIS to do scientific work in this very exciting and challenging world of foam research.

1.2 Objectives

Though the fundamentals of foam formation and evolution are well understood, still many interesting scientific questions appear if we look around in the field of microfluidics, microbubbles, monodisperse systems, particle stabilisation of foams, liquid layers, wet foam dynamics, or the role of gravity [6, 7].

The driving force behind the ADMATIS projects detailed above was to develop a new type of foaming method for aluminium foams and to introduce an alternative manufacturing process for shaped aluminium foam parts using direct gas introduction.

The objectives of my PhD thesis were formed by considering both scientific and technological interests and can be grouped into three points:

[1] ADMATIS (ADvanced MATerials In Space) is a small R&D venture founded in 2000.

[2] ID: AO-99-075, contract no: 98009

[3] FOCUS is part of the SURE (International Space Station: a Unique Research Infrastructure) project, financed by ESA, ID: SURE AO-019 / PECS 98045, and co-funded by the EC project SURE, contract no: RITA-CT-2006-026069.

[4] Investigation of particle stabilised foams under macrogravity, TP-212

1. To investigate particle-stabilisation effect in aqueous foams and to find relation experimentally between the particle contact angle and the foamability of the system.

2. Utilising the benefits of FOCUS FG, my aim was to study the role of gravity and the direction of foaming measured to gravity vector in the foamability and stability of FOCUS suspension (see below).

3. Further aim was to investigate the change in foam structure and bubble size distribution by varying the foaming direction and gravity environment, using FOCUS FG and FOCUS suspension (see below).

Chapter 2

Foams everywhere

2.1 What is a foam?

2.1.1 Basic characterisation

By definition, foams are a uniform dispersion of gas in a second phase. This second phase can be either liquid or solid. The gas content of a foam should be, let's say, at least 50V/V%. Below this value we can only speak about bubbly liquid, or porous material. The term 'foam' usually applies for liquid foams. Solid foams are regularly made of liquid foams, by the solidification of the liquid phase. One more important note: the liquid always contains surface active molecules (surfactants, electrolytes, polymers, proteins) or particles that can stabilise the films between the bubbles [8, 9].

Liquid foams consist of gas and liquid, but oddly, they can act as a solid material. A spoon of whipped cream on the top of your cake won't flow down, although it is made of milk and air[1]. The mechanical behaviour of foams is very important and it is under intensive scientific research. The key parameter from this viewpoint is the *liquid volume fraction* (ε) of the foam (Eq. 2.1). This is the volume ratio of the liquid content and the foam volume given in percentage. Thermodynamic, acoustical, and rheological properties are also highly influenced by ε.

$$\varepsilon = \frac{V_{liquid}}{V_{foam}} \tag{2.1}$$

Based on the liquid volume fraction we can speak about *dry* and *wet* foams [5, 8]. Dry foams contain less than 1% liquid, while ε can reach even 36% in the wet case. Althoug there is no well-defined limit, we can say that foams are wet from cca. $\varepsilon \approx 15 - 18\%$ [11, 12].

A really wet foam ($\varepsilon > 36\%$) is nothing more than a bubbly liquid, where the spherical *bubbles* can move easily and the separating walls are thick. Dry foams

[1] Whipped cream is very interesting: it is made by beating air into the cream with at least 26-30% fat content. The foamy structure of the whipped cream is initially stabilised by proteins and then by tiny fat globules. [10]

consist of polyhedral *cells* and the films between them are very thin. Wet foams are often mentioned as *spherical* foams, while dry ones are called *polyhedral* foams, based on the shape of the bubbles. There is a phase transition from wet to dry, and we can also speak about 'transitional' foams: where the foam begins to react to mechanical interactions (shear stress) as a solid material. This occurs at the critical liquid volume fraction, cca. $\varepsilon_c \approx 26\%$, which is the hexagonal close packing of the bubbles. The bubbles begin to get into contact at cca. $\varepsilon \approx 36\%$ (random close packing). This effect is also called 'jamming' transition. [8, 13, 14].

An example of a usual aqueous foam can be seen in Figure 2.1. Thanks to the liquid drainage from the top of the foam towards the liquid/foam interface due to gravity, we can observe all dry, transient and wet regions.

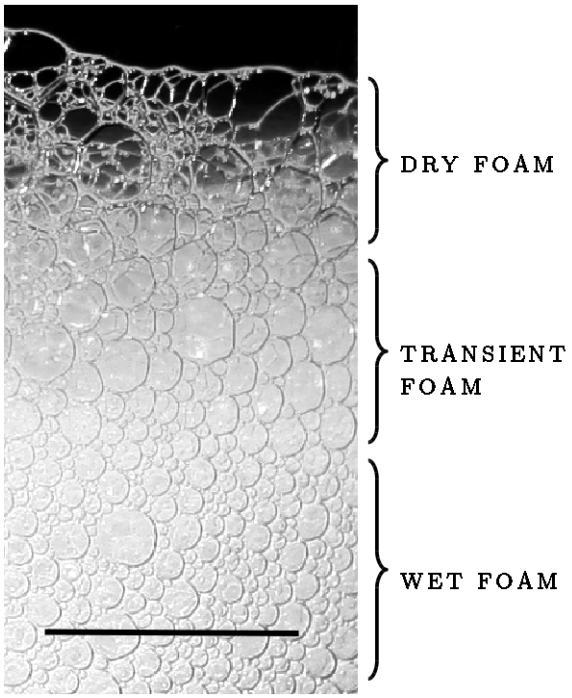

Figure 2.1: Close-up photo of an aqueous foam, consisting of a wet, a transient and a dry region. Scale bar is 4mm

In the case of solid foams we often use the term *relative density* that is, the apparent density of the foam (ρ_{foam}), divided by the density of the bulk material (ρ_{bulk}) from which the foam is made of (Eq. 2.2). ρ_{rel} ususally varies from 0.001 to 0.3. Above 0.3 we speak about porous materials ([15], cited by [16]).

$$\rho_{rel} = \frac{\rho_{foam}}{\rho_{bulk}} \tag{2.2}$$

Another very important parameter is the size and the size distribution of the bubbles that build up a foam. A foam made of equal size bubbles is called *monodisperse*

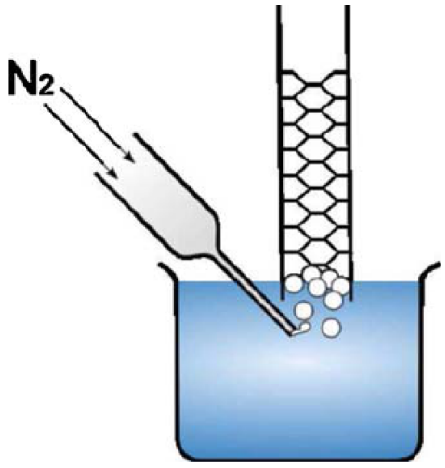

Figure 2.2: A simple method for producing ordered foam structures: ideal systems for testing foam theory [17].

foam. Foams are *polydisperse* when they consist of many different sized bubbles. Note that the critical liquid volume fraction ε_c for the 'wet limit' can be lower for polydisperse foams. Polydisperse systems are *disordered*, but monodisperse ones can easily evolve into *ordered structures* when the size of the bubble is comparable to the size of the container in wich the foam exists (see Figure 2.2). Ordered structures are good model systems for testing general foam theory [12].

It is very easy to create polydisperse foams, but you have to be a bit more careful when making monodisperse ones. Formerly, monodisperse foams were not of much interest because they cannot be found in nature and they cannot be maintained for a long time due to decay processes — gas diffusion between the bubbles and film rupture — that soon lead to polydispersity. William Lawrence Bragg together with John Nye in the 1950s created two dimensional monodisperse soap bubble rafts for the demonstration of crystallographic structures and defects (e. g. dislocations, stacking faults). Cyrill Stanley Smith used soap froth as an analogue for grain growth in metals and ceramics [18–20].

Thanks to the recently developed bubbling techniques with outstanding bubble size control down to a micrometer scale and advances in physical chemistry monodisperse foams and emulsions now have moved into the focus of scientific research in microfluidics and lab-on-a-chip technologies [12, 14].

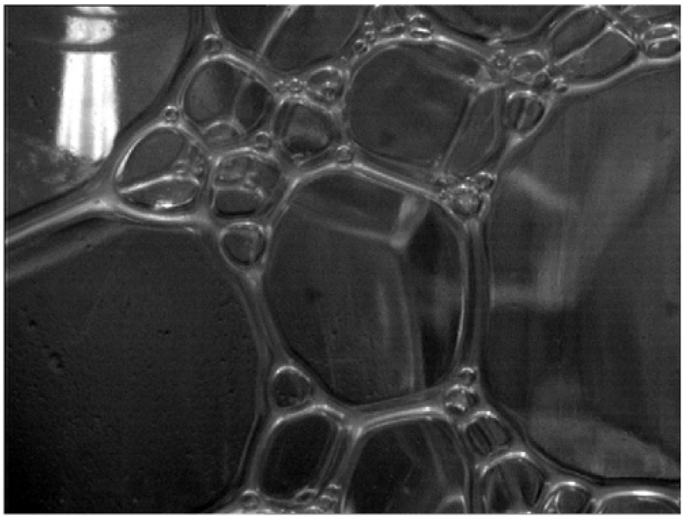

Figure 2.3: Macrophoto of a polydisperse foam. Photo was taken at the FOAM Group at Brandenburg University of Technology lead by M. Meier.

Figure 2.4: Monodisperse foam: a crystal made of bubbles! [21].

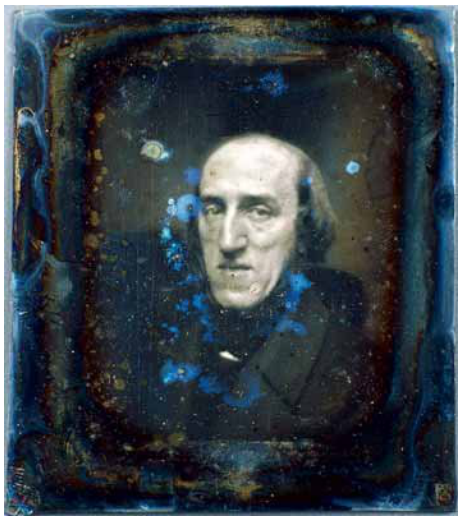

Figure 2.5: Daguerreotype portrait from 1843 depicting the Belgian physicist Joseph A. F. Plateau (1801-1883), author unkown. Credit: Joseph Plateau collection, University of Ghent [23].

2.1.2 Foam structure

The characterisation of foam structure and the exploration of the physics behind is connected to a more than hundred year old work of a Belgian scientist called Joseph Antoine Ferdinand Plateau (1801-1883) [6, 22].

Plateau investigated the form of floating oil droplets in water-alcohol mixture and he experimentally proved that molecular forces acting in a thin surface layer dominate the formation of *equilibrium surfaces*. He could also observe[2] equilibrium surfaces of thin soap films, using more than 80 different wire figures, made by himself. In his work called 'Statique expérimentale et théorique des liquides soumis aux seules forces moléculaires' he published the following basic laws for the formation of thin soap films, nowadays called as *Plateau's rules* [22, 24]:

1. Each wire edge supports one film.

2. At a liquid edge no more than 3 films can come together; they then form angles of 120° ($\arccos(-\frac{1}{2})$).

3. The liquid edges that come together in one point are always in the number of 4 and form angles of 109°28' ($\arccos(-\frac{1}{3})$).

[2] At that time, in 1843-44 Plateau lost his sight and for his experiments, as well as for all related deskwork colleagues and family helped him. His wife, Fanny Clavareau and his sister Joséphine supported him day by day by reading papers and articles. His sister, as an accomplished artist probably helped with the drawings in the publications [22].

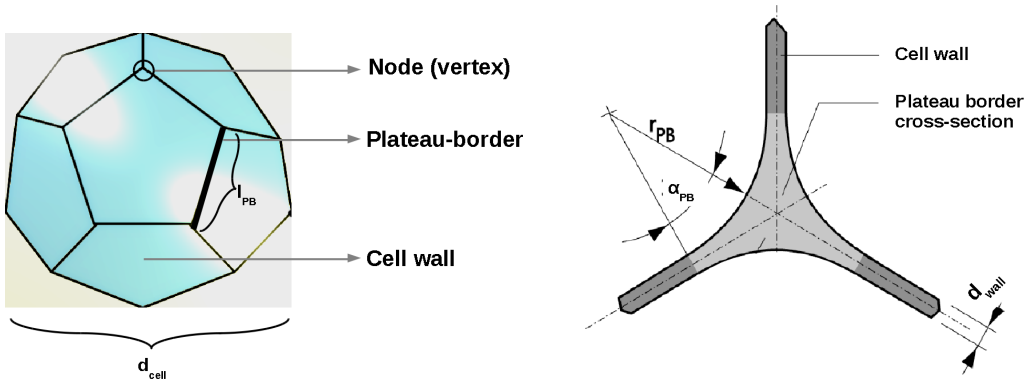

Figure 2.6: Left: a pentagonal dodecahedron cell from a dry foam [25]. Right: Cross-section of a PB and the related definitions [16, 25].

We can observe the same features when looking into the structure of a dry foam built up of polyhedral cells. Each cell in a foam consists of *cell walls* (thin liquid or solid film). In the case of solid foams we can distinguish *open* or *closed-cell* foams, depending on the permeability of the cell wall, meaning that the cell walls can be either ruptured, or totally missing. Open cell solid foams are often called 'sponges'. The edges where three cell walls (two from the selected cell and one from its neighbour) meet are called *Plateau-border* (henceforth PB). Four PB-s, or on the other hand, six cell walls abut into a *node* or *vertex* [16].

The foam cell geometry can be featured with its overall size d_{cell}. This can be defined for example as the maximum distance between two arbitrary points (p_1, p_2) that are elements of the center (bisector) plane of the cell walls (eq. 2.3).

$$d_{cell} = max[d(p_1, p_2)], \quad p_1, p_2 \in \text{cell walls bisector plane} \tag{2.3}$$

The cell wall is characterised by its thickness d_{wall}. PB found at the joining of three cell walls have a lentgh l_{PB} and a curvature that is characterised by its radius (r_{PB}) and arc (α_{PB}). These values can vary for each cell wall or PB even within one cell, since foam cells can take on a wide variety of different polyhedra [16, 26].

The reason behind Plateau's rules is the energy-minimizing principle — nature reduces the interfaces in order to have the least amount of total energy to maintain, and thus enclose a given area/volume with as little perimeter/surface area as possible. The general problem of determining the shape of the minimal surface constrained by a given boundary is also mentioned as *Plateau's problem*. Minimal surfaces have a total curvature equal to zero in every point. Ernest Lamarle, a Belgian mathematician in the 1860s gave a proof that only four soap films can meet at a point, vertices having more films are unstable [27, 28].

More than a century had to pass till the connection between the above empirical findings and the energy-minimizing principle was mathematically proved by Jean

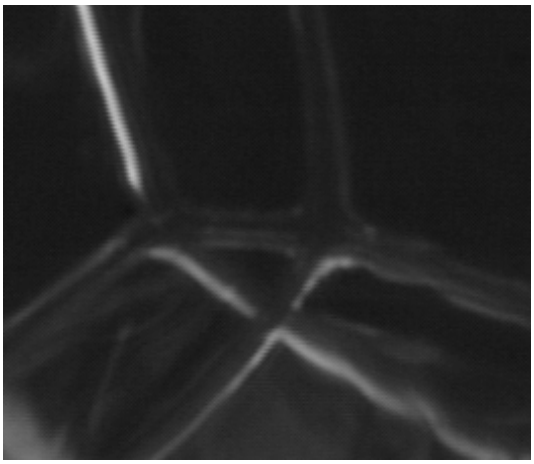

Figure 2.7: Macrophoto of nodes in a dry aqueous foam. Photo was taken at the FOAM Group at Brandenburg University of Technology lead by M. Meier.

E. Taylor together with Fred J. Almgren in 1976 using geometric measure theory [29–32].

Divide up space into cells of equal volume using the minimal surface area — foams can do this. The solution of this problem in 2 dimensions is the 'honeycomb' structure (Figures 2.8, 2.14). László Fejes Tóth, a great Hungarian mathematician, determinative personality in the mathematics of packing proved the honeycomb conjecture under the hypothesis that the cells are convex. Interestingly, the *general* proof of the honeycomb conjecture is not too old, published only in 2001 by Thomas C. Hales [27, 33].

The solution in 3D, which is a 14-sided polyhedra built up of six square and eight hexagonal faces was proposed in 1887 by Lord Kelvin (Sir William Thomson).

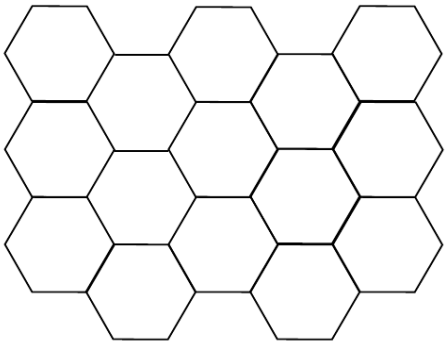

Figure 2.8: Honeycomb structure: any partition of the plane into equal area regions has a perimeter at least that of the hexagonal honeycomb tiling [33].

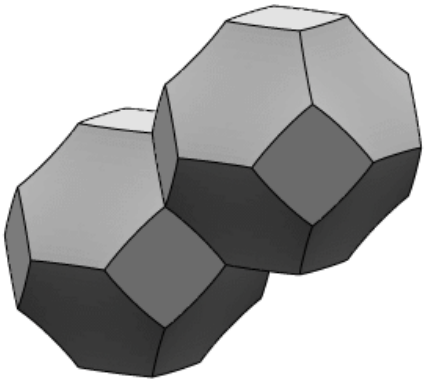

Figure 2.9: Partition of space into equal volume cells: Kelvin's tetrakaidecahedra [35].

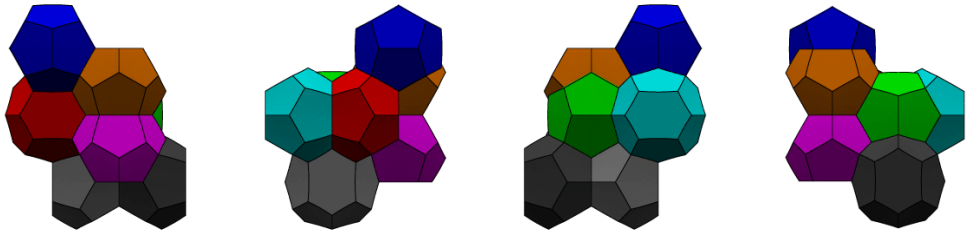

Figure 2.10: Selected views on Weaire-Phelan structure [35].

Kelvin's solution is in fact the 3D generalization of the hexagonal honeycomb in 2D. Two of Kelvin's *tetrakaidecahedra* can be seen in Figure 2.9. Note that the hexagonal faces are slightly curved in order to satisfy Plateau's rules. [34, 35]. Matzke in 1946 showed that the most frequent polygon inside a foam is the pentagon and the average number of a monodisperse foam faces is 14 ([26], cited by [16]). He also made a statistical investigation of cca. 600 bubbles in a monodisperse soap froth but did not observe any Kelvin cell. This strange finding was later confirmed by simulations[3] as well [36–39]. Weaire and Phelan in 1994 proposed a new structure that has a lower surface area than Kelvin's partition by cca. 0.3% [40, 41]. The so-called Weaire-Phelan structure can be seen in Figure 2.10.

[3] The Surface Evolver developed by Kenneth Brakke is an open access interactive program for the modelling of liquid surfaces shaped by various forces and constraints [36, 37].

Figure 2.11: Reticulite specimen from a lava fountain photographed near the Pu'u Loa petroglyphs in Hawaii Volcanoes National Park on April 3, 2007. [44].

The unit cell consists of two dodecahedra, and the other six are 14-sided with two opposite hexagonal faces and 12 pentagonal faces. The 14-sided cells stack into three sets of orthogonal columns, and the dodecahedra fit into the interstices between the columns [35]. The same structure can be found in *clathrates*, or 'cage compounds', like methane hydrate (methane captured in ice) under special pressure and temperature circumstances [16, 42]. *Reticulite*, a glassy volcanic rock is an open-cell polyhedral solid foam, consisting of a network of twelve- to fourteen-sided cells, a few tenths of a centimeter in size. The closed cell form is called *pumice*. Cell morphologies are also close to the model found by Weaire and Phelan [43, 44].

There is still room for searching better solutions than Kelvin's conjecture, since there is no proof for the ultimate conformity of the Weaire-Phelan partition. We have only proof that solution exists for the general n-dimensional space and a certain domain of the so-called tetrahedrally close packed structures[4] (TCP) has a lower surface area than Kelvin's partition. More recently in 2009 Gabrielli found another counter-example to Kelvin's conjecture. Whilst this new shape, made of four different polyhedra doesn't beat the Weaire-Phelan structure, the newly developed mathematical method could lead to a better solution to the Kelvin's problem [45, 46].

Interestingly, the outer wall of the Beijing National Aquatics Center, raised for the Olympic Summer Games of 2008 was built using the Weaire-Phelan structure, inspired by the natural formation of soap bubbles in the foam [47].

[4] These polyhedra consist of only pentagonal and hexagonal faces [45].

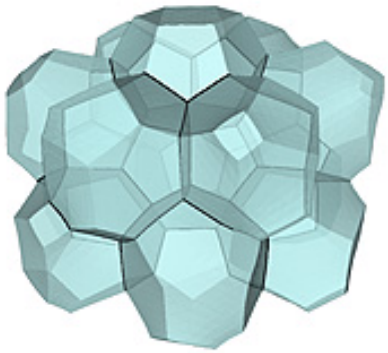

Figure 2.12: A new counter-example to Kelvin's partitioning by R. Gabrielli, using an alternative technique for mathematically modelling the structure of foam [45, 46].

Figure 2.13: A bird's view of the 'Water Cube' in Beijing, China [47].

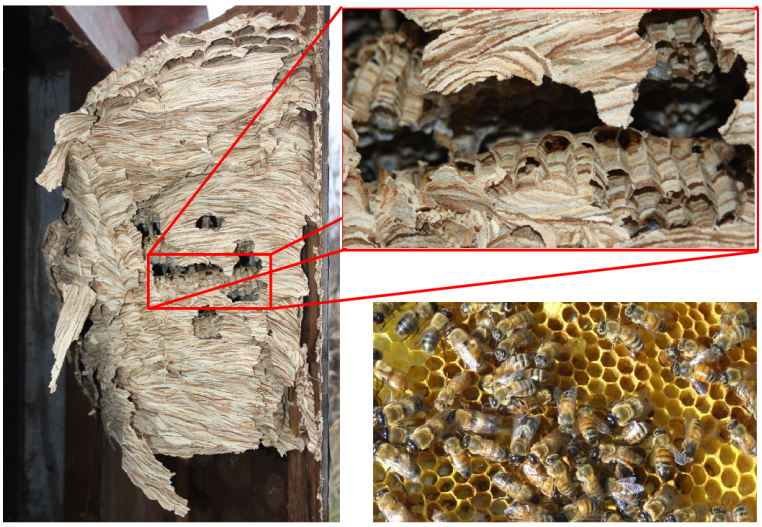

Figure 2.14: Left and insertion: European hornet (vespa crabro) nest, made of cellulose from decayed wood. Right: An example of the honeycomb structure: close-up photo of a beehive [49]

2.2 Natural foams - artificial foams

2.2.1 Foams in nature

Walking on the seashore, we often see froth along the beach. Taking a closer look on a leaf we meet conformations similar to a polyhedral foam. Living nature prefers foam-like structures or cellular materials against dense or compact architecture. Think about bone, or wood: we always find cellular material where we need strength, stiffness and light weight together. Prof. M. F. Ashby's famous saying, which is very often cited in almost every work dealing with cellular materials, draws the attention to the above finding: 'When modern man builds large load-bearing structures, he uses dense solids: steel, concrete, glass. When nature does the same, she generally uses cellular materials: wood, bone, coral. There must be a good reason for it!' ([48], cited by [16]). A typical example of a natural cellular building is the nest of various social insects, like bee, wasp, or the European hornet, shown in Figure 2.14.

But foams are good not only because of their unique mechanical features. Liquid aqueous foams show exceptionally diverse functions in biology. Foam nests of various insects[5], frog[6] or fish[7] species enable external fertilizing, gives mechanical protection and also shields the embryos or larvae from microbial, chemical or parasitic attack [50, 51]. More generally, organization of cells in various tissues are often similar to foam structure [26].

[5] e. g. Philaenus spumarius
[6] e. g. Chriomantis xerampelina
[7] e. g. Trichogaster trichopterus

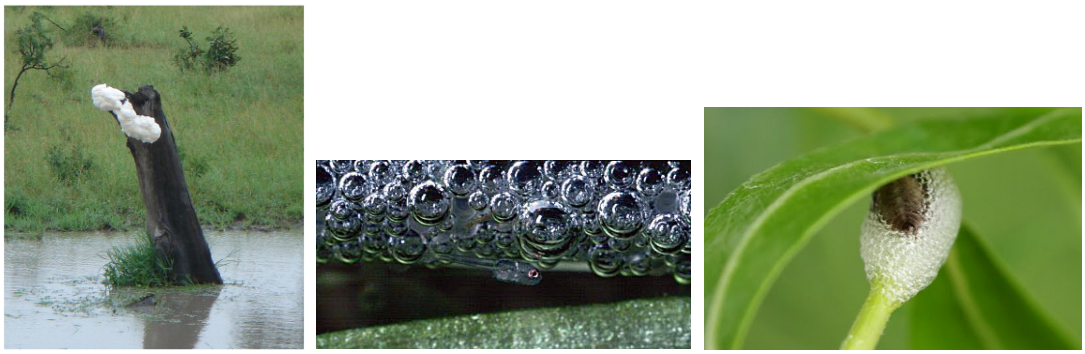

Figure 2.15: Left: Foam nests of the African foam nesting tree frog (Chiromantis xerampelina). Photo: Alan Cooper [50]. Middle: Fry of cosby gourami under bubblenest (Trichogaster trichopterus) Photo: Wiljo Jonsson [52]. Right: Protective bubble nest, or the 'cuckoo-spit', of spittle bug nymphs [51]. Photo: Csaba Pásti [53]

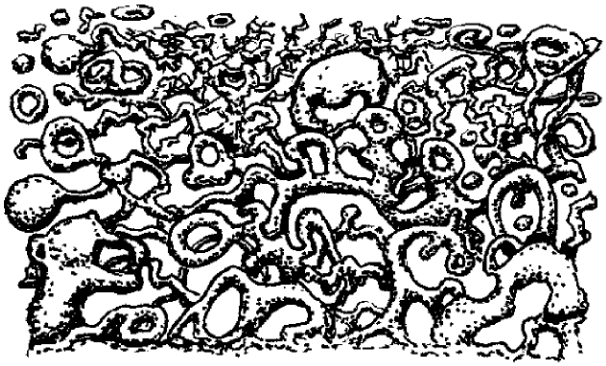

Figure 2.16: The foam-like nature of space-time at the Planck scale of 10^{-33}cm or 10^{-43}s [56].

Furthermore, we should never forget that the whole Universe, according to recent observational and theoretical cosmological studies has a large scale structure similar to foam. This is the heritage of the quantum stage space-time fluctuations [54, 55].

2.2.2 Foams in industry

Since nature is an inexhaustible resource of knowledge and new ideas, our artificial environment is predominantly formed following natural patterns. Foams as functional and/or structural materials appear in many different industrial processes and products. Of course they can also outcrop as unwanted by-products in some cases e. g. in paper industry, oil recovery or metallurgy.

The production of foams made of many different materials relies on empirical knowledge, but the scientific understanding is also very important in order to reach safe and reliable mass production of foam products with well defined features. The most important control parameters in foam production are the bubble size and the size distribution [14]. A brief summary of different foam production technologies is given in section 2.2.3.

Liquid or solid artificial foams can be easily grouped based on the cell wall material:

- aqueous foams (beer, fire extinguishing foam, dish-water, foam of cleaning supplies, shaving foam, etc. ...)
- polymer foams (polyurethane, polystyrene, polyethylene, bread, chocolate mousse, ice-cream, sponge-cake...)
- ceramic foams (glass foam, aluminium-oxide, silicon carbide foams, slag foam, concrete foam, carbon foam ...)
- metallic foams (aluminium, steel, titanium, magnesium, copper, lead, zinc...)
- composite foams (metallic sponge coated with polymer, or ceramic foam coated with polymer or metal layer, etc. ...)

Aqueous foams are the most common ones, and they are widely used in food industry — a foamy sweet after lunch or a mug of beer are always enjoyable. Oil or benzine fires can be extinguished using aqueous foams since they are less dense than oils and can cover the flaming surface. This feature is utilized as well when inhibiting the evaporation of toxic volatile liquids. Foam sprays loaded with irritating materials can be used in law enforcement or self-defense. There is also a vast amount of products for different cleaning, pharmaceutical or beauty industry applications. Aqueous foams can also be used as model materials for scientific investigations [57, 58].

Microfluidic technologies enable us to generate monodisperse aqueous foams down to a micron scale with very sharp control. The idea is to inject gas and liquid through micro-channels with well controlled flow rates. John Nye's first experiments on bubble rafts can be considered as the roots of these techniques. Such ordered aqueous foam structures and finescale foams now are under intensive scientific research, since

Figure 2.17: Aqueous foams: foaming must during fermentation (left), and fire-fighting show with foam fire extinguisher (right)

Figure 2.18: An everyday and a high-tech application of polymer foams: PS foam for crash absorber in bike helmet and PUR foam inserts in bike gloves (left). Space shuttle external tank covered with PUR insulating foam (right) [62].

they have a potential for direct applications in discrete microfluidics and lab-on-a-chip technologies e. g. for pharmaceutical industry [6, 14, 17, 20].

Solid open or closed cell *polymer foams* can be found around us everywhere. Almost every polymer can be foamed. They are prevalent as packaging materials or energy absorbers thanks to their advantageous elastic/plastic features (PUR). Soft polymer foams are often used in cushioning of furniture. Rigid products can be used as lightweight structural elements. Building industry uses them as thermal insulator/noise attenuator materials (PE, PS). Nowadays polymer foam production is one of the best established technology in chemical industry. Recent challenges are the recyclability and the restricted usage of CFC-s as foaming agents.

There are edible polymer foams as well: just think of bread, sponge-cake or chocolate mousse. Surface active agents for foaming are proteins, fats and alcohols in food production. The cell wall material of biscuits, snacks and cookies are a certain blend of biopolymers, like starch and different proteins [59–61].

Ceramic foams are rigid and lightweight materials, used as thermal/acoustic in-

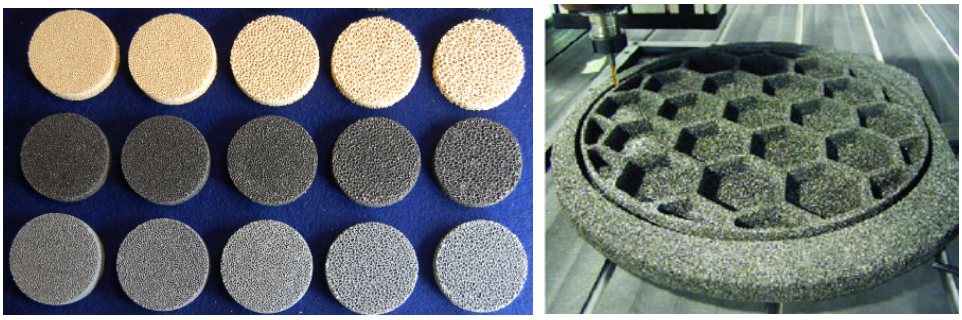

Figure 2.19: Ceramic foam high-tech applications — different pore size ceramic filters (left) and lightweight space mirror support (right) [65].

sulators at moderate or high temperatures (glass foam), or filters for example in metallurgy (SiC, Al_2O_3, Si_3N_4). They are also suitable for catalyst supports and pollutant adsorbers and we can meet them in special applications in defense/aerospace industry. Closed cell ceramic foams can be used as lightweight, but stiff and thermally stable base structures for primary mirrors in telescopes, or high energy laser optics [60, 63–65].

Metallic foams are the youngest members of the foam family, their story began in 1948 with the patent of B. Sosnick about the foaming of Al-Hg mixture in a pressurized container through the vaporization of Hg around the melting point of Al by ceasing overpressure [66]. From lightweight constructions to noise damping in closed cell form, and from flame arrestors to electro-chemical applications in open cell form, cellular metallic structures are very promising materials, and tend to conquer those empty niches where polymer or ceramic foams cannot come through. Comprehensive study from the design and production to the potential structural or functional applications of metal foams are presented in [9, 67–69].

The research and development of aluminium foams has some Hungarian relations as well. Pál Bárczy at the University of Miskolc initiated an application oriented research work on aluminium foams. A co-operation between the Austrian LKR Leichtmetallkompetenzzentrum Ranshofen and Miskolc University began and an excellent PhD thesis titled 'Ceramic Particles Stabilized Aluminium Foams' was born in 2003 by Norbert Babcsán.

ADMATIS Ltd. started its metal foam activity in 2003 inside the ESA project called 'Advanced Foams under Microgravity', as a co-investigator and facility supplier. The next step forward was the FOCUS Experiment: the second Hungarian materials science experiment in space after thirty years since the BEALUCA[8] programme [16, 70].

FOCUS Experiment is essential part of this work and the detailed experiment description is available in Chapter 3. The main purpose of the experiment is al-

[8] BEALUCA was a controlled crystal growth experiment using twelve different probes made of Al-Cu alloys. The programme was conducted by Erik Fuchs and executed by Bertalan Farkas onboard the Salyut-6 space station [70].

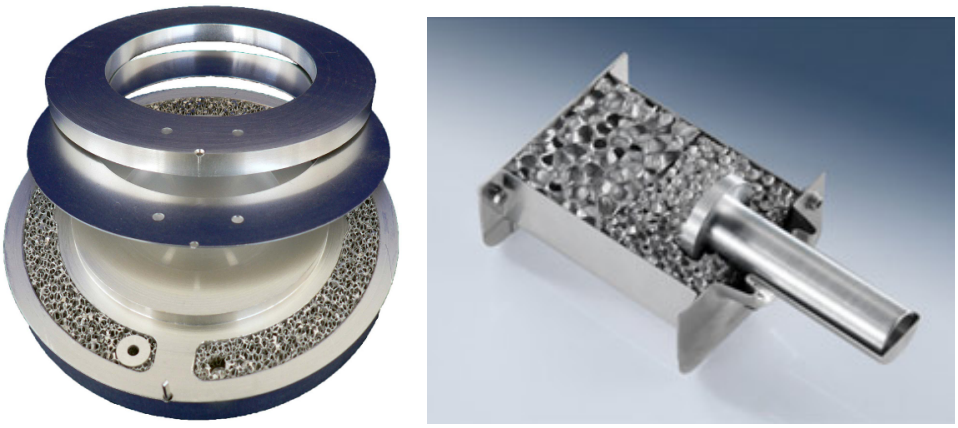

Figure 2.20: Left: Heat exchanger with open cell metallic foam inserts (DuoCel) [74]. Right: closed cell aluminium foam crashbox for automotive industry (MetComb) [75].

ready described in Section 1.1. Recent achievements of ADMATIS Ltd. are the implementation of FOCUS foaming technique for aluminium foams and further improvement of the so-called AluBone[9] intermediate good: complex shape metal foam with protective shell ensuring advanced mechanical properties [70–72].

Recently, the Group of Materials Development at Bay Zoltán Foundation for Applied Research in Hungary, lead by N. Babcsán have notable achievements in alternative aluminium foam production methods: using acoustic detachment of bubbles during foaming and to use nanoparticles for stabilising aluminium foams in order to increase stability and to improve workability [73].

As a summary, some typical end-products or processes are enumerated in Table 2.1. Beyond the four main groups *composite foams* also occur mainly in specific high-tech applications. A recent development is the so-called graphene-foam, made of graphene and PDMS [76].

Due to the similar properties of solid foamed materials, like good strength to weight ratio, high surface area, good thermal insulation or energy absorption characteristics we can find significant overlapping in the fields of application in different industries. The selection of the appropriate material always depends on the specific requirement. For example, metal foam liners (FML) near the aircraft engine fits well to the collection of requirements in aero-acoustics: efficient noise attenuation at specified frequency range and at high temperature, including flame resistivity, high stiffness, etc [77].

[9] AFT, Shaped Metal Foam Technology, Ányos Jedlik Programme, NKFP-07-A2-METFOAM8 2008-2011 and FTF GOP-1.3.1-11/C-2011-0039

Table 2.1: Selected foam (or sponge) products from different materials and typical (or potential) applications linked to various fields of industry.

Industry	Material			
	Aqueous [57]	Polymer [60, 78–80]	Metal [9, 67, 74, 77, 81, 82]	Ceramic [60, 63, 74, 83–85]
Food	Must, champaign, beer, cola	Bread, sponge-cake, ice-cream	-	-
Transportation (automotive, marine, railway)	-	Insulation, shock/energy absorption, furniture element, flame retardancy, vibration damping	Al-foams as shock/crash absorbers (bumper), structural element — Siemens Combino, Audi Q7	Catalyst carrier, exhaust filter (open cell), buoy
Aerospace	Airplane de-icing, fire-fighting	Insulation, structural reinforcement, energy absorption (SPF), Last-a-Foam®	Heat-exchanger (DuoCel®), meteoroid impact shield, Al-foams as helicopter tailboom, crash element, Ti-foam sandwich panel (Boeing), noise redustion, turbine structural parts, Li-Mg foams, breather plugs, flame arrestors	Catalyst support, SiC thermal protection systems (spaceship re-entry)

Industry	Material			
	Aqueous [57]	Polymer [60, 78–80]	Metal [9, 67, 74, 77, 81, 82]	Ceramic [60, 63, 74, 83–85]
Defense / military / security / law enforcement	Fire-fighting, sticky-foam, OC pepper foam, blast attenuation, noise suppression	Shock / explosion damping (in sandwich structures), bomb-suit		Shock/blast absorption, radar sign absorption (CFOAM®), lightweight structure
Building / Construction	-	Water/heat/noise insulation (PUR, PS, PE)	Structural element, decoration, noise insulation	Heat insulation (glass foams), foamed lightweight concrete
Cleaning / Beauty / Pharmaceutical / Medical	Shaving foam, carpet cleaning foam	Cleaning sponge, memory foam, eyeshadow applicator	-	Foot file (pumice)
Furniture	-	Matress, spacers	Decoration, design elements	
Chemical / Environmental	Volatile liquid sealing, vapour suppressing, odour control	Mechanical/chemical filter (open cell)	Electro-chemical application (Pb-foam, Ni-foam batteries), high-temperature filter (finescale open cell metals)	Mechanical/chemical filter (open cell), furnace thermal insulation, adsorber

2.2.3 Foam production

How can foams be made? A wide spectrum of foam production techniques is developed and used, but the purpose is the same: to somehow mix and disperse the gas into the liquid under controlled conditions and to achieve the desired foam structure. Two groups can be distinguished: *dispersion* and *segregation* methods. A non-exhaustive list together with short descriptions and examples are listed below [9, 14, 16, 73, 86–89]:

- **Dispersion methods**
  1. **Gas blowing:** This is the simplest method for foaming. Gas is introduced using single- or multi-capillary, porous frit, plate or sparger immersed into the foamable liquid. Foam properties depend on the capillary size, gas flow rate, etc. Typical application is froth flotation or bubble separation in mining industry. Also used in metal foam production (MetCOMB, Cymat).
  2. **Pouring:** Liquid stream is poured onto a pool of the same liquid causing gas bubble engulfment. This method is used for foamability estimation of different fluids (e. g. detergents).
  3. **Mechanical mixing:**
     (a) Mixing the liquid with gas using propeller-stirrer, vortex mixer.
     (b) Whipping (beating) air into the liquid.
     (c) Simultenaous feed of liquid and and gas jet onto porous plate or gauze, typical application is the in-situ generation of fire-fighting foam using special air-mechanical and mixing foam generators.
     (d) Liquid and gas co-flow through porous material gives foam. This method is used e. g. for oil recovery process simulations.
     (e) Microfluidic technologies, such as confined co-flow, flow-focussing, or cross-flow of liquid and gas at milli- or microscale. Potential applications in lab-on-a-chip technologies, biochemistry and medicine.
  4. **Shaking:** A vessel filled with liquid and air is shaken.
- **Segregation methods**
  1. **Aerosol method:**
     (a) Creation of gas bubbles in a supersaturated liquid by sudden pressure decrease. (e. g. shaving foam)
     (b) Nucleation of gas bubbles in a supesaturated liquid due to temperature increase — low boiling point solvents mixed into the foamable liquid (PS foams).

2. **Dissociation:** Mixture of solid powder and foamable liquid. The powder dissociates due to temperature increase or chemical reaction by releasing gas. Typical metal foam production route is mixing TiH_2 into Al liquid (Alporas).

3. **Chemical reaction:** Gas generation during polimerization, or reaction between multi-component fluids — used in PUR foam production.

4. **Propellants:** Special additives decomposing to gas and thus foaming (PVC foams).

The above enumeration does not contain those alternative technologies where the gas and liquid are not directly mixed, like chemical vapour deposition, investment casting, casting around space holders or other solid state processing of materials. These technologies are widespread in ceramic and metal foam/porous metal production [9, 84].

2.3 Foam evolution

Liquid foam is a beautiful but sensitive building, subject to various physical and chemical effects from generation to its disappearance.

Foams are thermodinamically unstable systems due to the excess surface energy and the absoute equilibrium state is the total collapse. Despite this fact we can observe foams that exist for a long duration, even for years. This signifies the existence of local equilibrium and meta-stability. Redistribution of the liquid inside the foam leads to hydrostatic equilibrium state determined by the capillary pressure and the pressures inside the gas and liquid. Based on the lifetime, we can distinguish *transient* and *permanent (metastable)* foams. Transient foams last for a few seconds, but metastable foam lives can vary from minutes to years [90, 91].

Figure 2.21 illustrates the life of a foam through its volume change with time. The life of a foam starts with gas dispersion into the foamable liquid (see Section 2.2.3). The most usual foaming process is to inject gas from below through an orifice into the liquid. A constant gas flow creates bubbles and due to density difference they rise up to the liquid/gas interface. In this first stage of foaming, bubbles move up with the gas velocity (v_g), so the foam volume increase is linear in the beginning [11]. Then the decrease in the slope becomes more significant based on the fact that the bubble lifetimes follow a Weibull distribution, which means increasing film rupturing probability with time [92]. The foam grows until reaching a steady-state value where the speed of foaming and decay is equal. Stopping gas introduction, only decay processes remain, leading to the sudden death or a long-lasting metastable state of a foam.

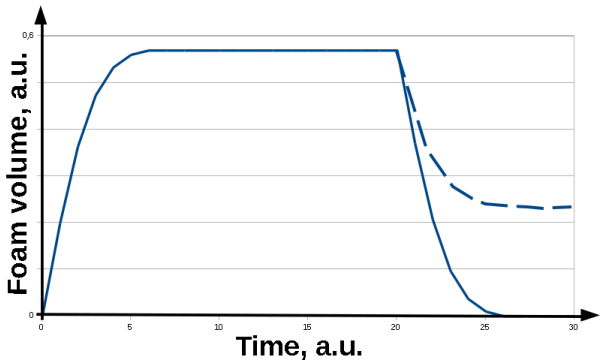

Figure 2.21: An illustration of the foam volume change with time from the beginning of foam generation to the complete disapearance (solid line), or a metastable state of a foam (dashed line).

2.3.1 Foam stabilisation

Single-phase liquids are not suitable for foam-making — the fluid films rupture almost immediately due to any thermal or mechanical perturbations. The key to survival is the modification of the surface properties. Regardless to the preparation method, a 'surfactant' is always needed to achieve long lasting foams. These additional materials can be *surface active molecules*, like in a soap froth, or *particles*, like in metallic foams. These materials have the capability to stabilise the thin liquid film against rupture. Fundamental mechanisms of foam stabilisation can be traced back to the stabilisation of single films or single PB-s. Particles and surfactants stabilise the films (foams) in different ways, as it is summarized below.

Surfactants, based on the hydrophillic part of the molecule, can be *non-ionic*, *cationic*, *anionic* or *zwitterionic* [87]. The main function of a surfactant molecule is to lower the surface tension and increase the surface elasticity of the liquid film through the adsoprtion onto the interface [16, 90]. The key phenomenon is the Gibbs-Marangoni mechanism in relatively thick liquid films (>100nm). The Gibbs surface elasticity (E_G) of the liquid is defined by

$$E_G = \frac{d\sigma_{lg}}{d\ln A}, \tag{2.4}$$

where σ_{lg} is the surface tension and $d\ln A$ is the relative change in the surface area. The above equation tells us that stretching a liquid film leads to surface tension increase through reducing the concentration of adsorbed surfactants. This is called the Gibbs-effect. E_G is determined under isothermal equilibrium conditions, with no re-establishement of the equilibrium surfactant concentration after deformation. The Marangoni-effect occurs thanks to the surface tension gradient caused by stretching: the liquid flows towards the streched region thus re-thickening the surface and providing a resistant force to further thinning. The surfactant concentration has to be in a certain range to achieve stable films (and foams) thanks to the strong

Gibbs-Marangoni mechanism. Too low concentration gives only low surface tension gradient, but too high concentration enables forming of very thin films that can easily rupture [16, 87, 90, 93].

The stability of thin (<100nm) foam films is determined by the *disjoining pressure* between the two surfaces. This disjoining pressure besides the Laplace capillary pressure ($p_c = \sigma_{lg}/r_{PB}$) , contains the electrostatic double layer repulsion (Π_{el}), van der Waals (Π_{vdw}) interactions and forces of steric origin (Π_{st}). The variation of the disjoining pressure vs. film thickness is called the disjoining isotherm. The shape of the isotherm depends on the surfactant type and concentration [16, 86, 90].

Particles, similarly to surfactants can adsorb at the interfaces and stabilise the liquid films in the foam structure. For example in the metallic foam regime surfactant molecules are not to be thought of — only ceramic particles can stabilise the foam films at such high temperatures. We can meet bubble-particle aggregates and particle containing foams in many natural and industrial processes: froth flotation, waste water treatment, oil-well drilling, etc. Binks and Horozov were the first to demonstrate that liquid aqueous foams can be stabilised solely by particles with certain contact angle, size and shape [94]. The detachment energy (ΔG_d) for a particle to be removed from the liquid/air interface is as follows:

$$\Delta G_d = \pi R^2 \sigma_{lg} (1 \pm \cos\Theta)^2, \tag{2.5}$$

where R is the particle radius, σ_{lg} is the surface tension and Θ is the contact angle of particle to the liquid [95]. Due to the high energies of attachment particles are irreversibly adsorbed (unlike surfactants). Particle stabilised aqueous or ceramic foams can last for years without any sign of structural changes with time [95–97].

According to Eq. 2.5 the largest energy value takes place at $\Theta = 90°$. A lot of experimental study arose investigating the connection between particle contact angle and foamability, and it was found that the optimum contact angle is usually below 90°. The solution is hidden inside the interfacial forces that arrange the particles into various structures in the liquid film thus inhibiting coalescence [7, 96].

According to [7], six different typical particle arrangements exist that can effectively separate the two liquid-gas interfaces:

- CP1: Closely packed single layer of particles
- LP1: Loosely packed single layer of particles
- CP2: Closely packed double layer of particles
- LP2C: Loosely packed double layer of clustered particles
- CP2+: Closely packed 'double+' layer of particles
- LP2+C: Loosely packed 'double+' layer of clustered particles

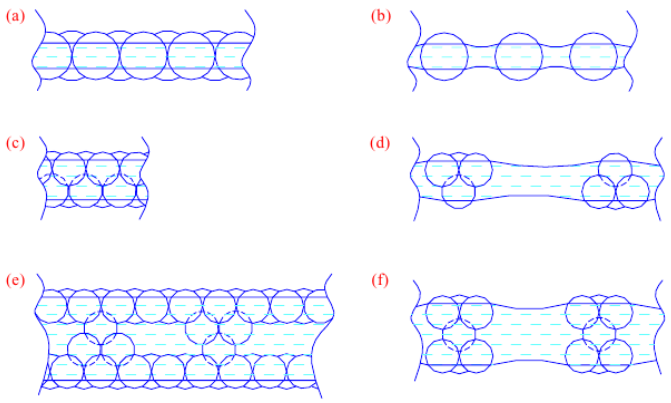

Figure 2.22: Part of the cell walls with different structures build up of the stabilising particles (schematic cross section): (a) 'CP1', (b) 'LP1',(c) 'CP2', (d) 'LP2C', (e) 'CP2+', and (f) 'LP2+C'. In (d) and (f) other particles may also be present, but are not shown for simplicity [7].

To stabilise liquid foams with particles, three subsequent event is needed, and the probabilites (p) of these events were deduced theoretically by G. KAPTAY in [7].

1. Stabilisation of bubble-particle agglomerates (p_1)

2. Stabilisation of two neighbouring bubbles against coalescence (p_2, p_c, referred to non-clustered and clustered particles, respectively)

3. Stabilisation of the foam against drainage and collapse (p_2)

The probabilities of particle-stabilised foam generation is proportional to the following two quantities for non-clustered and clustered particle arrangements:

$$p_\Sigma = p_1 {p_2}^2 = \frac{(1-\cos\Theta)(\cos\Theta+z)^2}{((1/f)-1+\cos^2\Theta)^2} \tag{2.6}$$

$$p_\Sigma^c = p_1 p_c {p_2}^2 = \frac{(1-\cos\Theta)(\alpha-\cos\Theta)(\cos\Theta+z)^2}{((1/f)-1+\cos^2\Theta)^2} \tag{2.7}$$

where

Θ:	contact angle between the liquid and the particles
z:	geometrical factor, depending on the type of particle arrangement (see Figure 2.22)
f:	cell wall coverage factor (ratio of the total cross section of particles attached to the cell wall, to the total cell wall)
α:	ratio of solid surface energy to liquid surface tension

The optimum contact angle depends on the particle arrangements, and it is situated somewhere between 50° and 90°. Depending on the contact angle, particles can act as foam stabiliser, but also as antifoamer.

The particle size and shape are also very important parameters in foam stabilisation. For aluminium foams, generally max. 30μm sized particles can be used. The maximum size of particles for aqueous foam stabilisation is 3μm [7, 96].

An alternative approach to investigate particle stabilisation is to consider the pressing force required to coalesce two bubbles decorated with particles. Particles affect the stability of films by reducing the thinning due to drainage [96]. The general equation for the so called maximum capillary pressure can also be derived for various particle structures [98]:

$$p_c^{max} = \pm 2\, p\, \sigma(\cos\Theta \pm z)/R, \tag{2.8}$$

where + is for o/w emulsions or foams, - is for w/o emulsions or foams, R is the particle radius, σ is the interfacial energy, Θ is the contact angle, and p and z are functions of the particle arrangements. The higher is the p_c^{max}, the higher pressing force can be tolerated by the liquid film.

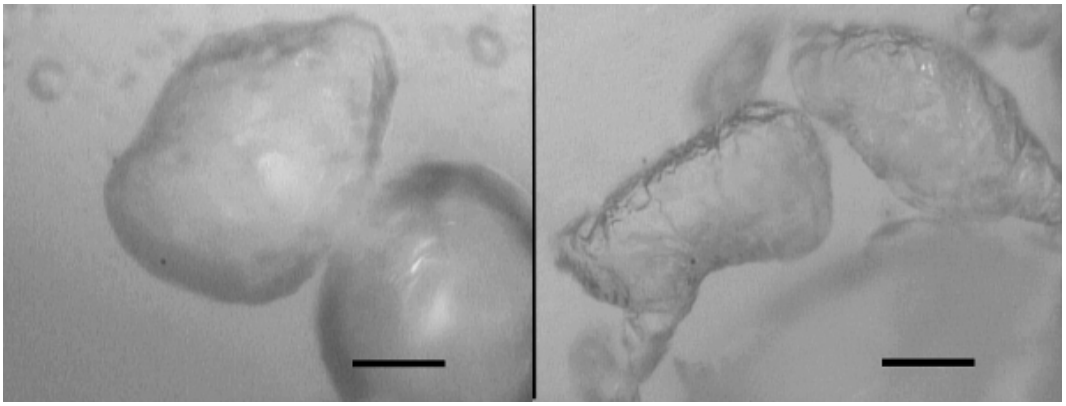

Figure 2.23: Optical microscopy images of foam bubbles stabilised solely by fumed hydrophobic silica nanoparticles. Scale bar is 5μm [99].

2.3.2 Foam decay

Right after the beginning of foam generation various decay processes start to take effect, finally leading to the complete disappearance or to a metastable state of the foam. The time evolution of foams is governed by four phenomena: *drainage*, *coarsening*, film *rupture* or bubble *coalescence*, and bubble flow (Figure 2.25).

Drainage is the irreversible flow of liquid through the foam in the direction of the gravity vector [101]. The liquid through the PB-s cross sections ooze downward due to gravity. As the steady foam volume is reached (see Figure 2.21), capillary

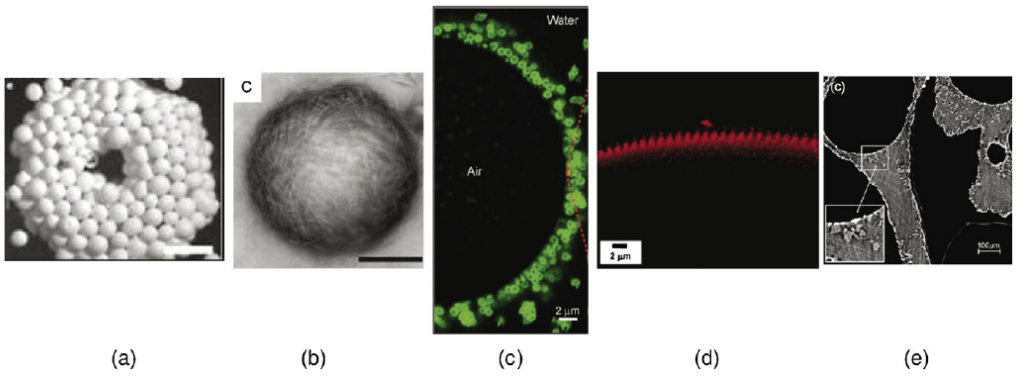

Figure 2.24: Examples on particle stabilised superstable foams: (a) toroidal air bubble stabilized by ground zirconium particles (bar = 0.5mm); (b) hairy air bubble covered by a layer of adsorbed rods (bar = 50µm); (c) air in water bubble stabilised by Janus particles; (d) air bubble stabilised with PS particles; (e) tomographic image of plane through a solid aluminium foam stabilised by SiC particles. The images were taken from [6].

suction with air flow balances gravity driven drainage [4]. The top of the foam becomes quickly dry and the bottom remains wet. The thickness t of the wet foam layer is determined by the ratio of the average bubble diameter (d) and the squared capillarity length (l_0^2), which depends on the ($\sigma/\rho_l g$) of surface tension (σ), liquid density (ρ_l) and the gravitational constant (g). The smaller are the bubble size in a foam, the thicker is the wet layer [11].

$$t = {l_0}^2/d \tag{2.9}$$

The past decade was full of advanced experimental and theoretical studies regarding drainage. The foam drainage equation can be derived from the balance of gravitational, capillary and viscous forces. The surfaces of PB-s (depending on-the surface viscoelasticity) can be rigid or mobile, resulting Poisuille-like flow, or plug-flow, respectively. These two regimes and even the transition can be observed experimentally [4, 102].

Foam coarsening (Ostwald-ripening) can be traced back to gas diffusion through the cell walls. Larger bubbles grow at the expense of the smaller ones due to differences in their chemical potential which is due to the difference in their capillarity. The growth occurs by diffusion of dispersed component (gas) through the continuous phase (liquid) [11, 103].

The bursting of a single film is a two-stage process: first the film thickness should decrease (film drainage) and then short range attractive forces should act between the two surfaces of the film resulting *rupture* [4].

It is clear that bubble coalescence, coarsening due to diffusion, or film rupturing all depend on foam liquid fraction and they are interconnected through the gravity-driven drainage [100, 102]:

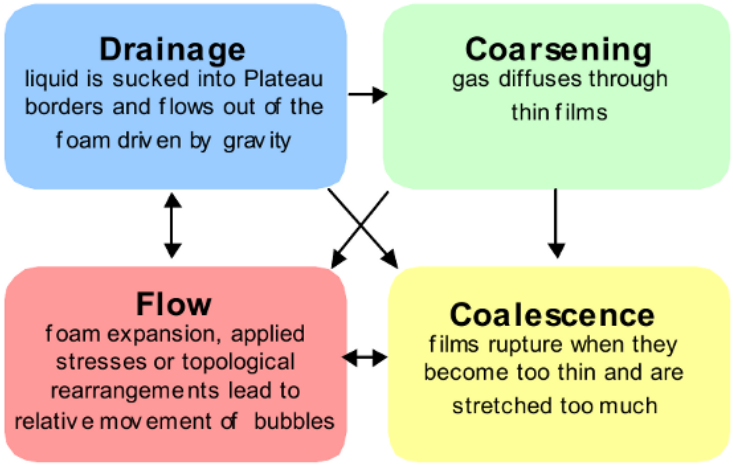

Figure 2.25: Interdependence of four principal phenomena in liquid foams [100].

* The yield stress of the foam increases with decreasing liquid volume fraction (ε)
* Coarsening enhances drainage through making wider PB-s and thus increasing drainage speed
* Drainage induces bubble coalescence/film rupture by thinning the film thickness
* Drainage induces bubble sorting (flow) and thus the foam structure changes
* etc. . .

Two research directions are envisaged: to understand basic phenomena by separation and elimination of the interconnections, and, on the contrary, to create the theory for coupling them (drainage *and* coarsening, drainage *and* rupture, etc.). Coarsening can be eliminated using insoluable gases for foaming. Elimination of gravity-driven drainage is possible using microgravity, or to create foams from microbubbles. Microgravity also provides an ideal environment for the investigation of very wet foams ($\varepsilon > 20\%$). The regions still unexplored in foam physics are illustrated in Figure 2.26.

2.4 Foam research in microgravity

Foams naturally degrade with time, because both capillary forces and free drainage thin the cell walls which eventually leads to film rupture and bubble coalescence. Capillary forces are mostly determined by the material properties while the drainage is influenced by gravity.

Eliminating gravity gives the possibility to separate gravitational drainage from other processes like coalescence, coarsening or film rupture, that lead to the death of

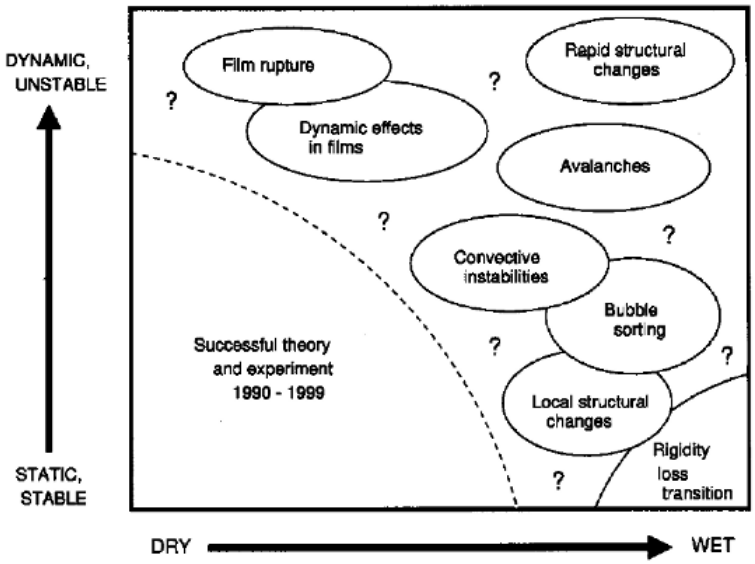

Figure 2.26: Challenges in the physics of foams [11].

a foam [5]. Dynamic effects at the wet foam limit becomes also available by reaching microgravity [2]. There are several ways to modify the gravity environment. Facilities are selected based on the desired magnitude and duration of hyper -or microgravity. A non-exhaustive list of the basic representative data of various experimental platforms can be seen in Table 2.2.

The first relevant gravity related foam experiments were made in the early '90s using short-term microgravity (sounding rockets, parabolic flights, drop balloons), mainly investigating industrial processes like flotation or metallic/polyurethane foam forming. We also find some activites back in the '70s: the feasibility of producing closed-cell metal foams were investigated at NASA in 1977 under the Space Processing Applications Rocket project, SPAR 2 [108, 109]. There were also some demonstrations on the Skylab space station back in the '70s using soap films [11, 110–113]. The Russian MIR Space Station (on orbit from 1986 to 2001) was an ideal platform for long term microgravity experiments in the field of materials science. For example, Merzhanov et al. synthesised closed cell ceramic foam materials for combustion experiments [114].

Besides the application-oriented research, theoretical study of liquids and foams in microgravity became more and more popular. A large number of micro-g experiments together with simulations and theoretical work helped to better understand the liquid motions and bubble dynamics inside the foam. Monnereau et al. showed experimentally in parabolic flights that transient foams can be stable in microgravity environment, and due to gravity increase spherical bubbles take polyhedral shape accompanied by numerous topological changes [3, 115].

Caps et al. [116] found in parabolic flight experiments on 2D foams that the liquid imbibition into the foam in the absence of gravity is a diffusive process. These

Table 2.2: Various experimental platforms for micro - and hypergravity research [104–107].

Platform	g-level/range	Duration	Max. payload mass
Drop tower / drop shaft	10^{-5}	5-10s	125kg
Balloon drop	10^{-3}	20s	500kg
Sounding rocket	10^{-4}	2-15min	450kg
Parabolic flight	$10^{-2} - 1.8$	20-30s	50kg
Retrievable capsules	$\leq 10^{-5}$	12-18d	500kg
Space station (ISS)	$10^{-3} - 10^{-6}$	years	4000kg
Hyper-g centrifuge	$1 - 30$	NA	1000kg

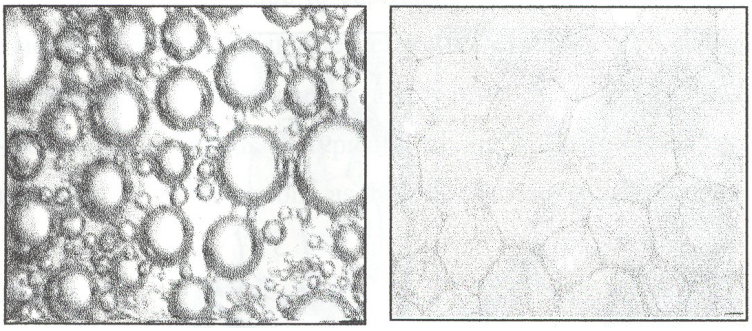

Figure 2.27: View of an SDS + Dodecanol solution foam at 0g (left) and at 1.8g (right) [3]

observations were studied as well by numerical analysis using the drainage equations for mobile and rigid interfaces [117, 118].

Foams containing solid particles were investigated both in micro - and increased gravity [119]. The role of particles in foam stabilising[10] is under intensive research and a lot of progress was achieved in the last few years in various fields: from aqueous systems to metallic foams, both theoretically and experimentally [7, 95, 96, 98]. Wübben et al. [120] showed in parabolic flight experiments that metallic foam films are stabilised solely by the network of solid particles. First in-situ X-ray radioscopy experiment on Al foams using sounding rocket with cca. 6 minutes of micro-g revealed that the bubble coalescence rate does not change significantly with the magnitude of gravity [121, 122].

The most significant microgravity programme for aqueous and metallic foams is called F O A M: Foam Optics and Mechanics[11], with the collaboration of several European and US foam research communities. The project started at the beginning

[10] A short insight can be read about particle stabilisation on page 25.
[11] ESA ref: AO-1999-108, NASA ref: NASA/TM-2002-211195 AIAA-2001-4961

Figure 2.28: ESA Astronaut André Kuipers with the FOAM-Stability equipment. [126]

of the third millenium [2, 59, 123]. The main objective of the project is to achieve long term microgravity onboard of the ISS in order to explore the realm of wet foams, including the phase transition ('melting') when the foam reaches the critical $\varepsilon \approx 26\%$ liquid volume fraction.

More than a hundred publications were born during the ten years of active theoretical and experimental work, based on several short-term micorgavity experiments on parabolic flights and sounding rockets (MAXUS[12] flights). The project has developed into two main area, called 'FOAM Stability' and 'FOAM Coarsening'.

FOAM-Stability investigated foams that would be unstable on Earth. While the difference between foaming and not-foaming solutions is clear, the case of slightly-foaming products is more complicated. For the latter, although agitation does not produce stable bubbles and liquid films on Earth, some liquid solutions can nevertheless produce foams in microgravity, as it was demonstrated during parabolic flight experiments performed in autumn 2007 [125].

FOAM-Stability experiment was carried out on the ISS in 2009. The experiment consisted in shaking various solutions both on Earth and in the ISS in order to study the influence of gravity on foamability and stability of foams. For that purpose, a small rack was built containing 12 transparent cylinders filled with various solutions with $\varepsilon \approx 30\%$. Foams were formed by hand-shaking by the astronaut and then mounted on a laptop screen (on the ISS) for illumination and their evolution was recorded (Figure 2.28). Researchers found cca. 2 times larger foamabilities for the selected liquids. Even slightly-foaming, non-foaming or anti-foaming agent containing solutions were able to foam under 0g. The foams were stabilised after forming and did not show any evolution in microgravity during the 1000s observing time. The unexpected behaviour of the solution containing anti-foaming agent raises new

[12] The MAXUS programme is a joint venture between SSC and Astrium Space Transportation used by ESA, providing cca. 14 minutes of microgravity for 785kg maximum payload mass [124].

fundamental questions for future research [127].

FOAM Coarsening is to study foam coarsening in the function of liquid fraction with novel experimental technics in space. The ultimate goal is the design and use a delicate experimental facility for the ISS for foam research. A series of technological tests were carried out in parabolic flights and MAXUS flights. A special microgravity cell has been developed and tested in 2009, allowing both drainage and rheology studies in space conditions. The hardware enables optical and electrical diagnostics of foam evolution. The planned experiments on the ISS will try to find the answer to the questions arise in the characterisation of very wet foams, transient foam stability, and the role of particles. These investigations are very important in order to be able to further optimize industrial foam processing in various technologies [5, 59, 101, 125, 128].

Chapter 3

Experimental

This chapter collects all foaming experiment data, including the equipments and materials used and the methods of experiment preparation. Before going into the details some definitions have to be pinpointed with regard to the methods of foaming experiments and materials characterisation. Unless otherwise stated, these definitions are applicable for all experiments discussed in this work.

3.1 Definitions

- **Foaming time** is the duration of gas introduction during foam making (from opening to the closing of the gas valve).

- **Foam volume** is the volume of the generated foam with homogeneous cell structure. Cells ('holes') that have sizes greater than 10% of the entire volume are not considered as part of the foam. This criterion is needed for technological reasons: foams needed to be homogeneous enough to find their way in industrial applications. See Figure 3.1. These regions may be also called as 'coalescence area' [109].

- The **initial foam volume** is the total volume generated with a fixed foaming method. This features the foamability of the system.

- **Foamability** is the capability of a liquid to foam. The more amount of foam can be made with a given method, the better is the foamability of the liquid. Note that the foamability in our increased and decreased gravity experiments applies not only to the given liquid (FOCUS suspension), but the suspension and the FG together.

- **Foam stability** means how long a foam can survive. This can be characterised by the ratio of the foam volume after a given period of time (e.g. three minutes) and the initial foam volume. The above general statement can be narrowed to

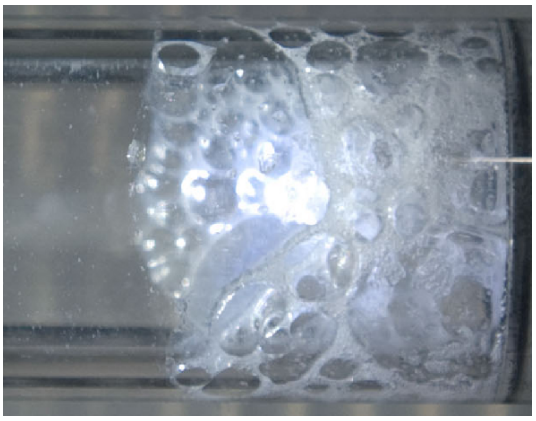

Figure 3.1: A typical 'hole in the foam' macrophoto from FOCUS Experiment. The hole is located at the bottom right of the image.

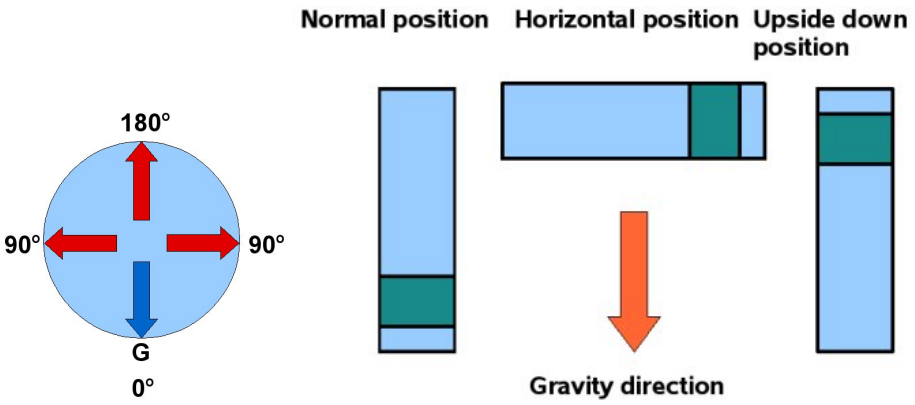

Figure 3.2: Definition of foaming direction measured to gravity vector and typical FC positions [131].

various definitions based on the selection of time elapsed after stopping foam generation:

  - **Foam life** is the time elapsed from foam generation until total disappearance. This definition is not very suitable because the observation of total disappearance can be very ambiguous. Therefore to select the time of reaching the one tenth of the foam's initial volume or the half of the original volume is a much better choice. The latter is called the **half-life** of the foam: $t_{1/2}$ [129, 130].

- **Foaming direction** is the direction of foam generation measured to the gravity vector. 180, 90 and 0° means 'downward', 'horizontal' and 'upward' foaming [131]. See Figure 3.2.

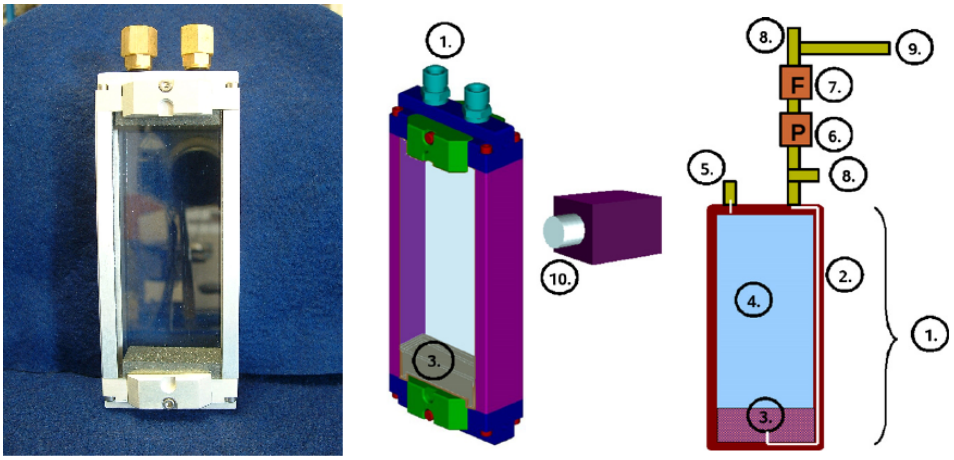

Figure 3.3: Left: Photo of UMFA-LT foaming cartridge. Right: Schematic drawing and the experimental set-up. (1) Foaming cartridge; (2) routes inside the cartridge; (3) porous SiC ceramic sparger; (4) glass sidewalls; (5) gas outlet; (6) pressure gauge; (7) flow meter; (8) valve; (9) pipe toward gas container; (10) webcamera [132].

3.2 Equipments

The following subsections describe the equipments used during the foaming experiments. All equipments described here were designed and manufactured at ADMATIS Laboratory. Other equipments used are mentioned briefly in the results section.

3.2.1 UMFA LT Cartridge

Universal Multizone Foaming Apparatus (UMFA) is a special open furnace equipped with eight heating zones capable of testing various foam or emulsion samples under controllable temperature environment[1]. The apparatus can be tailored to different investigation techniques: from optical imaging to X-ray radioscopy.

Separate foaming cartridges, designed for various purposes can be placed into the UMFA. The low-temperature (LT) foaming cartridge was used during the foaming experiments of PVC-water-ethanol solution. It has two removeable glass sidewalls enabling optical imaging and visual observation of foaming. A porous SiC ceramic sparger with cca. 17% open porosity together with the gas routes are also built into the cartridge (see Figure 3.3). The overall volume is cca. 40cm^3 [132].

3.2.2 Macro-g test pad

Macro-g test pad was developed for making fully automatized foaming experiments except sample change. The test pad was successfully integrated into the ZARM

[1] The apparatus was designed and manufactured under the ESA PECS contract ID: AO-99-075, no: 98009

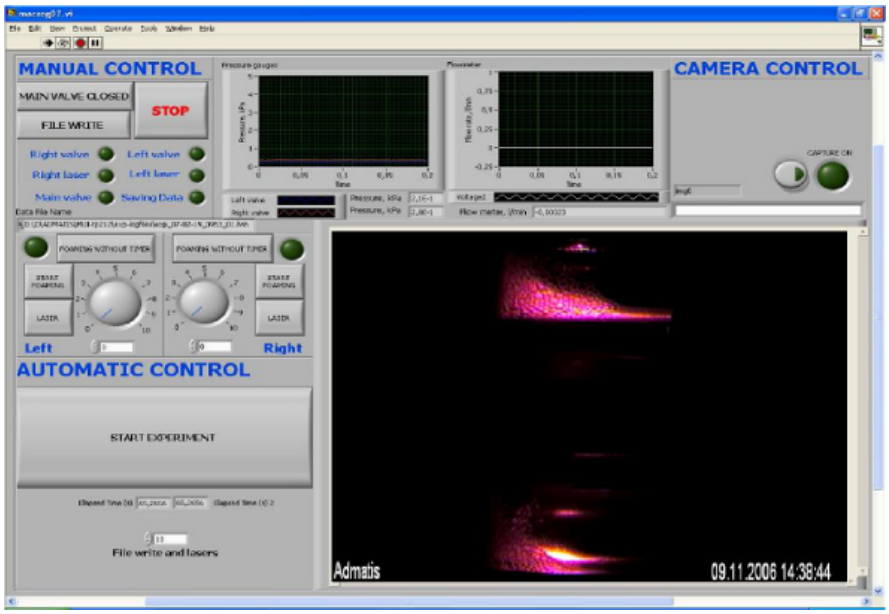

Figure 3.4: Measurement control software of Macro-g test pad [131].

Hyper-G Centrifuge in Bremen. Measurement control — valves, lighting, data collection and imaging — was solved using a special control software, 'Virtual Instrument (VI)' developed in LabVIEW^{TM} frame system (see Figure 3.4). The VI enables the user to switch between hand and automatic experiment control.

The rotatable disk enables varying the foaming direction measured to the gravity vector with 1° accuracy. Two foaming cartridges (FC) can be fixed onto the disk. Red line laser illumination (Roithner Lasertechnik) gives good contrast on the view of the foams. The test pad is equipped with a Panasonic Colour WV-CP480/G CCTV camera.

Foaming pressure and flow rate can be adjusted manually and the data can be recorded for each foaming cartridge separately at maximum 100Hz. External gas tank or pressurised air line can be connected to the test pad. The essential parts of the equipment are shown in Figures 3.5 - 3.6.

The centrifuge at ZARM Institute is often used for both scientific experiments and industrial applications (testing & qualification). Maximum centripetal acceleration is 30g and the maximum equipment size is 1000x800x1500mm. The macro-g test pad was deployed onto a universal platform, which can be inserted in both the Hyper-g centrifuge and into the drop tower of ZARM [105, 130, 131].

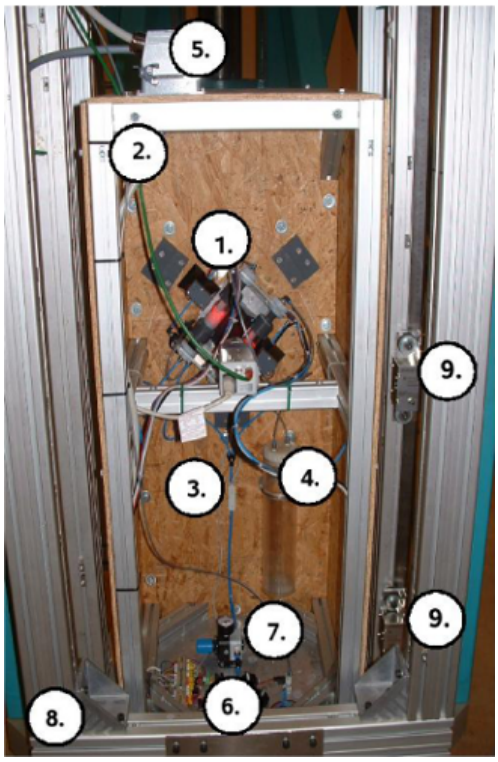

Figure 3.5: Macro-g test pad: (1) Rotatable disk; (2) Gas introduction; (3) Flow meter; (4) Liquid overflow tank; (5) Power supply; (6) Relays; (7) Pressure reducer; (8) Macro-g platform; (9) Accelerometers [131].

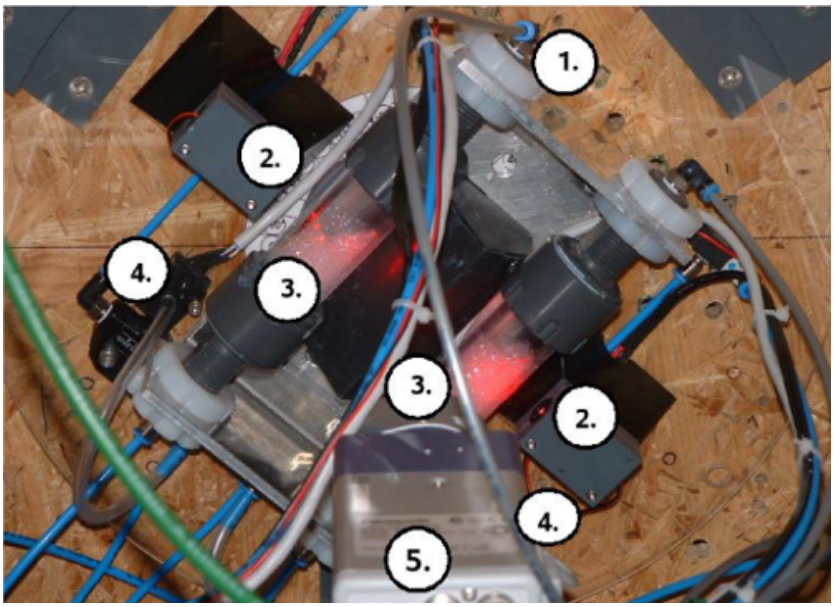

Figure 3.6: Close-up view of macro-g test pad: (1) Rotatable disk; (2) Red line laser module; (3) Foaming cartridges; (4) Pressure sensors; (5) CCTV Camera [130, 131].

Table 3.1: Main characteristics of foaming cartridges [133, 134].

FC name	FG material	FG placement	FG diameter (mm)	FG height (mm)	FCH height (mm)
Macro-g FC (FC01)	K2790 blue polyurethane foam	Fixed	24	15	73
Modified macro-g FC (FC02)		Exchangeable	24	15	73
FOCUS FC (FC-FOC)	K2790 grey polyurethane foam	Exchangeable	19	15	72

3.2.3 Macro-g and FOCUS foaming cartridges

The foaming cartridges were under constant development in order to achieve better usability and control of experimental parameters. Foaming cartridges consist of a cylindrical foaming chamber (FCH) and a foam generator (FG). The liquid or suspension can be infiltrated into the FG prior to foaming. During foaming, gas penetrates into one side of the FG and foam comes out from the opposite side. Liquid and gas is mixed inside the porous structure of the FG. More detailed description of the FG material can be read in Section 3.3.

Table 3.1 below summarizes the different stages of foaming cartridge development during the macrogravity and decerased gravity experiments. The first series of FC-s had fixed FG-s inside. Second generation enabled to change, replace, or refill the FG-s, and to adjust the liquid content. For the FOCUS Experiment we needed to change the geometry of the foaming cartridges in order to integrate them into the experiment container (EC — see Section 3.2.5). Also a vent hole was put onto the FCH-s.

FC01 type cartridges were used during the macrogravity and its reference experiments. FC02 types were used in the characterisation of the so-called FOCUS-suspension (detailed in section 3.3), and during the FOCUS pre-experiments. FC-FOC type cartridges were used in the microgravity and its reference experiments [133, 134].

3.2.4 FOCUS Test Pad

Pre-experiments on FOCUS suspension and FOCUS micro-g hardware testing was done using the modified macro-g test pad. Modifications enabled to insert single FC-s into the rotatable disk and to make sequence of high resolution images at 1fps frame rate. FOCUS hardware could also be fixed onto the disk. Flow rate and

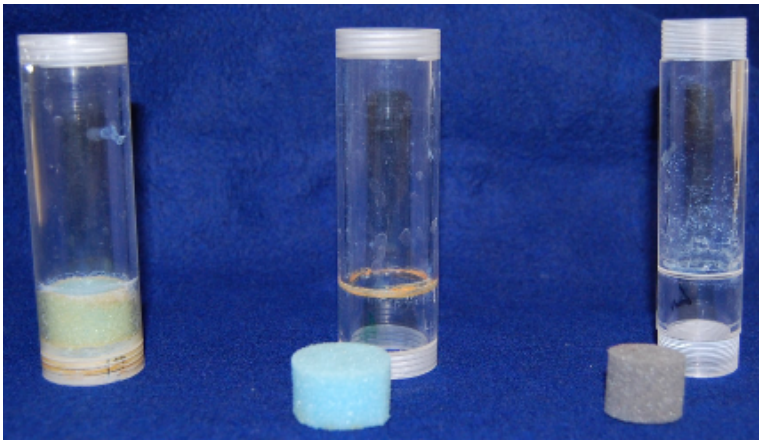

Figure 3.7: Three generations of foaming cartridges [133].

pressure data were recorded, and an extra pressure sensor was added to measure the pressure inside the FOCUS EC during foaming.

3.2.5 FOCUS Hardware

FOCUS Hardware was used during the microgravity experiment on board of the International Space Station (ISS) and the terrestrial reference experiments at ADMATIS Lab. Four identical items were manufactured, two of them were the flight and the flight spare, one model was built for training and one for testing purposes. The purpose of the development was to have a compact and totally stand-alone hardware capable to carry out foaming (or other simple fluid physics) experiments with astronaut assistance.

FOCUS Hardware consists of three foaming cartridges (FC-FOC type, see Table 3.1) included in a dedicated Experiment Container (EC) that inhibits any leakage into the ISS atmosphere and enables observation through its sight window (Figure 3.9). FC-s have three parts: Illumination System (IS), a transparent Foaming Chamber (FCH) and the Gas System (GS) with the gas container and valve (Figure 3.9). The foamable suspension can be filled into the porous foam generators (that is inside the FCH) prior to assembling and foams can be generated by blowing gas through them. The hardware is fully independent of ISS onboard facilities and can be manually operated without any tools by using the gas and light knobs. Nikon D2xS and Nikon D40 type DSLR camera on a camera support (multi-use bracket) were used for sequential imaging on the ISS and in the reference experiments, respectively. The on-board configuration is shown in Figure 3.10 [71, 134].

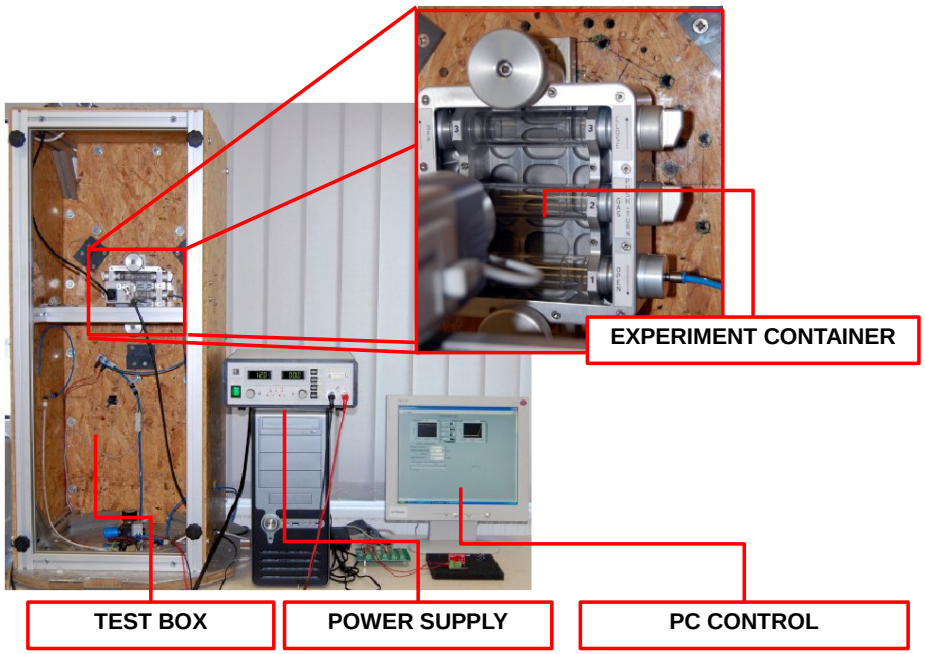

Figure 3.8: FOCUS Test Pad [71].

3.3 Materials

3.3.1 PVC-water-ethanol solution

Ethanol-in-water solution was selected to observe the influence of the contact angle between a solid stabilizing particle (PVC) and the liquid phase during the process of foam making.

The PVC particles were produced by emulsion polymerization process [135]. The PVC resin, purchased from Vestolit under the trade name of Vestolit B7021, had a K-value of 57, i.e. the average molecular weight is $M_w = 87000$g/mol measured according to DIN53726 standard [136]. In this regard, the molar weight of the polymer does not have an effect on the surface properties. Emulsion type PVC was selected because it has much more regular spherical shape and lower average particle size than suspension type PVC. SEM image of the particles can be seen in Figure 3.11 where the spherical shape and the agglomeration behaviour of the smaller particles are visible [132].

Particle size analysis was carried out using laser diffraction method (Sympatec Helos 12KA/LA Sympatec GmbH, Germany). Particle size is deconvoluted using the Fraunhofer theory [137]. The results of the laser scattering measurements are shown in Table 3.2.

The surface of the emulsion type PVC particles was contaminated by sulphur

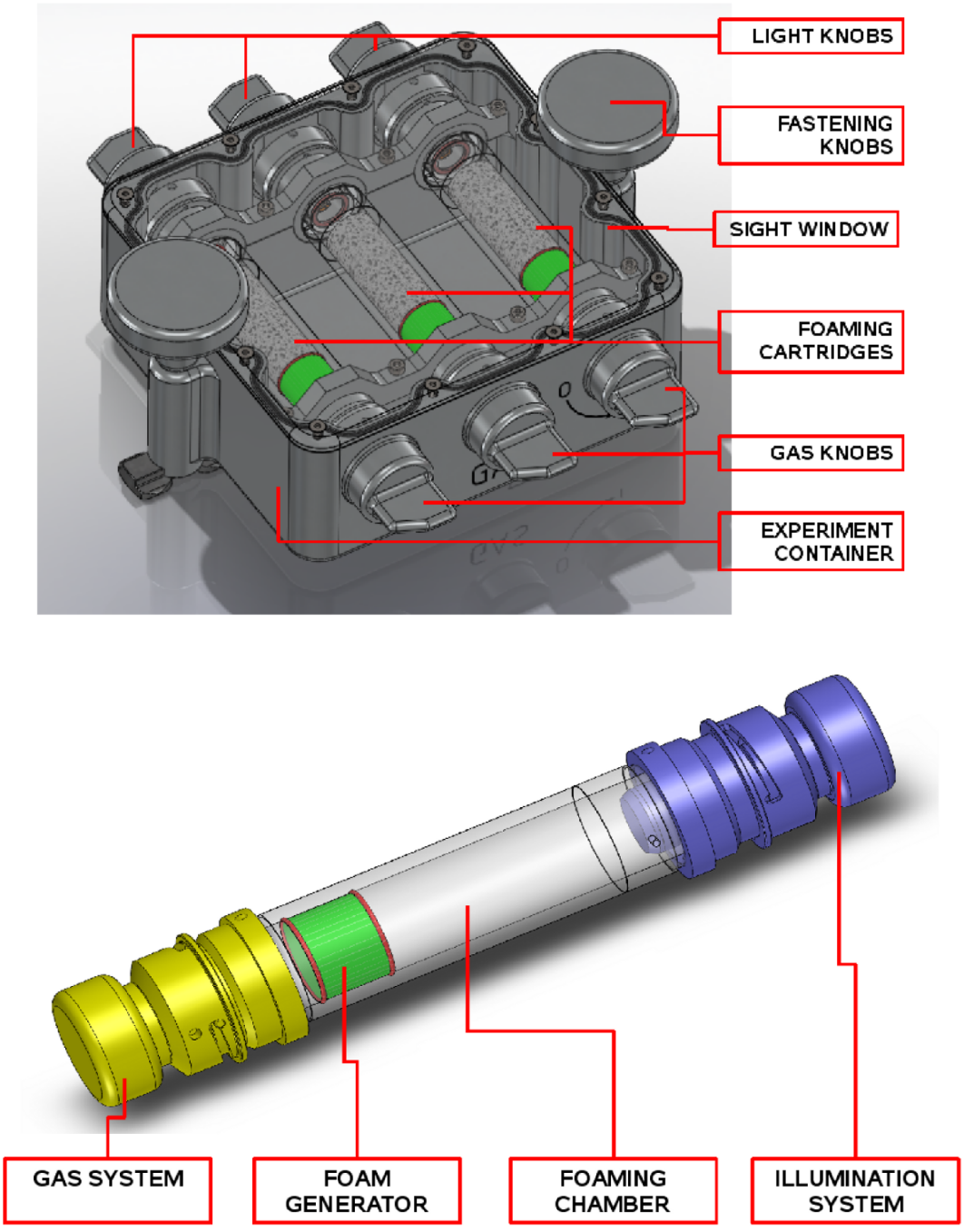

Figure 3.9: Up: FOCUS Experiment Container. Down: FOCUS Foaming cartridge [134].

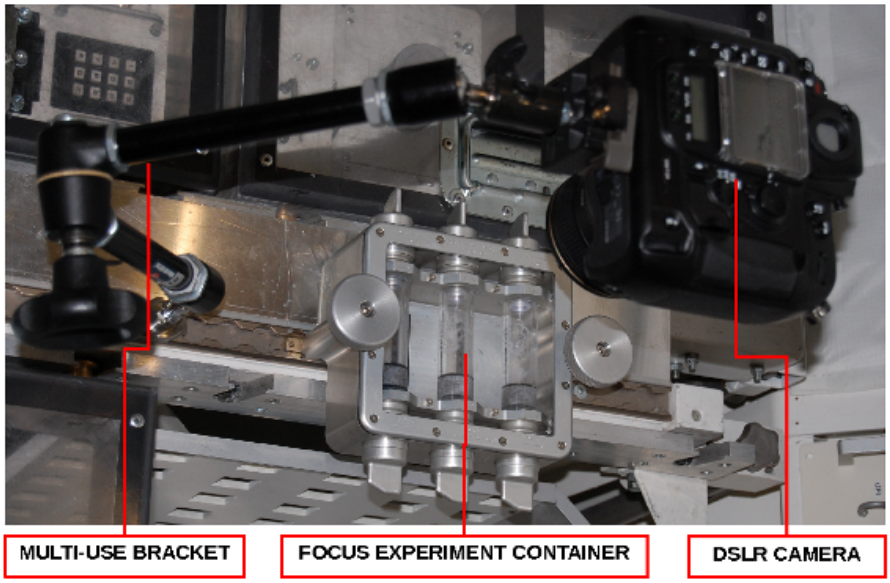

Figure 3.10: FOCUS on-orbit configuration. Photo was taken during the experiment sequence test in 2009 July at EAC Cologne.

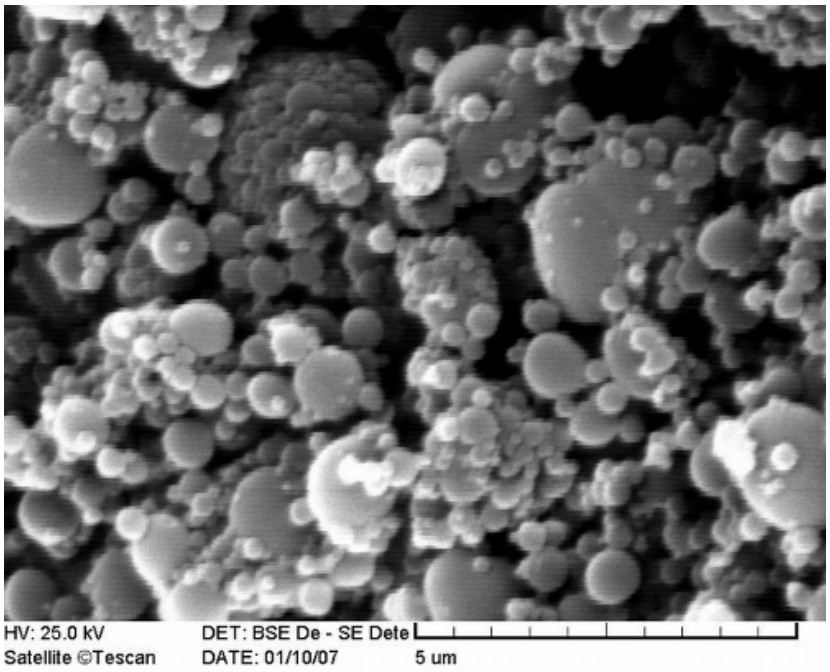

Figure 3.11: SEM image of PVC powder after washing procedure [132].

Table 3.2: Particle size distribution using laser light diffraction method [132].

Factor	Particle size (μm)
X5	0.61
X10	0.80
X30	1.50
X50	**2.62**
X70	5.79
X90	**14.67**

X5 means that 5% of the sample are smaller than 0.61μm, X10 means that 10% of the sample are smaller than 0.80μm, and so on.

containing surface active layer. To assure reproducible experimental conditions the particles were cleaned before the experiments with a high rotational speed centrifuge using distilled water. The concentration of the PVC powder was set to 10wt% in every washing cycle. The centrifuge operated at a speed of 7000min^{-1} and for 5 minutes. The conditions of the washing liquid above the settled powder were checked after each wash cycle in order to have information about the status of decontamination as follows.

Foams were generated from the washing liquids by simple hand-shaking in a test-tube, using 10ml of the liquid, shaking for 10s and reading foam heights after 5 seconds. The foam heights decreased exponentially with the increasing number of the wash cycles, indicative of the reduced concentration of surface active contaminations contained in the system.

Surface tension (σ) of the washing liquids were also measured by pendant-drop method. This method determines the surface tension through analyzing the drop shape which is formed by the balance of gravity and surface forces [138]. One measurement lasted approximately 3 hours because we had to wait for the equilibrium state of the drop. Figure 3.12 shows the change of the foam heights and the surface tension of the washing liquids as a function of the number of washing cycles. The washing procedure was repeated until the surface tension of the washing liquids show convergence to a certain value. After eleven cycles the surface tension of the washing liquid tended to a typical value of $\sigma = 52$mN/m [132].

SEM investigation showed no significant difference in particle size distribution between the unwashed and washed powder; average particle size remained around 10μm. The powder was dried after the washing procedure at T = 40°C and p = 8kPa in a vacuum dryer [132].

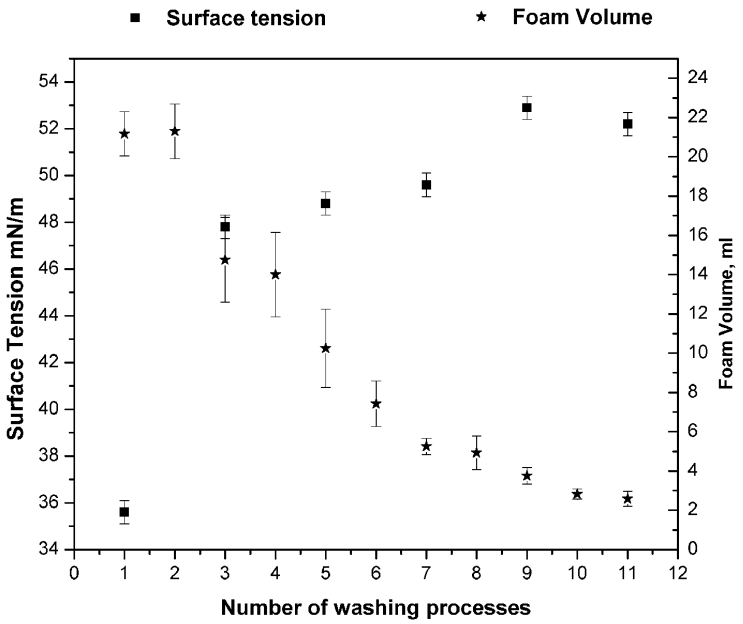

Figure 3.12: Variation of washing liquid properties. Left axis shows the change of surface tension of the washing liquid and the right axis shows the foam volume. Squares are for the surface tension and stars are for the foam volume. [132].

Figure 3.13: Main stages of FOCUS suspension preparation: dosage of SDS, dosage of powder, stirring, and the ready-to use suspension (thick creamy layer can be seen forming on the top) [133].

3.3.2 FOCUS Suspension

The liquid used in the increased and decreased gravity experiments and in the terrestrial reference measurements was a suspension of 2wt% hydrophobic fumed SiO_2 nano-particles in aqueous solution of 0.05% SDS. The selection of SiO_2 nanoparticles was based on the result of simple foaming probes by hand-shaking of different nano-powders and distilled water mixture using air-tight test tubes [99]. HDK H15 procured from Wacker Chemie GmbH was selected due to its promising foaming properties. According to the manufacturer, mean primary particle size distribution is 18nm and the agglomerate particle size is above 50μm. Surface area is $120\pm20 m^2/g$ [139]. SDS (Sodium Dodecyl Sulphate, Rectapur®, $C_{12}H_{25}NaO_4S$) is an anionic surfactant, product of Fluka Chemie GmbH and VWR Prolabo product [130, 134].

Note that FOCUS project was also an attempt to investigate the functionality of FOCUS FG-s in decreased gravity for the purpose of later utilisation of the FG-s in aluminium foam production. Aluminium foam precursor materials were excluded during the FOCUS experiment preparation process because of safety and budget issues. Therefore, the driving force behind the selection of the above material was to find a foamable liquid where particle stabilisation is significant and foams can be easily and safely produced using FOCUS FG at room temperatures. From this viewpoint 'FOCUS Suspension' can also be considered as a room temperature analogous, or experimental simulation of aluminium foam precursor materials [71].

The suspension was prepared using magnetic stirrer by adding the surfactant first and then slowly portioning the silica nano-powder into the solution. Stirring speed was slowly increased up to $1200 min^{-1}$. The ready-to-use suspension was creamy white after 1.5 hours of stirring. Strong sedimentation and creaming occurred after switching off the stirrer. Particle agglomerations were investigated using TEM and

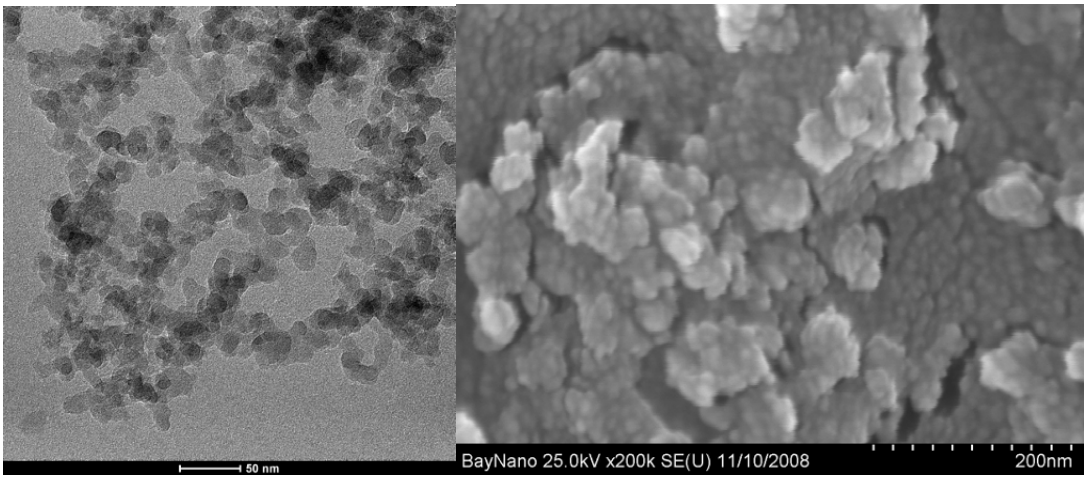

Figure 3.14: TEM (left) and HR-SEM (right) images of fumed silica nanoparticles used in FOCUS Suspension. Photos were taken at BAY-NANO Institute, Miskolc.

HR-SEM. The fresh suspension contained cca. 100nm particle agglomerates with cluster-like structure build up of single particles, which were cca. 20nm in size (See Figure 3.14). A certain amount of them was attached to bubbles that had been mixed into the suspension during preparation. These particle covered bubbles made up a cream (wet foam) on the top of the suspension. This top part was not used in the experiments.

The suspension was filled into the FGs by suction (in the case of increased gravity experiments) or by immersion and pressing (decreased gravity measurements) — see Section 3.4.

Investigations during the preparation of macrogravity experiments revealed that foams blown from FOCUS suspension using N_2 as foaming gas lasted much longer — 60-70 minutes — than the same solution without particles. This indicated the significant role of particles in foam stabilising. On the other hand, the suspension without any SDS can give only transient foam, disappearing within a few seconds [130].

A large number of pre-experiments were carried out in order to meet ISS safety and integration regulations prior to the microgravity experiment. These investigations pointed out that the FGs infiltrated with the suspension have limited shelf-life. During the shelf-life tests a 50% decrease in producable foam volumes occurred after two weeks of storage. Pre-experiments revealed the following reasons for foamability loss:

- Gravity-driven drainage of the suspension inside the porous structure of the FG.

- Strong sedimentation and creaming tendencies together with particle agglomerations inside the suspension. These phenomena were observed during storing the suspension in test tubes. Particles can lose their foam stabilising capability

Table 3.3: Basic properties of K2790 type PUR foam material [141].

Property	Related standard	Value
Net density	MSZ:10193/12-88	25-28kg/m^3
Compression resistance	DIN:53577	7.7-10.7kPa
Tensile strength	MSZ:10193/11-88	min. 150kPa
Ultimate elongation	MSZ:10193/9-79	min. 15%
Permeability	MSZ:10193/5-78	237±40l/h

due to agglomeration, strong sedimentation and adsorption to the inner surface of the FG.

- Surfactant adsorption onto the inner surface of the FG and onto the surface of the nanoparticles.

Due to the limited shelf-life, age of the pre-infiltrated samples became a crucial parameter. Macrogravity probes were carried out using freshly infiltrated suspension, but the decreased gravity experiment was carried out 11 days after suspension preparation and filling because of the shipping and integration time. Therefore also 11 day old samples were used for the reference measurements. Particle size distribution change with time during storage was determined using dynamic light scattering method. 11 days old samples had 100nm average particle size with high polidispersity. [130, 133, 134, 140].

3.3.3 Foam generator material

Blue and grey K2790 type partly open cell polyurethane foam, product of Eurofoam Hungary Ltd. (Sajóbábony) was selected as the material for FG both for increased and decreased gravity measurements. The colour difference did not mean any significant physical or structural difference [133, 141]. The material was selected from several other polyurethane and other porous polymer structures, based on their foam generation properties. The largest and most homogeneous foams using the macro-g test pad (see section 3.2.5) with fixed N_2 flow rate, foaming time and suspension amount were reached using K2790 type material. The microstructure and permeability of the materials were also investigated [142, 143].

Some basic properties of K2790 type PUR foam are collected in Table 3.3.

Permeability of the material was characterised with a simple method using the macro-g test pad. 30kPa overpressure using N_2 was applied on one side of the FCH while the other side was sealed. The gas moves through the FG to equalize pressure inside the FC and the pressure build-up curve, typical for each FG material type was recorded. The plot for K2790 FG material is shown in Figure 3.15.

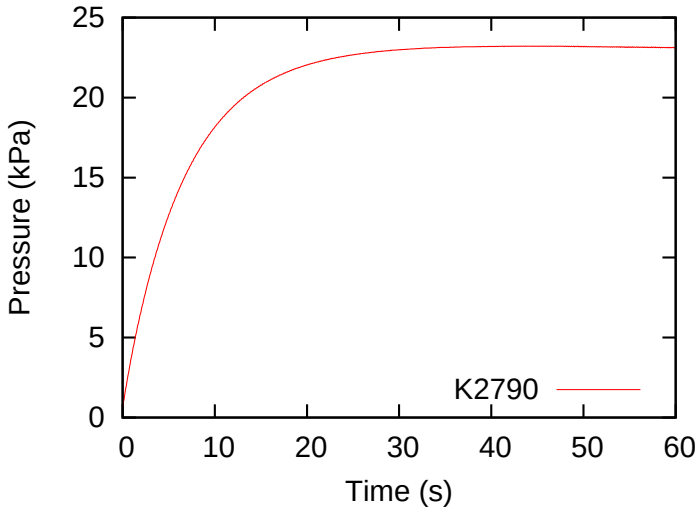

Figure 3.15: Pressure build-up curve for k2790 type FG material applying 30kPa overpressure [143].

Average cell size was investigated using optical microscopy images. K2790 is highly polydisperse and the cells are only partly open, meaning that most of the cell walls are broken or hollow, but there is also a significant amount of intact ones. Examples of optical and SEM images can be viewed in Figure 3.16.

Cumulative cell size distribution of the selected FG material was calculated based on a large amount of macrophotos using image analysis. Result is presented in Figure 3.17. All cells are smaller than 1mm^2 and more than 60% of the cells are smaller than 0.5mm^2. The open porosity of the FGs was above 95% [133].

Cylindrical FGs were used in all cases. For experiment integration reasons, FG dimensions had to be changed for the decreased gravity experiments. See Table 3.1 on page 39.

An 'initiation process' was carried out on each FG prior to any experiment in order to achieve equal material structure and to get rid of contaminations. The FG-s were washed in deionised water and then squeezed several times and dried at room temperature (RT) for three days [133].

3.3.4 Foaming gas

For the PVC-water-ethanol solution foaming we used dry N_2 of industrial quality. Air and dry nitrogen were used during the increased gravity measurements and the reference measurements, respectively.

During the decreased gravity measurements and its reference experiments we used HFC-245fa (Honeywell product) as a foaming gas. We selected this kind of gas in order to avoid high pressures inside the FOCUS hardware because of ISS safety prescriptions. HFC-245fa (Genetron 245fa in other name) gives 125kPa absolute pressure at 20°C, which is enough for a modest foam generation speed.

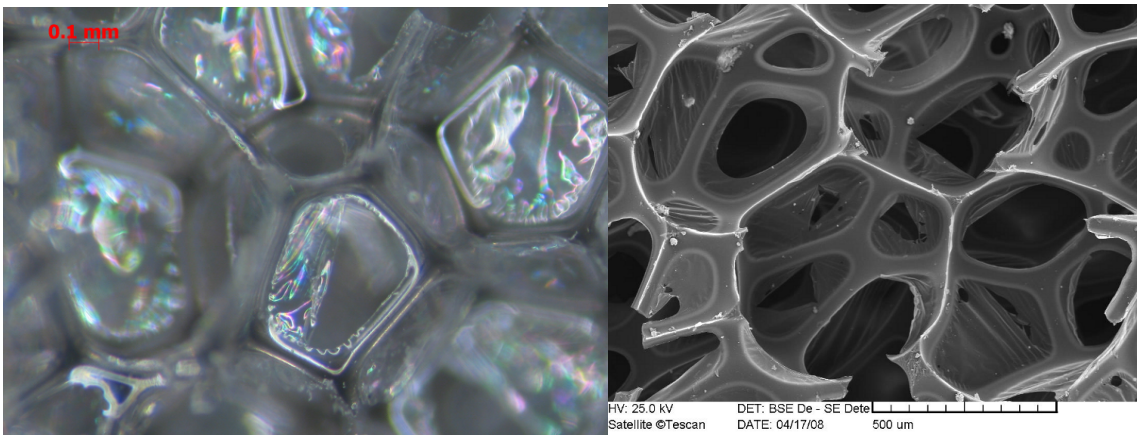

Figure 3.16: Optical (left) and SEM (right) images of K2790 type foam generator material. Photos were taken by P. Bárczy and Á. Kovács.

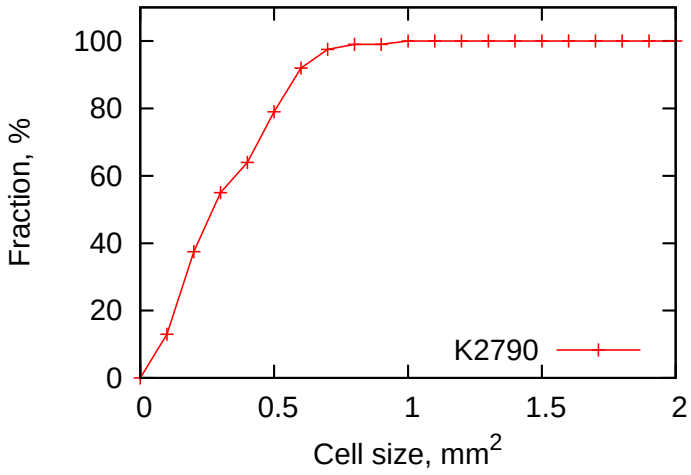

Figure 3.17: Cumulative cell size distribution of K2790 type foam generator material.

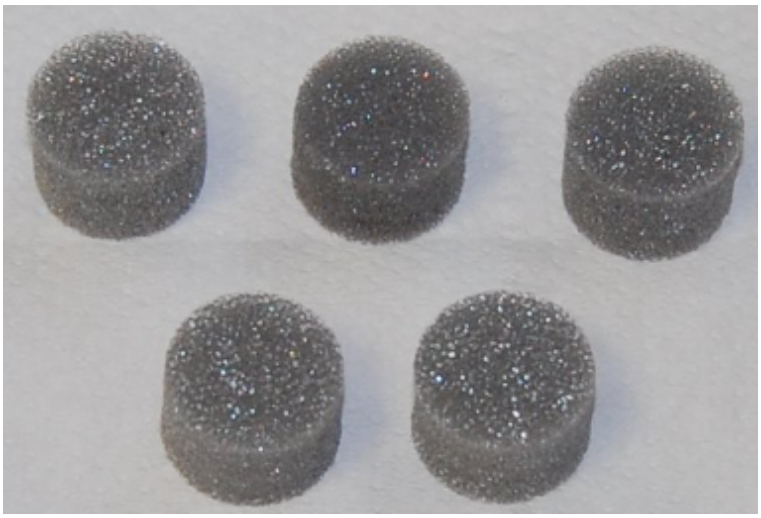

Figure 3.18: K2790 type foam generators for FOCUS experiment [133].

Table 3.4: Selected physical properties of HFC-245fa [134, 145, 146]

Chemical name:	1,1,1,3,3 pentafluoropropane
Molecular formula:	$CF_3CH_2CHF_2$
Molecular weight:	134.0g/mol
Liquid density:	1339kg/m^3
Boiling point:	14.9°C
Vapour pressure @ 25°C:	149kPa
Water solubility	7180mg/l

The only disadvantage of this gas is the high water solubility that can speed up foam coarsening [115, 144]. Some selected physical properties of HFC-245fa can be read in Table 3.4. The same gas was used during the reference experiments as well [134, 145, 146]. During the shelf-life tests of FOCUS Suspension we used N_2 (see page 47) [133, 140].

3.4 Methods

3.4.1 PVC-water-ethanol foaming experiments

UMFA-LT foaming cartridge (see Section 3.2.1) was used in the foaming experiments of PVC-water-ethanol solution. The foams were produced using a 0, 33, 55, 78, 90 and 96 vol% ethanol with distilled water and a constant PVC particle concentration of 10 wt%. Optical images of the foam formation and foam decay were recorded by

a commercial webcamera with 640x480 pixel resolution [132].

The sparger was characterised by measuring the bubble size distribution in distilled water in the function of the bubbling pressure. Bubble sizes were determined by image analysis using ultra-high shutter speed (1/15,000) images in order to achieve a clear view on the emerging bubbles [132].

During the foaming measurements of the PVC – ethanol – water mixture, two valves were responsible for the gas control. N_2 gas was used in the experiments. The flow rate of the gas was recorded with a flow meter inserted between the gas container and the foaming cartridge. The pressure gauge was placed before the sparger for measuring the bubbling pressure. Pressure, flow rate data and the control of the valves were carried out using ADVANTECH GeniDAQ control software. An optical image series was recorded during each foaming experiment to determine the foam heights. Using only optical observation it was impossible to get a closer look at the foam structure, because the foam was not transparent. During one foaming test the structure of the foam was recorded using a microfocus X-ray source (Hamamatsu) with combined panel detector [132, 147].

During the experiments, 10s foaming time at 0.3bar bubbling pressure was used. In order to avoid agglomeration of the particles, ultrasonic mixing was integrated before and during each experiment. A total of 9min of ultrasonic mixing was carried out before foaming each solution. 15ml of liquid was used in every experiment, which is $1/4^{\text{th}}$ of the entire volume of the cartridge. Flow rate and pressure data were recorded with a frequency of 6Hz.

The foamability of the solutions were characterised by measuring initial foam heights at different gas flow rate levels. By definition, the initial foam height means the attained height immediately after bubbling has ceased [132].

The optical image of the foam is shown in Figure 3.19a. The cellular structure is not detectable due to the light scattering of the PVC particles. The X-ray image of the foam gave observable cell structure which can be used in the future to follow the drainage and cell ruptures quantitatively if the image quality is improved (Figure 3.19b) [132].

The critical point in foam volume/foam height measurements is the flow rate of the bubbling gas. These data were also recorded, and the pressure sensor was set to provide the optimal flow rate values. But, at any given pressure level the flow rate has significant variation. This effect may be caused by the obstruction of the porous ceramic. Each solution was processed 10 times in order to achieve acceptable average values of foam heights [132].

Foam heights (h_{foam}) were simply measured from the images taken and the foam volumes (V_{foam}) were determined using basic geometrical calculations:

$$V_{foam} = A_{FC} \cdot h_{foam}, \tag{3.1}$$

where A_{FC} is the base area of the UMFA-LT foaming cartridge.

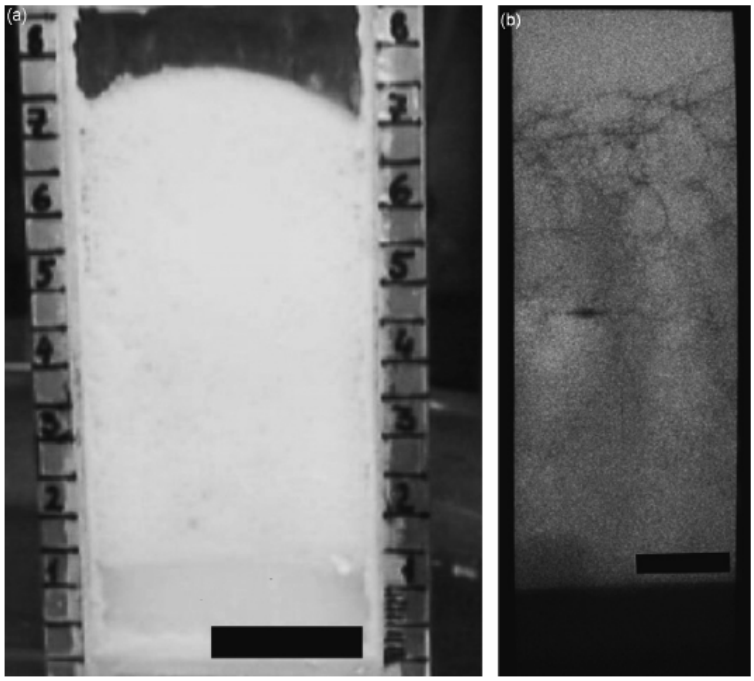

Figure 3.19: PVC particle stabilized foams: (a) visible light and (b) X-ray images. Scale bar is 2 cm. [132].

3.4.2 Increased gravity experiments

Increased gravity experiments were done using the macro-g test pad described in Section 3.2.2. This test pad was integrated into the ZARM Hyper-G Centrifuge in Bremen.

One experiment consisted of the following steps:

1. Infiltration of two FGs with 4.2 ± 0.2g of FOCUS suspension. This amount is cca. 65% of the FG pore volume. The overall volume of the FGs was 6.8cm^3.

2. Integration of the FCs into the macro-g test pad.

3. Setting of the gravity level on the hyper-g centrifuge.

4. Blowing gas (air) through the FGs sequentially for 10 seconds at a given flow rate (0.125l/min) at room temperature.

5. Foams were exposed to increased g-level for three minutes after generation.

6. Centrifuge was stopped and the samples were taken out.

7. Macrophotos were taken of each samples.

Figure 3.20: Left: NASA astronaut Jeffrey N. Williams during experiments execution. Right: FOCUS HW on board of the ISS Columbus Module. Credit: ESA Columbus Control Centre.

20 experiments were carried out under increased gravity, at 1.5, 2, 4, 6, 10 and at 15g in three different foaming directions. 25 reference experiments were made at 1g. Each experiment was carried out twice, by using two foaming cartridges. Foaming pressure (Pa), flow rate (l/min) and g-level were recorded. Pressure sensors were put directly in front of the FGs and the flow meter was placed in front of the pressure sensors. The primary pressure was set to 5bar and using the built-in reductor this was decreased to 1.5bar. Flow rate value and foaming time were pre-set to 0.125l/min and 10s, respectively. Foams were generated after reaching the desired g-level and they were exposed to increased gravity for 3 minutes after generation. The time to reach the given g-level varied from 20 to 80 seconds, depending on the magnitude of gravity. Accelerometer accuracy was 0.1g. Two sensors were put onto the macro-g test pad: one near the FG and another at the bottom of the test pad. The distance between the sensors was 500mm. The gravitational acceleration gradient along the FCs increased with higher gravity levels but reached only 0.002g/mm in the case of 15g acceleration. The measurement results of the sensors can be seen in Figure 4.6.

Average foam volumes and their standard deviations were determined from two samples evaluating the recorded videos at the initial state and 3 minutes later. Macro photos using a Panasonic Lumix DMC-LZ2 type digital camera were taken after each experiment (5 minutes after foaming) of the foams to determine the cell sizes.

The results evaluation and calculation of foam volumes and average cell sizes were the same as in the FOCUS experiment — see the the next subsection. The only difference is that the average cell sizes here were determined in pores per inch (PPI), measured along one horizontal line at a distance of 10mm from the FG.

3.4.3 Decreased gravity experiments (FOCUS)

FOCUS experiment was carried out on board of the ISS inside the European Columbus Module, by astronaut Jeffrey N. Williams on 7th February 2010. FOCUS EC

Table 3.5: FC settings [134]

FC ID	Flow rate (l/min)	Foaming time (s)
FC1	0.08	42
FC2	0.125	40
FC3	0.23	37

(see page 40) and a multi-use camera arm together with the onboard camera (Nikon D2xS) was fixed onto the seat track. Gas knobs were switched on sequentially right after turning the illumination and the imaging on. Foams were created with three different flow rates and correspondng foaming times (see Table 3.5) in the cartridges. Images (275 pcs in micro-g and more than 100 in each reference experiment) were taken in raw format on the foam growth and decay with cca. 16-18px/mm resolution in all cases. Imaging rate was 1fps during foaming ('dynamic' session), and minimum 2fpm during decay ('static' session). The whole activity of the ISS experiment was recorded using the onboard video camera [134].

Columbus cabin temperature, pressure and gravity level was 23°C, 0.97bar, and $<$0.016g, respectively. All the above conditions, timing and gas valve settings were kept during all terrestrial reference experiments, except gravity. FG-s were always filled with the same amount of suspension (3.8g). This means cca. 90% of the FG pore volume. The overall volume of the FGs was 4.3cm^3. For the basic properties of FG material and FG geometry see Section 3.3.3 on page 48 and Table 3.1 on page 39.

FOCUS Experiment was executed 11 days after payload handover. In order to have comparable data, all samples for the reference experiments were 11 days old, as it was in the 0g experiment.

Reference experiments were carried out in three different foaming directions (0°- downward, 90°- horizontal, 180°- upward) measured to the gravity vector (see Figure 3.2).

Regarding the experiment evaluation, automated image analysis scripts could not be used correctly due to the low contrast and the transparency of the samples. Foam volumes and the average bubble sizes were determined manually.

Foam volumes were calculated by multiplying the measured foam height (H) with the base area of the FG ($R^2\pi$). There were some cases when the foam volume needed to be calculated by approximation with a truncated cylinder. Figure 3.21 shows the notations for equations 3.2 - 3.4.

10% error in foam volume measurements was estimated based on repeated readings of the pixel values from the images. The same method was applied before during the increased gravity experiments [130, 134].

$$V = R^2\pi(H + \frac{h}{2}) \tag{3.2}$$

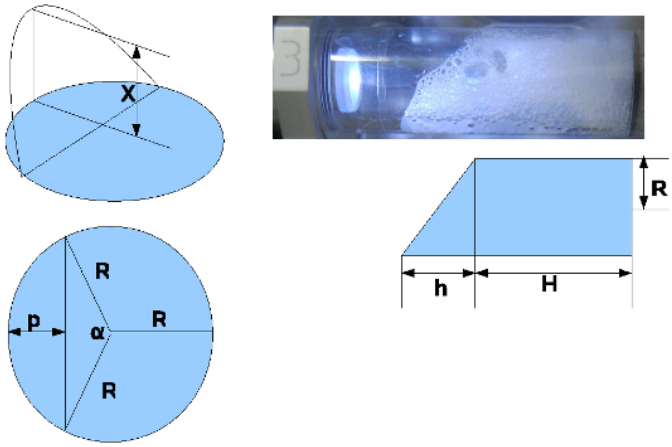

Figure 3.21: Calculation of foam volumes [134].

$$V = (\frac{R^2}{2}\alpha - \frac{((R-p)R\sin\alpha)}{2})\frac{x}{2}) \qquad (\alpha < \pi) \tag{3.3}$$

$$V = (R^2\pi - \frac{R^2}{2}\alpha + \frac{((R-p)R\sin\alpha)}{2})\frac{x}{2}) \qquad (\alpha > \pi) \tag{3.4}$$

Foam stability was characterised by the half-lives of the foams. Note that we have only one measurement in 0g so the errors of half life measurements are estimated from the foam volume determination errors. At 1g, standard deviations for 7 measurements are given.

Number of bubbles was counted along the half-perimeter of the FC at every 5 millimetres, measured from the FG surface. Only those bubbles that contacted the inner perimeter of the FC could be calculated precisely. These bubbles have different boundary conditions than the ones in the bulk foam, but only these ones were considered in all cases. Average bubble size (d) at a given distance from the FG was determined by dividing the half inner perimeter ($R\pi$) by the number of bubbles (n). Those cases where the foam did not fill the whole half perimeter of the cartridge, only the appropriate arc length (i) was considered [134]. The calculation of the arc length can be easily followed from Figure 3.22. y_1 and y_2 are the two endpoints of the arc.

$$d = \frac{R\pi}{n} \tag{3.5}$$

$$i = R(\arccos\frac{R-y_2}{R} - \arccos\frac{R-y_1}{R}) \tag{3.6}$$

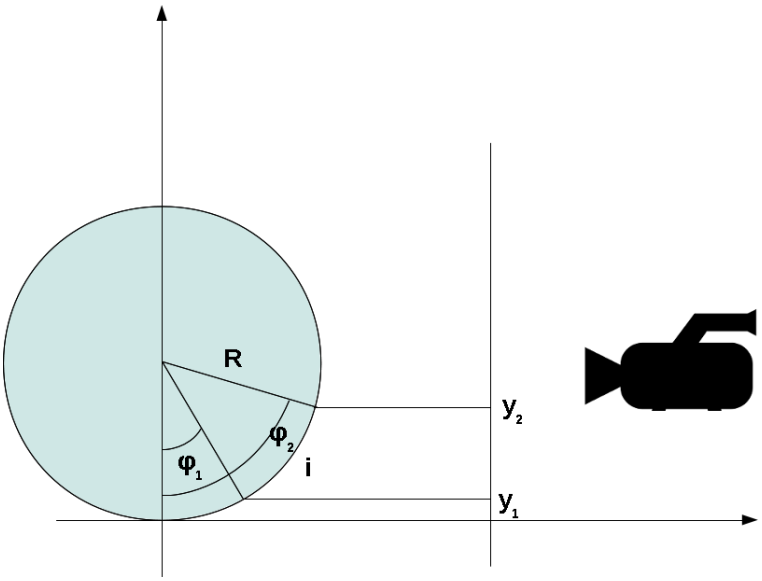

Figure 3.22: Calculation of arc length.

Chapter 4

Results and discussion

4.1 Foams made of PVC-water-ethanol solution

4.1.1 Surface tension measurements

Surface tension measurements were carried out using pendant-drop method on water–ethanol solutions with and without PVC particles. Mean errors were less than $\sigma = 0.1$mN/m. The PVC containing solutions had 10 wt% of PVC powder. Figure 4.1 shows the variation of surface tension versus the concentration of ethanol in the system. The surface tension decreases with the increasing concentration of ethanol. Particle containing liquids have a significantly lower surface tension. Possible reasons for this are either the remnant surface active contaminations (see page 44) in the liquid or the particles themselves have a surface tension decreasing effect [132].

4.1.2 Foaming properties

Before starting the foaming experiments with water-ethanol solutions containing PVC particles, we investigated the porous ceramic sparger in the UMFA-LT foaming cartridge. We measured the bubble size distribution in distilled water at different bubbling pressure levels. The higher was the bubbling pressure, the larger were the average bubble size and the standard deviation. Results are shown in Figure 4.2. For liquids with different surface tension we expect slightly different bubble size, but the tendency should be the same. In order to obtain homogeneous foam structure low bubbling pressure (0.2bar) was selected at the cost of longer foam producing time [132].

The foam height decrease after foam production was not visible because the white coloured liquid[1] sticked to the glass sidewalls of the cartridge. The coarsening observed on the X-ray radioscopy images revealed that the foam decayed inside [132].

[1] The liquid became white due to the PVC particles.

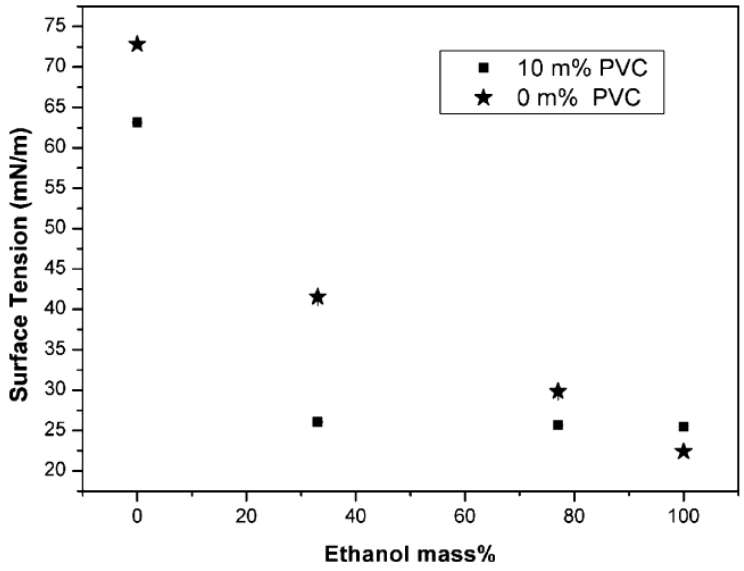

Figure 4.1: Surface tension of the liquids with and without PVC particles in the function of ethanol mass percentage. Stars stand for the data without PVC; black squares are for the liquids containing PVC [132].

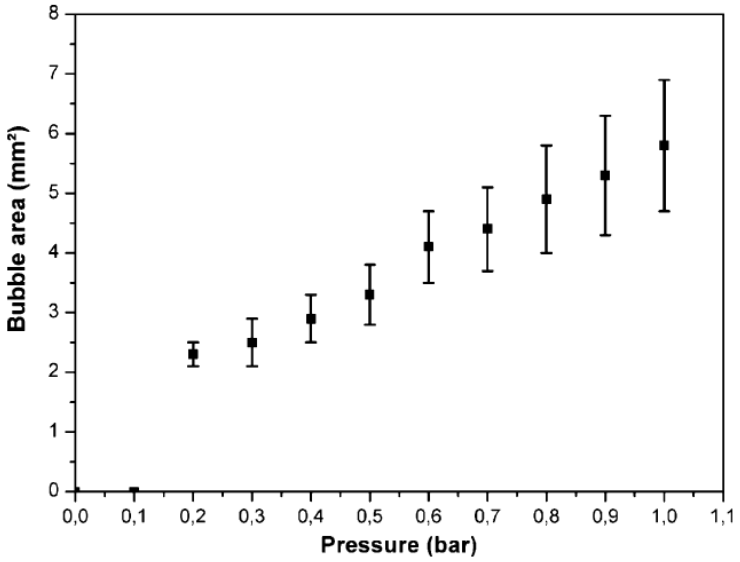

Figure 4.2: Variation of bubble size in the function of the bubbling pressure in UMFA LT FC. Bubbles started to form at 0.2bar [132].

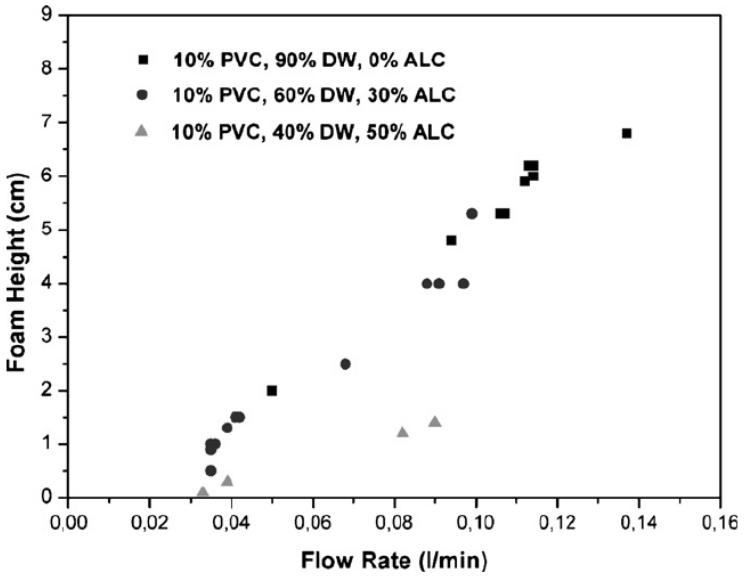

Figure 4.3: Variation of the initial foam height in the function of the flow rate using different concentrations of PVC, distilled water (DW) and ethyl-alcohol (ALC). At higher flow rates the foam height was bigger and there were also differences when changing the ethanol concentration in the system [132].

The initial foam heights were observed as a function of the flow rate. Results are shown in Figure 4.3. It is clear that the flow rate has a direct effect on the foam height. After a threshold foaming pressure, which is 0.2bar in the case of our experimental set-up, bubbles could form and build up foams. The relationship between the flow rate and the initial foam height follows a linear rule in the 0.03 – 0.15l/min region.

The higher the ethanol concentration is, the lower are the initial foam volumes. This means that at higher ethanol concentrations the PVC particles cannot build in well into the surface of the foam films and they cannot stabilise the foam effectively. This is due to the lower contact angle of the particles at higher ethanol concentrations. From 70 to 96% of ethanol concentration foam production was impossible. We also tried to make foams under the same conditions without PVC particles using only water and ethanol to no effect [132].

A fixed flow rate value, 0.09l/min was chosen from the experimental data to see the change of the initial foam height in the function of ethanol concentration. The contact angle, which is a key parameter in solid particles stabilised foams, can be varied by changing the ethanol concentration. The plot of the initial foam heights and the change of the contact angle between PVC particles and the liquid are given in Figure 4.4 [132].

The contact angles of the PVC with different ethanol–water mixtures and the surface tension of the solutions were taken from the literature [148]. Pure ethanol gives 0° contact angle with PVC which increases to 83° if pure water is used. Results show that the contact angle has a significant effect on the initial foam heights. At

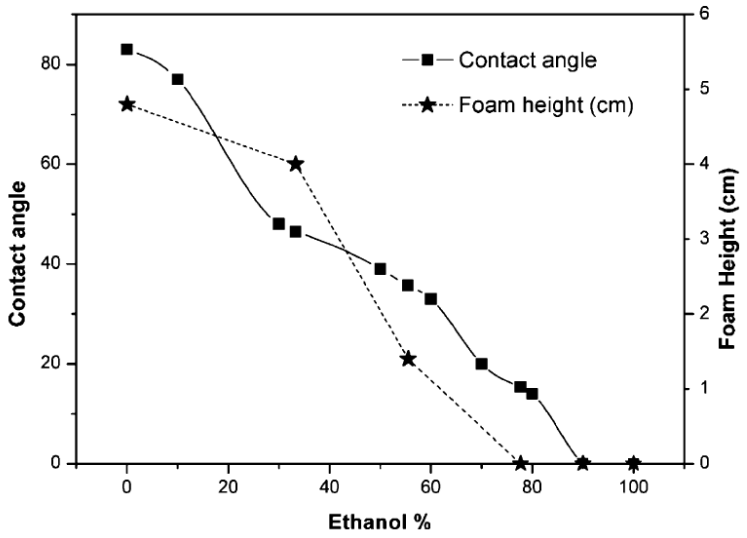

Figure 4.4: Decrease of foam height with the increase of ethanol concentration in the system, at a flow rate of 0.09l/min. Through varying the ethanol concentration we could vary the contact angle between PVC and the liquid as we can also see from the plot. Contact angle data were taken from [148]. Four points were interpolated from the literature data. [132].

high ethanol concentrations (>70%) there was no foam generation which corresponds to 20° contact angle. The best foamable system did not contain any ethanol. This stands for a contact angle of 83° between PVC particles and water.

Sun and Gao reported the lack of foam formation of PVC – water – ethanol suspension above 20vol% ethanol concentration (contact angle 63°) in their prior work [149]. The increasing foam stability tendency by increasing water concentration was found to be the same in their and our work. However, in our system using 55.5vol% ethanol (contact angle 36°) foam was able to form. This extra stability range at lower contact angle can be originated from the significantly smaller particle size used in this work (1µm) compared to the prior work (75µm). This finding might be overlapped by the effect of the residual surfactant in our system. Unfortunately we do not have information about the residues in [149]. Our improved foaming technique can also increase the stability range of the PVC suspension. In the prior work using the shaking technique the average bubble size has been reported for 0.2mm. Our bubbling technique using sparger produced 2–3mm diameter bubbles. Larger bubble size should decrease the stability via the larger cell walls. In spite of this our foaming technique improved foam stability by the well-defined controllable bubble sizes. The difference in particle concentration (10wt% in this study and 3.3wt% in the previous work) can also affect the stability but does not influence the minimum contact angle particles with which foam can be produced [132].

The foam heights reached in the function of contact angle can be compared to the so called 'product of probabilites' to stabilise liquid foams (see page 26, detailed in [7]).

Table 4.1: Q or Q^c values gained in the function of different selected parameter sets, together with standard deviation and structure data [7]. The typical structures are shown in Figure 2.22 and detailed in the text.

z	f	α	Q	Q^c	Standard dev.	Valid structure	Contact angle range
0	0.907	NA	3.03	NA	1.02	CP1, LP1	$\Theta < 90°$
0	0.8	NA	9.68	NA	1.58	CP1, LP1	$\Theta < 90°$
0	0.7	NA	17.96	NA	2.20	CP1, LP1	$\Theta < 90°$
0	0.5	NA	47.03	NA	2.81	CP1, LP1	$\Theta < 90°$
0	0.3	NA	156.56	NA	2.98	CP1, LP1	$\Theta < 90°$
0.633	0.907	NA	0.14	NA	0.68	CP2	$\Theta < 129°$
1	0.907	NA	0.07	NA	0.80	CP2+	$\Theta < 129°$
0.633	0.6	1	NA	4.94	0.34	LP2C, LP2+C	$\Theta < 129°$
0.633	0.6	2	NA	2.21	0.25	LP2C, LP2+C	$\Theta < 129°$
0.633	0.6	3	NA	1.42	0.28	LP2C, LP2+C	$\Theta < 129°$

We obviously cannot predict the foam volumes from equations 2.6 - 2.7 that can be generated from a given liquid using a fixed foaming technique, but it is interesting to put together our contact angle vs. foam height data and the above mentioned 'product of probabilities'.

To make the comparisons, a semi-empirical multiplier (Q and Q^c) was introduced for p_Σ and p_Σ^c, respectively:

$$\hat{p}_\Sigma = Q\, p_\Sigma \tag{4.1}$$

$$\hat{p}_\Sigma^c = Q^c\, p_\Sigma \tag{4.2}$$

The value of Q and Q^c was determined for different z, α and f values by fitting $\hat{p}_\Sigma$ or $\hat{p}_\Sigma^c$ (which applicable) on the three non-zero foam height data using Levenberg-Marquardt algorythm. The Q or Q^c parameter was calculated for those parameter sets that were presented in [7]. Table 4.1 summarizes the results for Q or Q^c values. The table also nominates the appropriate theoretical particle arrangements (structures on the cell wall, Figure 2.22 on page 26) for each parameter set, and the standard deviation of the probability curve from the foam height data.

From the table we can see that the lowest standard deviation (0.25) is gained at $z = 0.633$, $f = 0.6$ and $\alpha = 2$, with $Q^c = 2.21$. Therefore we can conclude that our PVC-water-ethanol foam was stabilised with LP2C or LP2+C type particle arrangement. Figure 4.5 also clearly shows that the $\hat{p}_\Sigma^C$ curve is in good correlation with our foam height vs. contact angle data.

As a conclusion, we were able to show experimentally that the contact angle has to be in a certain range (36-83°) in order to see the stabilisation effect of the above

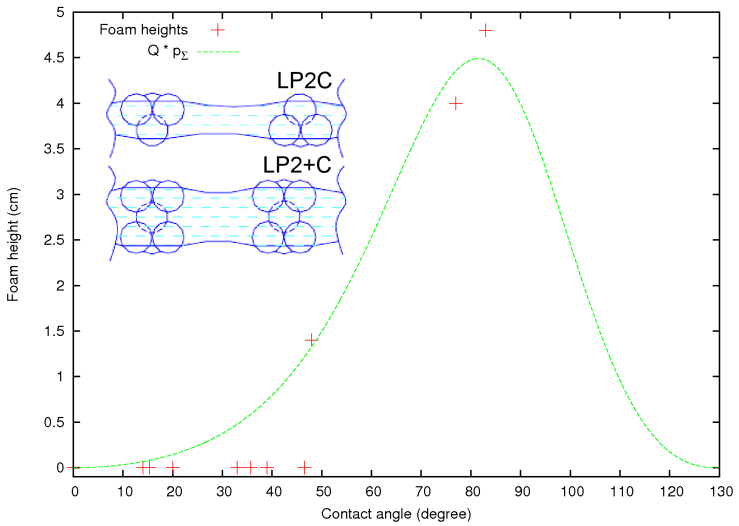

Figure 4.5: $\hat{p}^c_\Sigma$, shown together with the measured PVC-water-ethanol foam heights. $z = 0.633, f = 0.6, \alpha = 2, Q^c = 2.21$ The two most probable particle arrangements are also inserted.

described system (subsection 3.3.1), using direct gas injection method for foaming. The maximum foam volume was reached in the case of ethanol-free system which corresponds to 83° contact angle for PVC particles. Foams were created using 0.3bar bubbling pressure for 10 seconds. See page 84 for the related thesis.

4.2 Increased gravity measurements

The results of the increased gravity experiments can be grouped into three main parts:

- Foam volume measurements and foaming properties
- Analysis of cellular structure
- Analysis of pressure and flow rate data during foam generation

The experiments were carried out using the 'progenitor' of FOCUS FC (FC01, Table 3.1 pp. 39) and FOCUS Suspension (section 3.3.2 pp. 46). Gravity levels were set to 1.5, 2, 4, 6, 10 and 15g, respectively. The results of the g-level measurements can be seen in Figure 4.6.

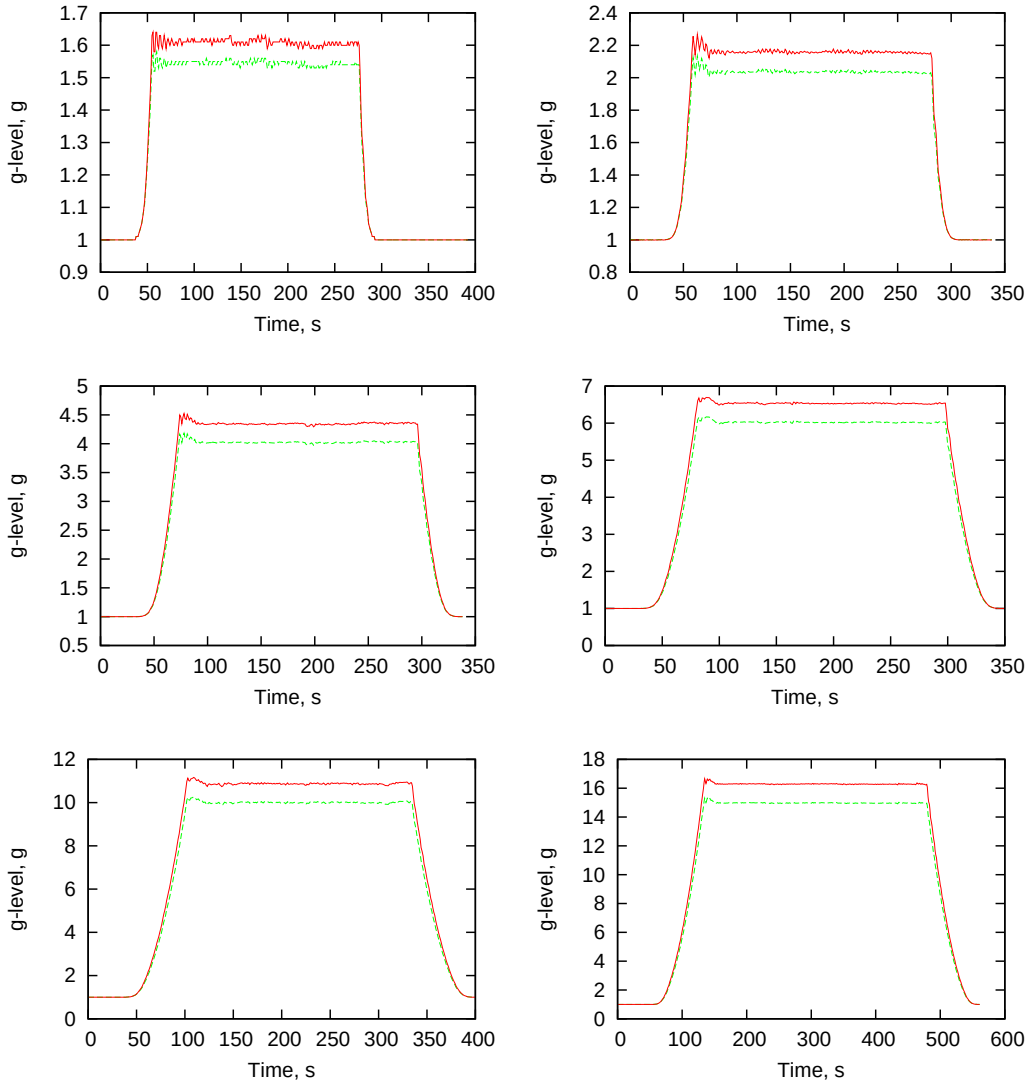

Figure 4.6: Set of g-levels at 1.5, 2, 4, 6, 10, 15g. Green line is for Sensor 1 and the red line is for Sensor 2. Sensor 1 was placed at the level of the FGs [131].

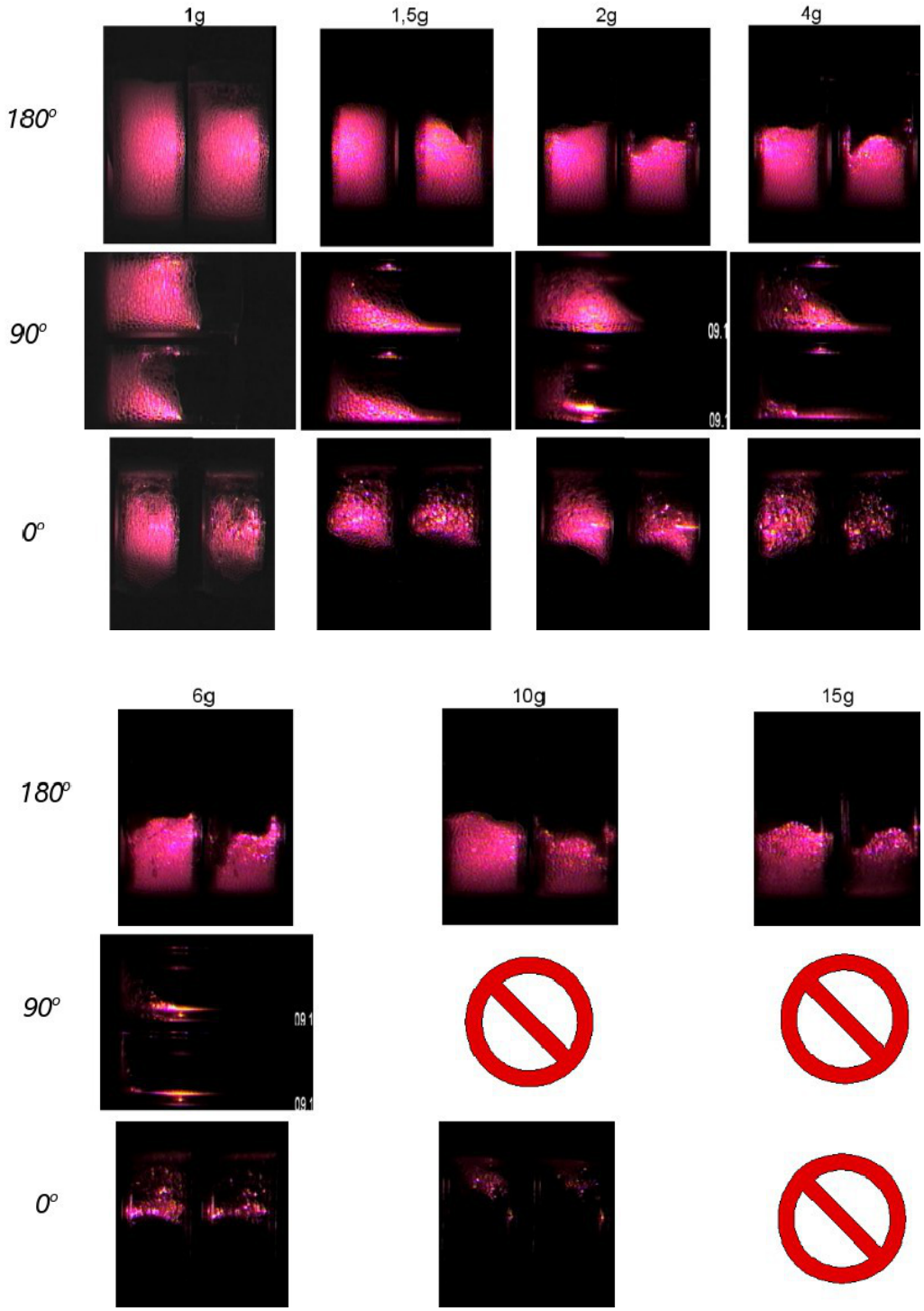

Figure 4.7: Photos of initial (left) and 3 minutes old (right) foam volumes at different g-levels and foaming directions. Foam generation was impossible at 10g/90°and at 15g/90°and 0° [131].

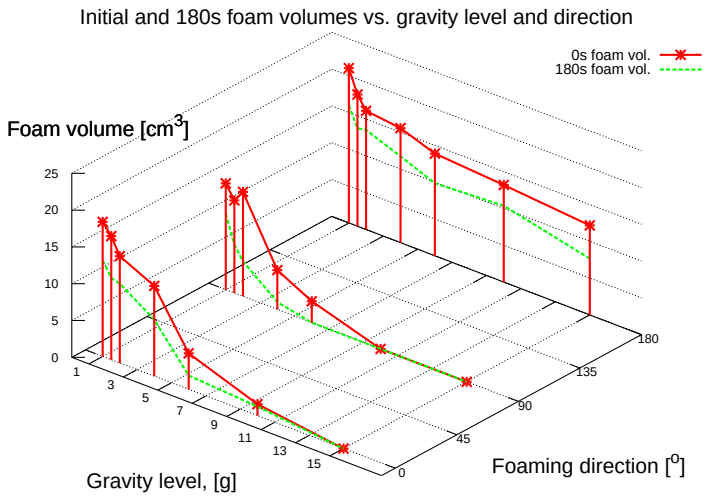

Figure 4.8: 3D plot of initial and 3 minutes old foam volumes at different g-levels and foaming directions [131].

4.2.1 Foam volume measurements

The effect of increased gravity (1.5 - 15g) and foaming direction upon foam generation can be primarily described by the foam volumes. By increasing the gravity level initial foam volumes decreased in all foaming directions. A collection of the initial and 3 minutes old foams can be seen in Figure 4.7. Figure 4.8 shows a 3D plot of the calculated initial and 3 minutes old foam volumes. Foam stability is characterised here by the ratio of the 3 minutes old and the initial foam volume data in percent. These percentage values together with the foam volumes can bee seen in Figure 4.9. The foam stability remained between 63 and 85% with increasing g-level (except one point at 6g/0°). The only significant decrease of foam stability was observed only at 90° direction where the generated foam was initially much coarser and decayed faster.

4.2.2 Cell structure measurements

Cellular structure of the foams blown in 180° and 0° was compared. The most homogeneous cell structure is reached at 180°. PPI data (Figure 4.10) does not change with the g-level, but it is conspicuously different in the two directions, as it is shown in Figure 4.11.

4.2.3 Pressure and flow rate data

The foaming pressure and the flow rate were pre-set in all experiments to 1.5bar and 0.125l/min. The variation of these values during the foaming were observed and recorded. These values varied with the alternation of g-level and foaming direction.

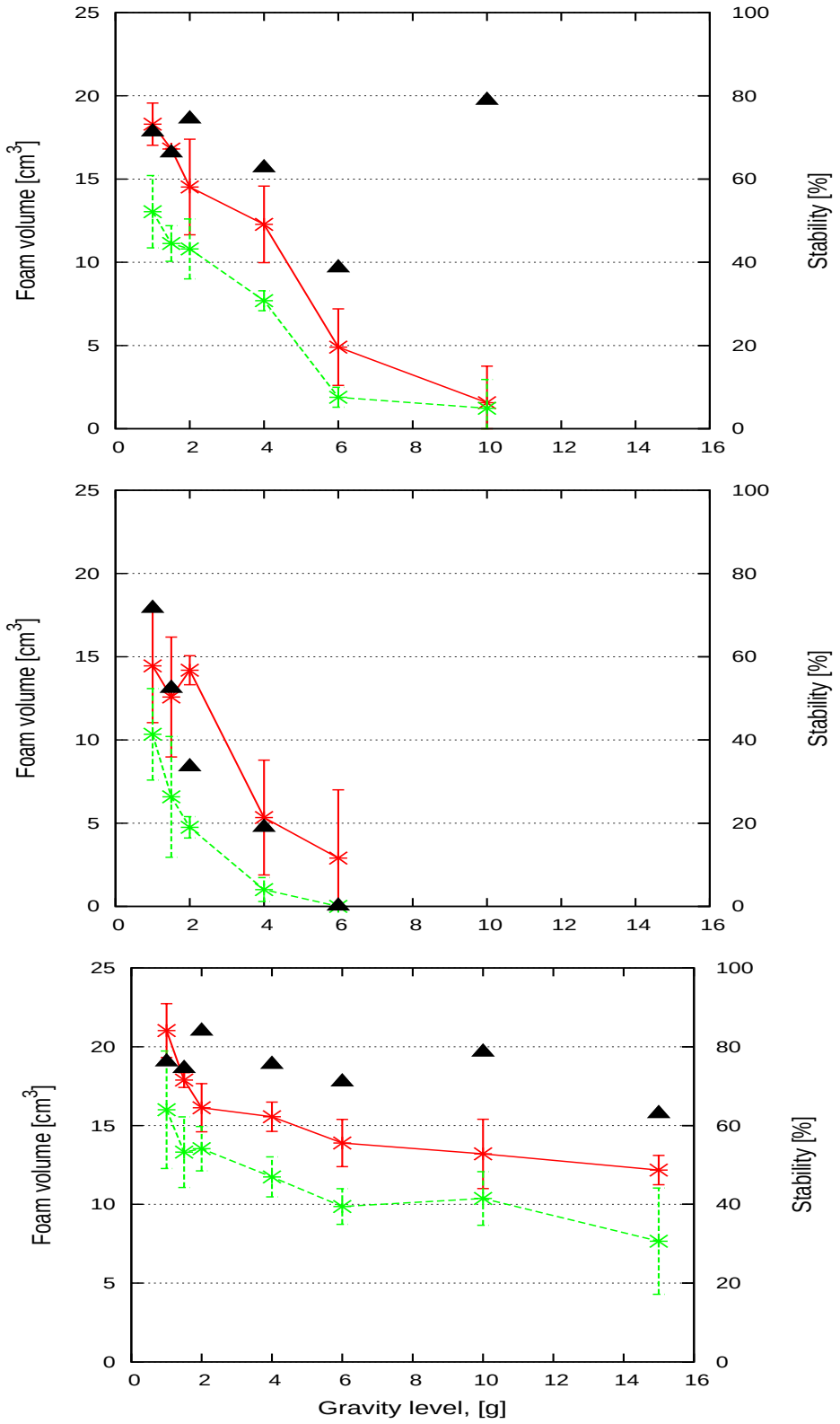

Figure 4.9: Initial (red) and 3 minutes old (green) foam volumes and calculated foam stabilities (black triangles) in the function of foaming direction and gravity level. Top: 0°, middle: 90°, bottom: 180° [130].

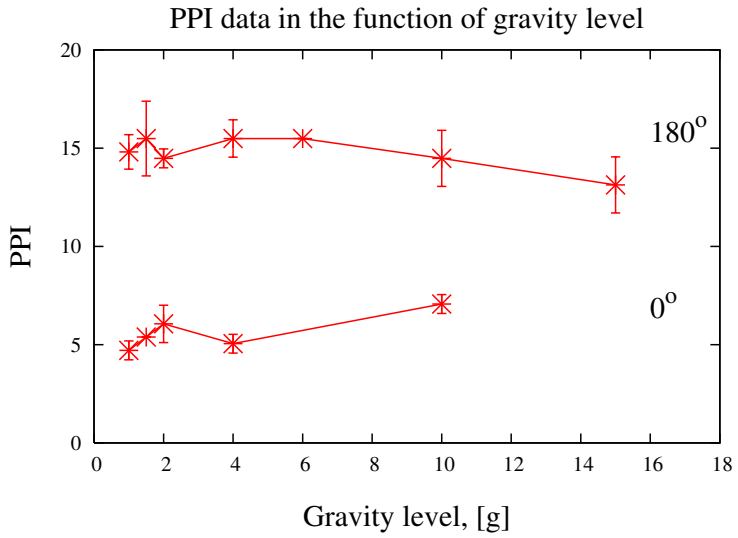

Figure 4.10: Bubble size as a function of the gravity level in 0° and 180° [130].

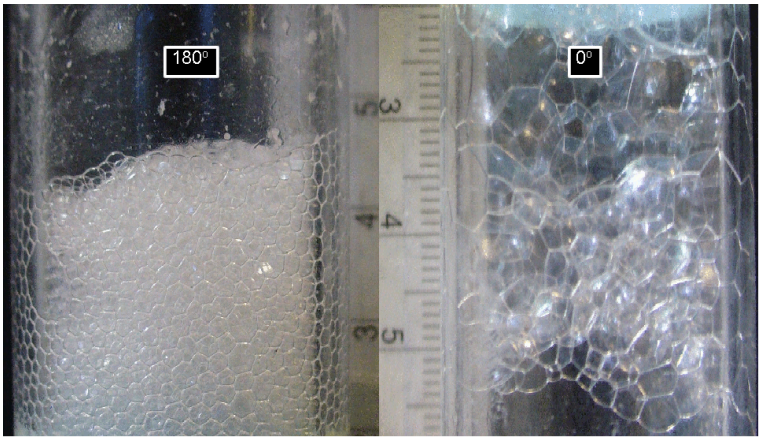

Figure 4.11: Two examples of typical cell structures observed in 180° and 0° foaming in increased gravity [130].

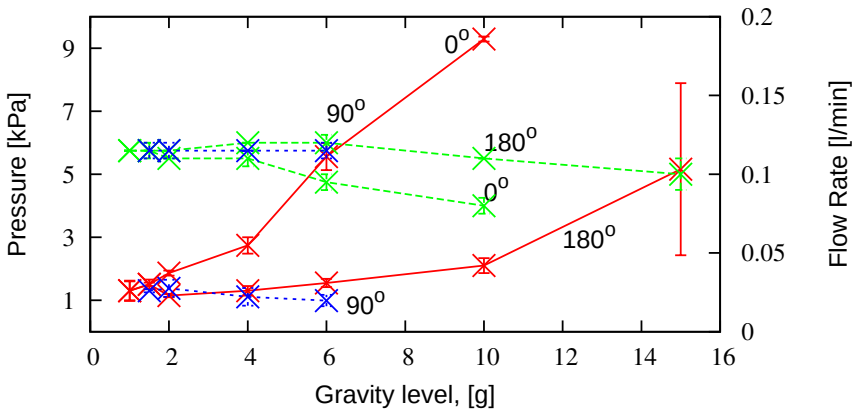

Figure 4.12: Average pressure and flow rate data at 0° and 180° from 1 to 15g [130].

The average pressure and flow rate values were determined taking into account the whole 10 seconds foaming durations. Average flow rates did not change significantly, remained around 0.11l/min. The average pressure shows a remarkable increase with g-level, mainly in the 0° direction (Figure 4.12). In the case of 90° foaming we did not observe significant average pressure increase [130, 131].

Pressure and flow rate curves during foaming bear plenty of information about the behaviour of the FGs. The collection of foaming curves — foam evolution with time — plotted together with these data can be seen in Figures 4.13 - 4.17. The foam volumes are signed with red lines, pressure data are green, and the flow rate is blue. The left y axis is for the pressure and flow rate curves, the right one is for the foam volume. Flow rate data are presented in 0.1l/min units for the purpose of making it visible.

Pressure curve characteristics were found to be similar in all gravity levels at a given foaming direction, but changing the foaming directions gives radical differences. It is clear that the flow rate decreased in line with pressure increase, signifying the obstruction of gas routes inside the FG.

By studying the foaming curves together with the pressure and flow rate data in the entire experimental series we can summarize the following typical cases:

- **Constant flow rate and pressure, linear growth of foam.** This means normal foam formation without or with constant gas loss in the system. The slope of foaming curves depends on the loss of gas. This was the case in all foaming experiments at 180°, 90° and at 0° at 1 and 1.5g. Initial foam volumes

decreased and the pressures increased with g-level.

- **Constant flow rate and pressure, poor foam growth that stops after a certain time.** This phenomenon was observed in the case of 90°/6g for example. The gas loss is significant because the gas can escape without any foam generation. Foam growth can also stop if steady state foaming occurs which means the equal timescale of foam formation and decay.

- **Fluctuating flow rate and pressure, linear/poor foam growth, or no foam at all.** Pressure increases were followed by sudden falls with foam evolution. Flow rate curves varied synchronously with pressure. This behaviour occured for example at 0° from 2g [130].

4.2.4 Discussion

The above enumerated measurement results give us an image on the functioning of our porous FG and the effect of gravity increase on foam formation. The processes during one foaming experiment can be divided into three phases:

1. Prior to foaming, the distribution and setting of the suspension inside the polymer structure is modified by moving in the gravity direction. Some pores deplete, some saturate. The suspension itself is exposed to gravity as well. The sedimentation of nanoparticle agglomerates intensifies inside the liquid composing a gradient distribution due to increased gravity. Many pores are clogged making the outflow of gas more difficult. This may also lead to improper foam generation through the reduced foamability of the suspension and obstructed routes of gas/liquid. Note that a strong sedimentation tendency of the particles was experienced as well during long-term storage of the suspension (see 3.3.2 on page 46.

2. During foaming, gas bubble movement is more difficult in the gravity direction, where clogged pores are dominant. This is why the foamability of the system will be different in 0° and 180° due to the gradient structure inside the FGs. At 0°, bubbles have to move in the gravity direction and to go trough clogged pores that lead to fluctuating pressure curves, increased average pressure and poor foaming. Continuous pressure increases are followed by sudden falls with bubble generation at 2-4g, but at 6 and 10g levels only pressure increases were observed. The penetrability of the pores is better from the bottom (180°), because the gas bubbles should move against gravity vector, from the denser part into the sparser regions. Depleted pores that enable the gas to escape without blowing bubbles can also lead to poor foaming, mainly in 90° case.

   Gravity-driven drainage can influence foamability and the cell structure as well. At 180°, draining liquid gets back onto the FG and into the lower part of the foam, causing a thicker liquid layer on the FG. This is not the case in the 90°

and 0° directions. The liquid leaves the foam in the shortest way at 90° and it cannot supply the foam structure, or the FG.

3. The foam stability itself is not affected strongly by the g-level in 0° and 180° which means that gravity-driven drainage takes place only during foam evolution and at the beginning of the decay process, causing a smaller foam volume.

We can conclude from the experiments, that the amount of foams generated from FOCUS Suspension using fixed air flow rate and foaming time with FOCUS FG-s, strongly depend on the gravity level. The higher the gravity is, the less foam volumes can be blown in all measured directions.

The stability of foams is not sensitive to elevated gravity levels. The ratio of the initial and 3 minutes old foam volumes (given in percents) remained between 63% and 85% regardless to the gravity level.

Average cell sizes also did not change markedly with the increasing magnitude of gravity, but the variation of foaming direction caused significant differences in the foam structure. 0°direction gives much coarser foams, with cca. 3 times less pores per inch value. Related theses (2, 4 and 6) can be found on page 85.

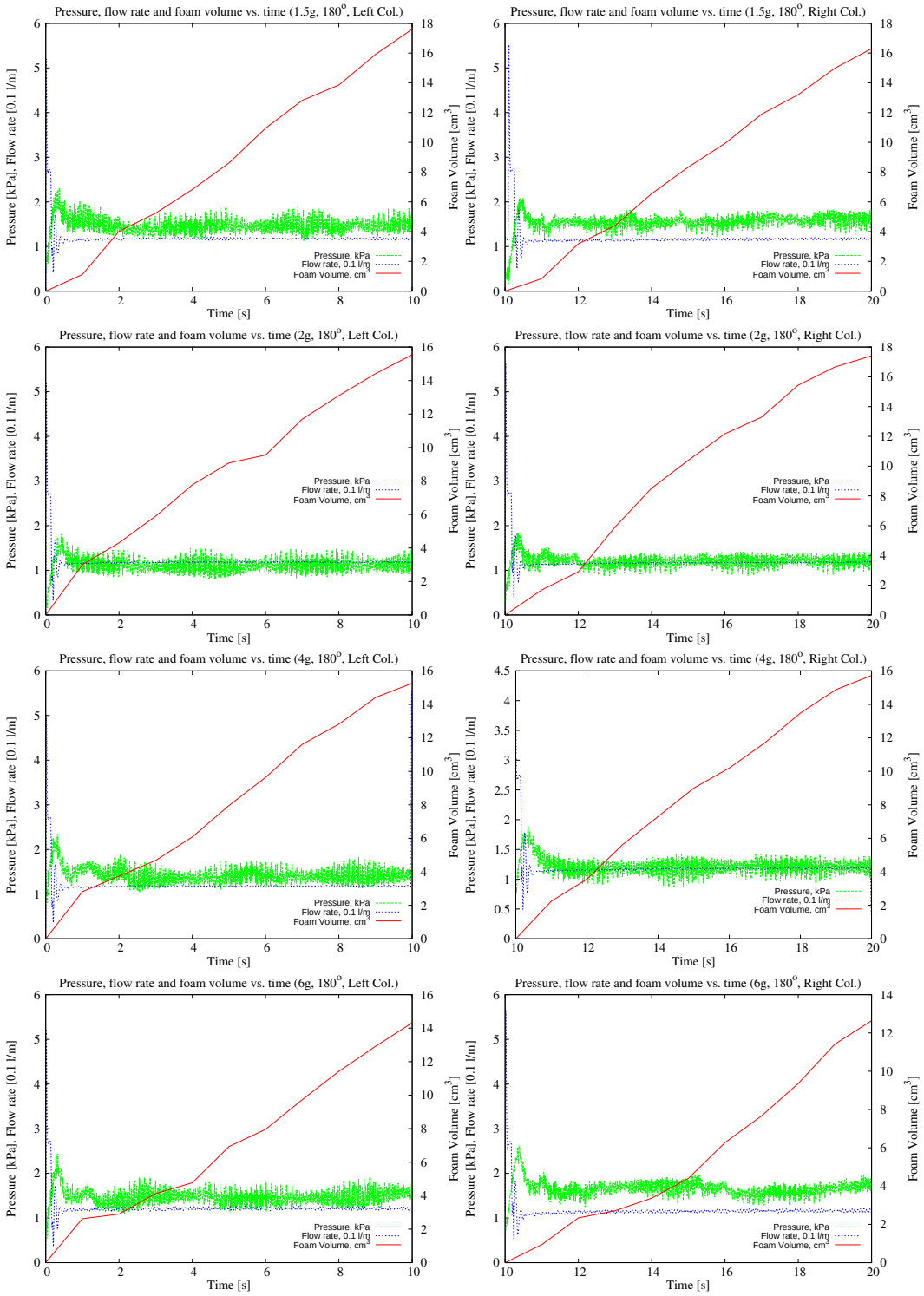

Figure 4.13: Foaming curves together with pressure and flow rate data from 1.5 - 6g at 180° foaming direction.

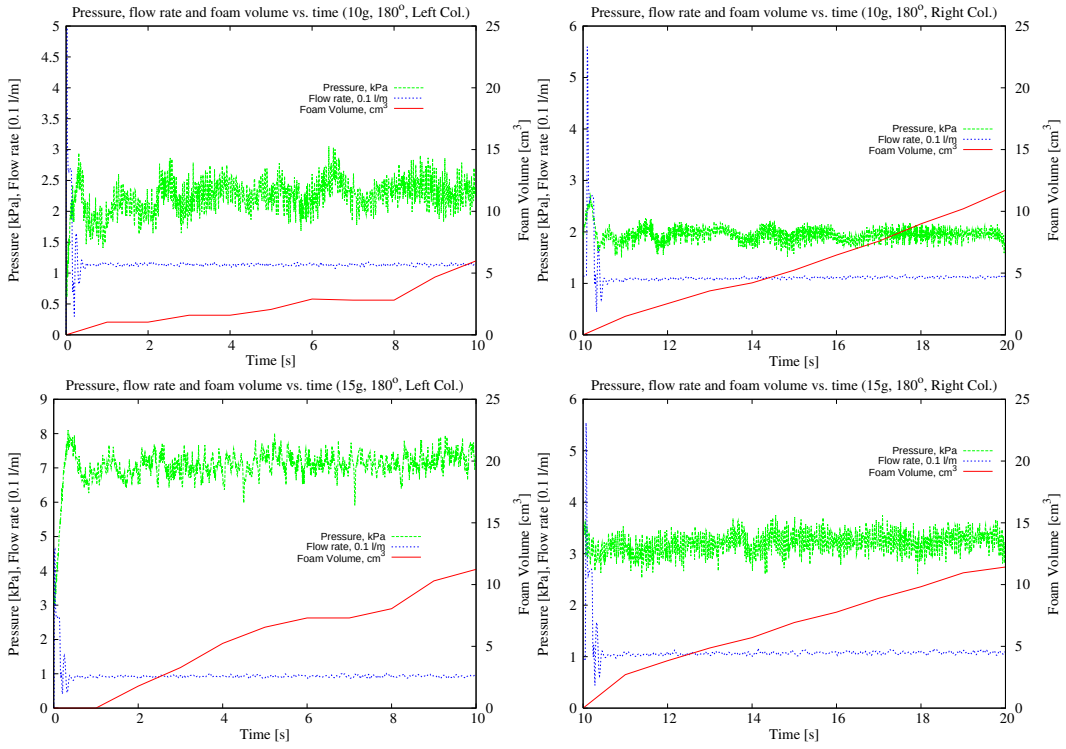

Figure 4.14: Foaming curves together with pressure and flow rate data from 10 - 15g at 180° foaming direction.

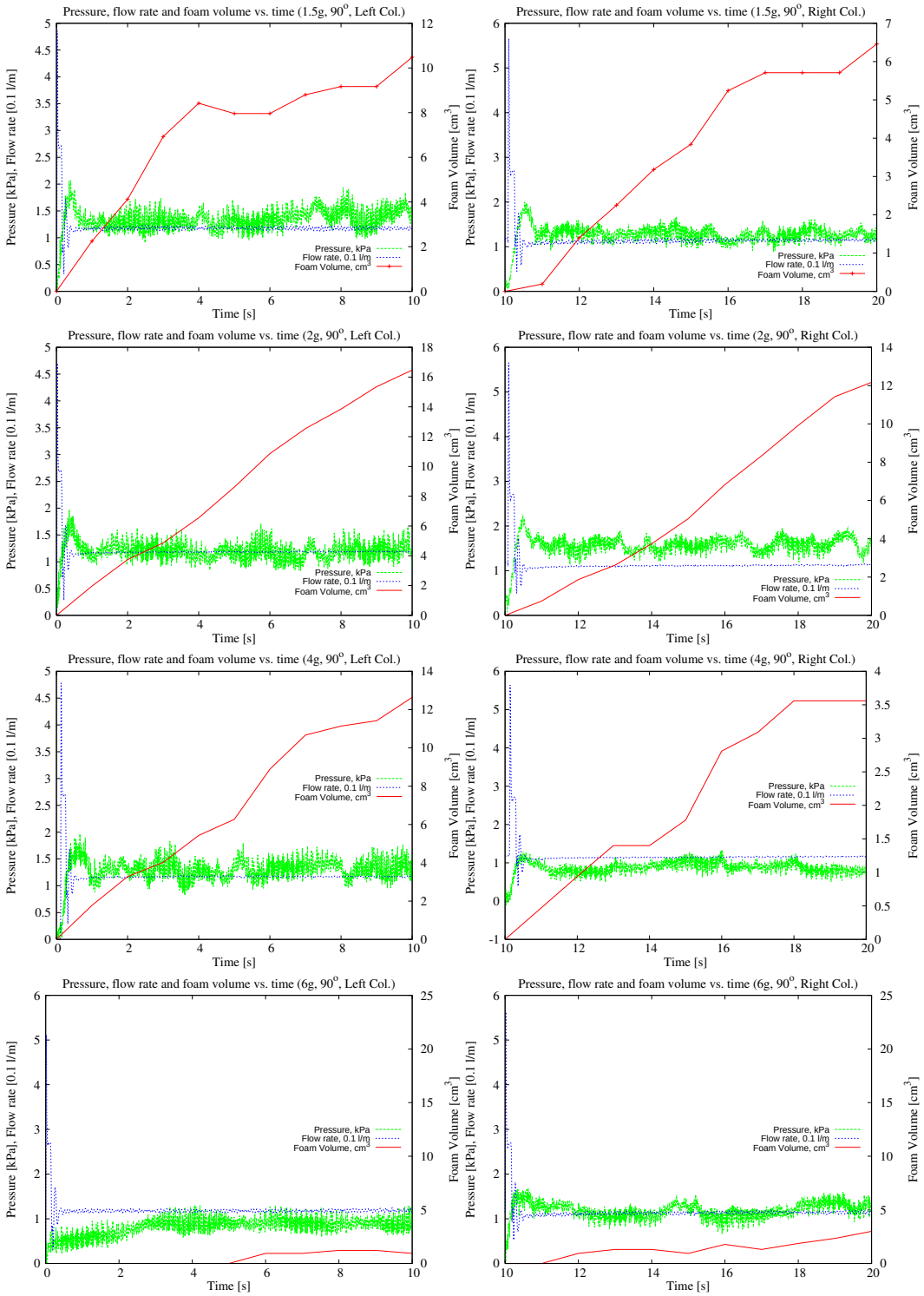

Figure 4.15: Foaming curves together with pressure and flow rate data from 1.5 - 6g at 90° foaming direction.

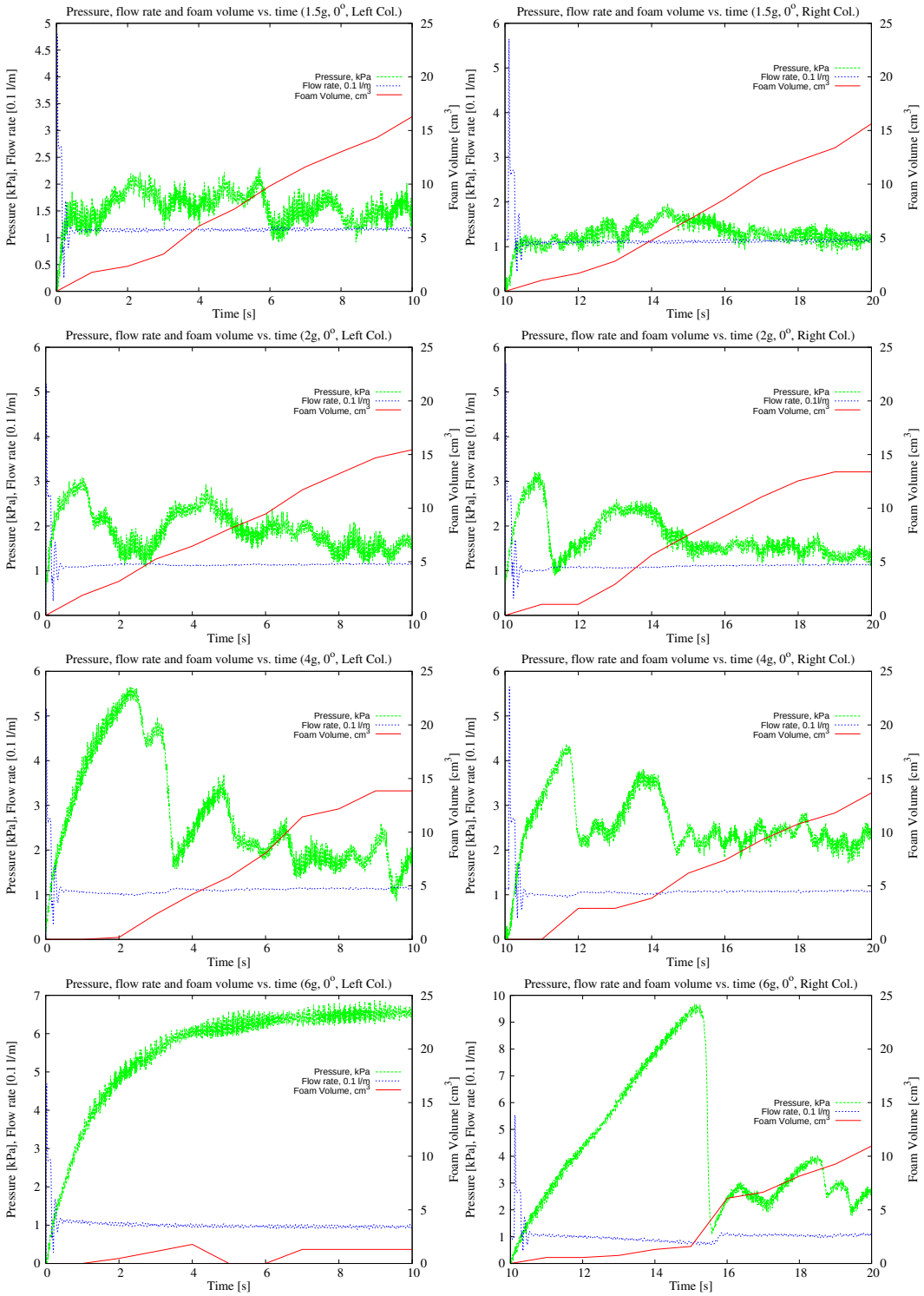

Figure 4.16: Foaming curves together with pressure and flow rate data from 1.5 - 6g at 0° foaming direction.

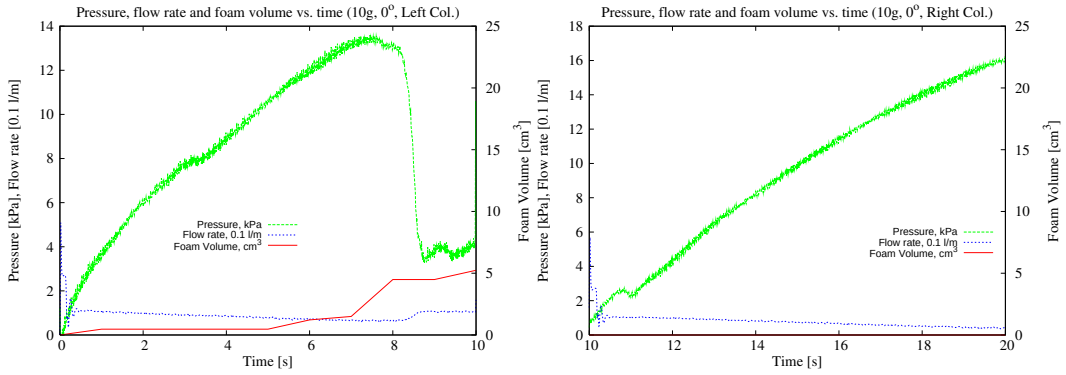

Figure 4.17: Foaming curves together with pressure and flow rate data at 10g, at 0° foaming direction.

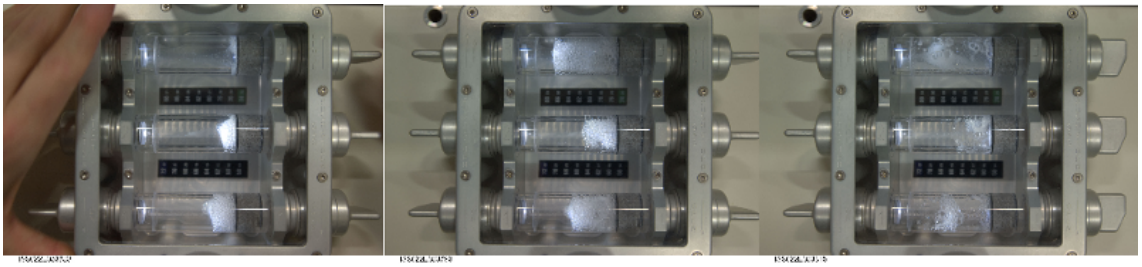

Figure 4.18: Three examples of the foam evolution stages in FOCUS Experiment. Left: Start of dynamic session; middle: end of dynamic session; right: static session. Credit: NASA.

4.3 Microgravity measurements

4.3.1 Foam volume measurements at decreased gravity

Foam evolution can be easily followed through the observation of the volume change with time. FOCUS experiment and the terrestrial reference experiments can be divided into two parts: a 'dynamic' session, when the gas valves are open, and a 'static' session, with closed valves after foaming.

Theoretically, under constant gas introduction, foam volume reaches a steady-state value when the speed of the foam evolution and the decay is equal. Stopping gas flow, foams evolve in a way determined by the processes that lead to cell wall rupture.

Figure 4.18 shows three examples of the photos taken about the developing foams during FOCUS Experiment.

Figure 4.19. shows the 'foaming curves' under micro-g and the comparisons with the reference experiments under 1 g using various foaming directions. Top-left subfigure shows the micro-g experiment results at 0.08, 0.125 and 0.23l/min flow rates, respectively [134].

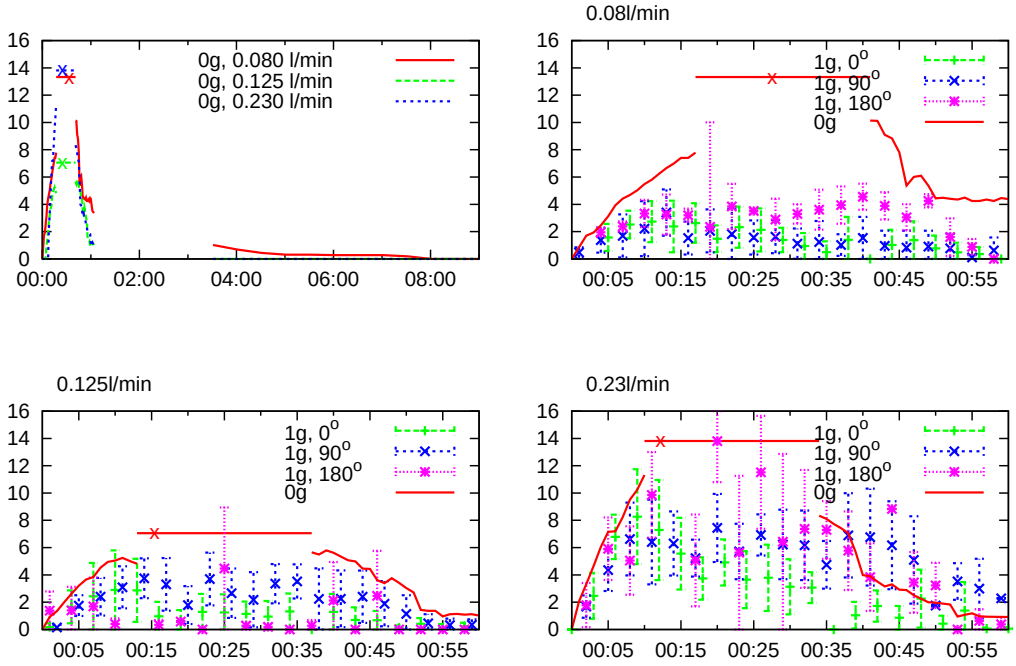

Figure 4.19: Foam volumes change in FOCUS experiment and reference experiments vs. time. Top left subfigure shows the microgravity experiment. Other subfigures show the micro-g experiment compared to the terrestrial reference experiments at different flow rates and foaming directions. X axis is the time given in MM:SS, Y axis is the foam volume given in cm^3 [134].

Table 4.2: Foam half lives (given in seconds) [134].

g-level/direction	Flow rate (l/min)		
	0.08	0.125	0.23
0g	8±1.5	12±3	5±2
1g/0°	5±2	7±2	7±1
1g/90°	9±2	6±2	22±7
1g/180°	11±2	6±5	11±3

A series of data is missing from 00:17 to 00:41 and from 01:05 to 03:30, because of improper timing during ISS experiment execution. However, the maximum foam volumes can be estimated in each FC from the suspension remnants on the FC walls by studying the ongoing images. This yields significant error in the estimation of the maximum foam volume and the time when the foam reached it, since we cannot decide whether the foams had reached this volume ever, because they could have included undetected holes (see Figure 3.1 on page 35). Therefore horizontal lines show the estimated maximum foam volumes in Figure 4.19. The corresponding estimated times when the foams reached their maximum are represented with asterisks. These values were determined by linear extrapolation using 00:00–00:17 data points.

The largest foam volume was reached using the highest flow rate (0.23l/min) and this was the case in the reference experiments as well.

The foaming curves of the reference experiments are given together with the 0g experiments, with the different flow rates separated (Figure 4.19., top right subfigure for the 0.08l/min, bottom left subfigure for the 0.125l/min and bottom right subfigure for 0.23l/min). These plots show the dynamic sessions only (first 1 minute), together with the standard deviations. Data points are the average of 7 experiments in each direction. Measurements were made in every second, but only every third data point is plotted for better visibility.

Foam half-life values in seconds can be read from Table 4.2. Due to the missing data in the microgravity measurements we can only estimate the half-life of the foams. The longest half-life was measured at 0.125l/min in microgravity. There is a salient value in 1g at 90° direction, 0.23l/min but with a serious standard deviation [134].

Though we have high standard deviations, foaming curves clearly show that reduced gravity gives larger foam volumes. The surprising result is that the foam stability did not increase in micro-g (except at 0.125l/min). The unchanged behaviour of our foam with and without gravity forces proves the dominant role of surface forces and negligible role of gravity related forces. This means that gravity induced drainage does not have an effect on the foam lives made of FOCUS suspension. Similar phenomenon was observed previously at elevated gravity levels, where the increase of gravity did not change the foam stability [130]. See Figure 4.9. for

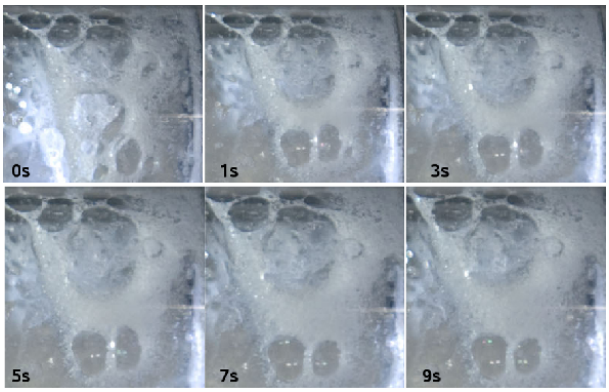

Figure 4.20: FOCUS Experiment, micro-g, 0.125l/min, static session. Rupturing at 0-1s. One little bubble at the bottom right side disappears due to coarsening. Cell walls getting thicker due to imbibition of the excess liquid. Bubbles become more and more spherical.

the stability data of increased-g foams. Therefore gravity-independent particle rearrangement (coagulation) should be primarily responsible to determine the stability of the cell walls and to influence foam life [134].

Note that aluminium foams are solely stabilised by particles and our FOCUS suspension also contains nano-particles for stabilisation purposes. Short term micro-g experiments on aluminium foams [122] showed also that the rate of coalescence is similar in micro- and normal gravity. Microgravity has a positive effect on the expansion of metal foams, but not on their stability. These foams were also found to be only stable even in micro-g, if they contain a certain amount of stabilising particles [120].

Splitting of the foam was observed quite often in 1g/0° direction. This was the case also in microgravity, but the main difference is that due to the lack of gravitational induced drainage, excess liquid from the ruptured bubbles did not move back to the surface of the FG, or dripped out of the foam (depending on the direction), but remained inside the foam structure, resulting spherical bubbles and thick cell walls in the end. Thanks to this imbibition effect remnant foams contained more liquid in microgravity. Figure 4.20. is an image series from 0.125l/min foaming at 0g, at the beginning of the static session. We can observe a rupturing event, coarsening and thickening of the cell walls.

4.3.2 Bubble size measurements

Average bubble sizes of the foams have a spatial distribution and they obviously also change with time. Figure 4.21. show FOCUS Experiment micro-g results for 0.08, 0.125 and 0.23l/min flow rates, respectively. Average bubble diameters are given in millimetres using colormap. This kind of visualisation enables us to see both time and spatial distribution of the bubble sizes in a condensed form. Zero average bubble diameter means that there is no foam at that range. The position is measured from

the surface of the FG. Note that data are missing between 00:17 and 00:41.

The linear foam growth in the beginning of the dynamic session is clearly visible in all cases. The first appearing bubbles are 1–2mm in size, having spherical shape and they form a wet foam on the FG. They travel on the top of the foam, as the next bubbles come out from the FG-s (see Figure 4.21). Newly generated bubbles are larger (see Figure 4.21a at 5s). The emerging foam gets coarser and dryer. Late bubbles (prior to valve closing) bear the features of a dry foam with thin cell walls and polyhedral shape. The FG exhausts of 'moveable' suspension. We can also assume that the suspension contains less amount of stabilizing particles in the end, because they had been previously built into the foam structure. This results bigger and less stable bubbles by the end of foaming. Smaller bubbles are still staying on the top of the foam (Figs. 4.21a-c at 40–50s). They are more stable than the upcoming bigger ones, due to the higher concentration of particles. Coalescence and coarsening make 'holes' to evolve from the larger bubbles, causing the foam to split (FC1 and FC3 cases). The movement of small bubbles can cause local virtual average bubble size *decrease* with time. See Figure 4.21c at 40–45s, 10mm position for example.

Apart from the spatial distribution, average bubble size in the overall foam can be calculated and plotted in the function of time, as it is in Figure 4.22. The comparison to the reference experiments for 0.08, 0.125 and 0.23l/min flow rates, respectively, can be read as well. These plots show the dynamic sessions only (first 1 minute), together with the standard deviations. Measurements were made in every second, but only every third data point is plotted for better visibility [134].

At the lowest flow rate (0.08l/min) there were no significant difference in the average bubble sizes, meaning that using this flow rate foam evolution is not sensitive to the magnitude and the direction of gravity. By increasing the flow rate, differences in the bubble sizes become more and more significant. The largest bubble sizes were measured in microgravity at 0.125l/min flow rate. A slight increase in average bubble size with time can be observed in all cases, regardless to the gravity level or flow rate values [134].

FOCUS experiment showed that the pre-infiltrated FG-s worked properly and foams could be made. On base of the comparison with terrestrial reference experiments we can take the following conclusions:

1. Minimal foam structure differences were found at 0.08l/min gas flow rate. At higher flow rates foams blown in microgravity have the largest average bubble sizes. The higher is the flow rate, the more significant is the difference in the average bubble size distribution. See Thesis 7 on page 85.

2. Based on the foam half lives data, foam stability was not improved by eliminating gravity. Similar phenomenon was found in previous macrogravity measurements using the same suspension [130]. Foam decay in the case of our suspension is therefore not connected to gravity induced drainage. See Thesis 4 and 5 on page 84.

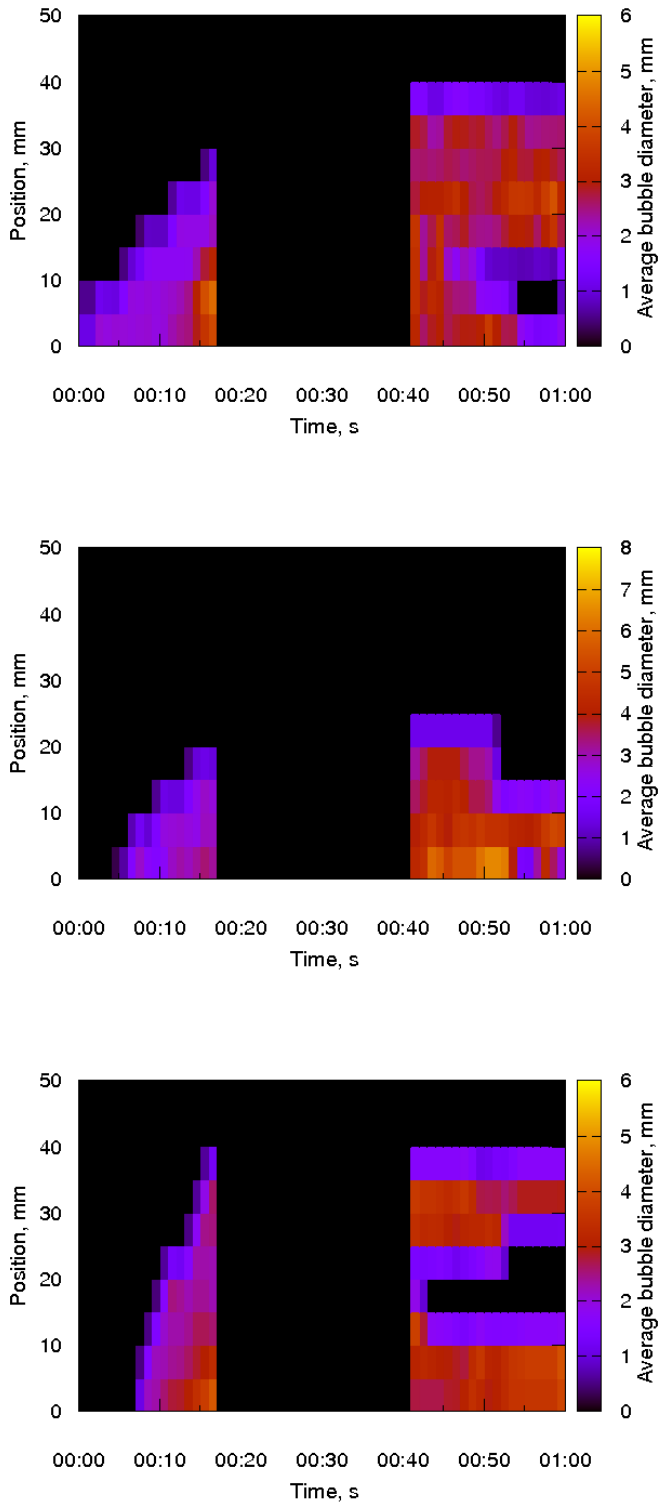

Figure 4.21: Average bubble size variation at 0g, 0.08l/min (a), 0.125l/min (b) and 0.23l/min (c), respectively [134].

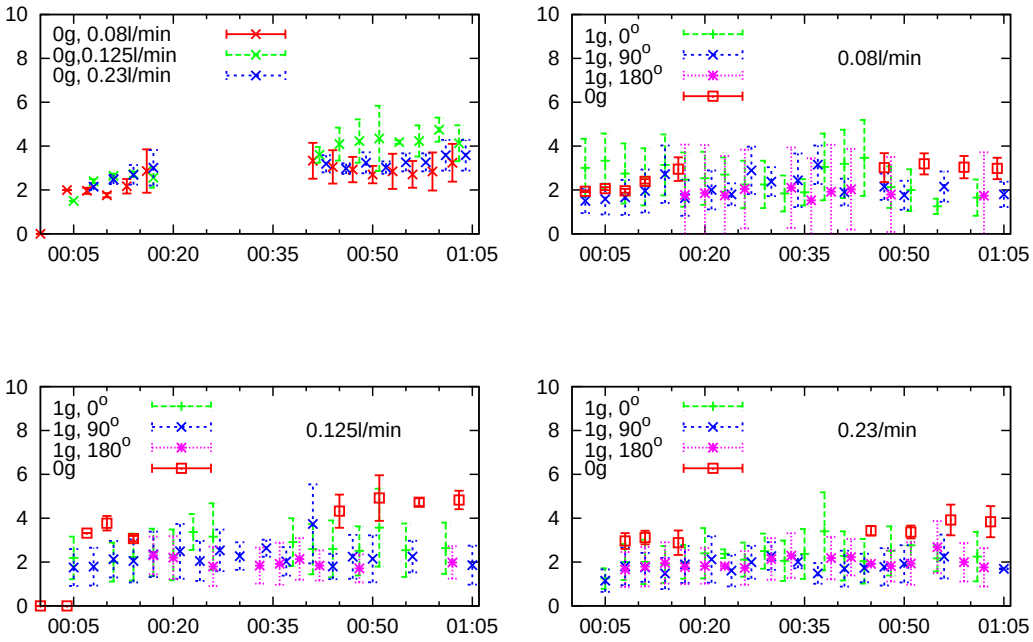

Figure 4.22: Average bubble size variation vs. time. Top left subfigure shows the microgravity experiment. Other figures show the micro-g experiment compared to the terrestrial reference experiments at different flow rates and foaming directions. X axis is the time given in MM:SS, Y axis is the average bubble diameter in mm [134].

3. Foam volumes increased during microgravity conditions and macrogravity measurements resulted reduced foam volumes. We can conclude that using the FG-s infiltrated with FOCUS Suspension, foam volumes depend on the gravity level as less gravity level gives larger foams. See Thesis 2 and 3 on page 84.

Chapter 5

Conclusions

Pure scientific research and industrial applications development should constantly interact in order to obtain results of great value, and this is exactly the case in foam research. Foams have an enormous application field as we outlined in Section 2.2.3. Here we investigated two specific areas separately and combined: one is the particle stabilisation of foams, and the other is the foam evolution in increased and decreased gravity environments. We experimentally showed for a certain system and foaming technique that the contact angle between the solid particle and the foamable liquid is of key importance and has to be in a specific range in order to make foams.

Increased and decreased gravity experiments were a real technical challenge for the ADMATIS team to carry out and to achieve scientific and technological results. The effect of foaming direction and the magnitude of gravity on an alternative foaming technique and the foams produced, using a suspension of nanoparticles resulted in interesting findings, and some achievements had been already transplanted into the metal foam scene of ADMATIS Ltd. The following subsection summarises the theses of the work.

5.1 List of theses

1. The effect of particle contact angle to the liquid in foam stabilising was investigated using 10wt% micron sized emulsion type PVC particles (Vestolit B7021, purified using distilled water) suspended in water-ethanol solution with various ethanol content. Through changing the ethanol concentration we could vary the contact angle between PVC and the liquid (0, 33, 55, 78, 90, 96 ethanol vol.% for 83, 46.5, 36, 15, 0, 0° contact angles, respectively). It was shown experimentally that the contact angle has to be in a certain range (36-83°) in order to see the stabilisation effect of PVC particles in water-ethanol solution, using direct gas injection through porous ceramic for foaming. The maximum foam volume was reached in the case of ethanol-free system which corresponds to 83° contact angle for PVC particles. Foams were created using 0.3bar bub-

bling pressure for 10 seconds.

2. The amount of foams generated from FOCUS Suspension (2wt% SiO_2 nanoparticles, 0.05wt% SDS in distilled water) using fixed air flow rate (0.125l/min) and foaming time (10 seconds) with FOCUS FG-s, depend on the gravity level: higher gravity gives less foam volumes in all measured directions (180°, 90° and 0°, measured to gravity vector).

3. The 'foaming curves' (foam volumes vs. time) of FOCUS Suspension (2wt% SiO_2 nanoparticles, 0.05wt% SDS in distilled water) showed that the largest foam volumes can be reached in microgravity, using FOCUS FG with HFC-245fa as foaming gas. Foams were generated at 0.08, 0.125 and 0.23l/min flow rates for 42, 40 and 37 seconds, respectively.

4. Foam stability in the increased gravity (1-15g) experiments was characterised by the ratio (given in %) of the 3 minutes old and the initial foam volumes. The stability of foams generated from FOCUS suspension (2wt% SiO_2 nanoparticles, 0.05wt% SDS in distilled water) with FOCUS FG, using air as a foaming gas remained between 63 and 85% showing only a slight decrease in the function of gravity level at 180° (Figure 5.1). Foams were generated at 0.125l/min flow rate for 10 seconds.

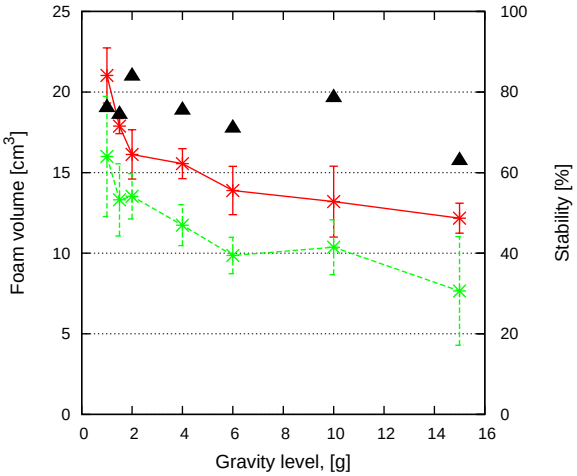

Figure 5.1: Initial and 3 minutes old foam volumes and calculated foam stabilities in the function of gravity level, 180° foaming direction.

5. The foam lives (i. e. stability) of FOCUS Suspension (2wt% SiO_2 nanoparticles, 0.05wt% SDS in distilled water) did not increase under microgravity environment. Foams were blown using HFC-245fa and FOCUS FG at 0.08, 0.125 and 0.23l/min flow rates for 42, 40 and 37 seconds, respectively. Foam

decay in the case of our suspension is therefore not connected with gravity induced drainage.

6. Average cell sizes of FOCUS suspension foams (2wt% SiO_2 nanoparticles, 0.05wt% SDS in distilled water) did not change markedly with the increasing magnitude of gravity, but the variation of foaming direction (measured to gravity vector) causes significant differences in the foam structure. 0° direction gives much coarser foams, with cca. 3 times less pores per inch value. Foams were generated using FOCUS FG, at 0.125l/min flow rate for 10 seconds with air as a foaming gas.

7. The largest average bubble sizes were reached in microgravity compared to 1g reference measurements using FOCUS suspension (2wt% SiO_2 nanoparticles, 0.05wt% SDS in distilled water) with HFC-245fa foaming gas. The higher is the flow rate, the more significant is the difference in the average bubble size distribution, when comparing 0g experiment with 1g reference experiments, using 0, 90 and 180° foaming directions, respectively. Foams were generated using FOCUS FG at 0.08, 0.125 and 0.23l/min flow rates with 42, 40 and 37 seconds foaming times, respectively.

5.2 Outlook

The results of FOCUS experiment and this PhD thesis is utilised in the development alternative metal foaming procedure of ADMATIS (patented). FOCUS foaming technique is successfully used in aluminium foam making at an experimental level. It is very important to further improve this foaming technique in order to achieve more effective and higher quality metal foam products. Gravity-insensitive foaming can be important at those technologies that use various foaming directions measured to gravity vector (e. g. injection moulding of metallic foams).

From the scientific point of view, interesting similarities were found on the investigation of foam stabilities of aluminium foams and our FOCUS Suspension — decreased gravity resulted larger foam volumes, but did not improve the stability. Further foaming experiments should be made using short-term microgravity both on particle stabilised aqueous suspension foams and aluminium foams for clarification. Though several outstanding works [2, 4, 7, 95, 96, 122, 150, 151] has been published yet, a comprehensive model for foam evolution and on the role of particles in foam stabilisation is still needed to be worked out and refined.

Nomenclature

A.U.	Arbitrary Units
ADMATIS	ADvanced MATerials In Space
AIAA	American Institute of Aeronautics and Astronautics
CCTV	Closed Circuit Television
CFC	Chloro-fluoro-carbon
DLS	Dynamic Light Scattering
DSLR	Digital Single Lens Reflex
EAC	European Astronaut Centre
EC	European Commission
EC	Experiment Container
ESA	European Space Agency
FC	Foaming Cartridge
FCH	Foaming Chamber
FG	Foam Generator
FML	Foam Metal Liner
FOAM	Foam Optics and Mechanics
FOCUS	FOam Casting and Utilization in Space
fpm	Frames per Minute
fps	Frames per Second
GS	Gas System

HFC	Hydro-fluoro-carbon
HR-SEM	High Resolution Scanning Electron Microscopy
HSO	Hungarian Space Office
IS	Illumination System
ISS	International Space Station
NASA	National Aeronautics and Space Administration
OC pepper	Oleoresin Capsicum (active ingredient in pepper spray)
PB	Plateau-border
PDMS	poly(dimethylsiloxane)
PE	Polyethylene
PS	Polystyrol
PUR	Polyurethane
PVC	Polyvinyl chloride
RT	Room Temperature
SDS	Sodium Dodecyl Sulphate
SEM	Scanning Electron Microscopy
SPAR	Space Processing Applications Rocket
SPF	Sprayed Polyurethane Foam
SSC	Swedish Space Corporation
SURE	International Space Station: a Unique Research Infrastructure
TCP	Tetrahedrally Close Pack Structure
TEM	Transmission Electron Microscopy
UMFA	Universal Multizone Foaming Apparatus
US	United States
VI	Virtual Instrument (LabVIEW^{TM})

Publications connected to the topic of thesis

Scientific publications

1. Bárczy Pál, Szőke János, Somosvári Béla M., Szirovicza Péter, Bárczy Tamás, Magyar anyagtudományos kísérlet a Nemzetközi Űrállomáson (Hungarian materials science experiment on board of the International Space Station), Bányászati és Kohászati Lapok, 2011/01.

2. B.M. Somosvári, P. Bárczy, J. Szőke, P. Szirovicza, T. Bárczy, FOCUS: Foam evolution and stability in microgravity, Colloids and Surfaces A: Physicochemical and Engineering Aspects 382 (2011), 58-63

3. Béla M. Somosvári, Norbert Babcsán, Pál Bárczy, Almuth Berthold, PVC particles stabilized water-ethanol compound foams, Colloids and Surface A: Physicochem. Eng. Aspects 309 (2007) 240-245

Scientific publications in conference proceedings

1. Béla M. Somosvári, Pál Bárczy, Péter Szirovicza, János Szőke, Tamás Bárczy, Foam Evolution and Stability at Elevated Gravity Levels, Materials Science Forum, 649 (2010) pp 391-397

2. Béla M. Somosvári, Norbert Babcsán, Foaming of Water-Ethanol-PVC System, ME Doktorandusz fórum (PhD Students Forum), 2005. 11. 09. ME-MAK szekciókiadványa, nyomdaszám ME. Tu-99/2007.

3. Béla M. Somosvári, Martin Meier, Experiments on Particle Stabilized Aqueous Foams, microCAD 2005. 03. 10-11, Miskolc, ISBN 963 661 658 2

Presentations and posters at conferences

1. Béla M. Somosvári, Pál Bárczy, János Szőke, Investgation of Shelf-Life and Foaming of Water-SiO_2-SDS Compound, poster, Colloids and Materials 2011, Amsterdam, 2011.05.08-11.

2. Pál Bárczy, János Szőke, Béla M. Somosvári, Péter Szirovicza, Tamás Bárczy, Foam Evolution and Stability in Microgravity, poster, EUFOAM 2010, Borovets, 2010. 07. 14-16.

3. Pál Bárczy, Csaba Mekler, István Budai, D. Madarász, Tamás Bárczy, Béla M. Somosvári, G. Kaptay, Conditions for homogeneous distribution of particles in liquid alloy suspensions to produce metallic foams by the liquid route, poster, MetFOAM 2009, Pozsony, 2009.09. 1-4.

4. Béla M. Somosvári, Pál Bárczy, Péter Szirovicza, János Szőke, Tamás Bárczy, Foam evolution and Stability at Elevated Gravity Levels, Solidification and Gravity 2008, presentation, Miskolc-Lillafüred, 2008. 09.03.

5. Béla M. Somosvári, Pál Bárczy, Péter Szirovicza, János Szőke, Tamás Bárczy, Foaming Experiments under Macrogravity Conditions, presentation, EUROMAT 2007, Nürnberg, 2007. 09.10.

6. Béla M. Somosvári, PVC Particles Stabilizing Water-ethanol Compound Foams, presentation, EUFOAM 2006, Potsdam, 2006. 07. 02-06.

7. Béla M. Somosvári, Pál Bárczy, Stabilization Effect of Particles in Aqueous Suspension Foams, poster, EUFOAM 2006, Potsdam, 2006. 07. 02-06.

8. Somosvári Béla M., Habnövekedés és gravitáció (Foam growth and gravity), presentation, MLR-RET Tudományos Diákfórum 2006, Miskolc, 2006. 06. 08.

9. Béla M. Somosvári, Foaming of Water-ethanol-PVC System, presentation, Winter School on Fluid Foam Physics: A Model for Complex Systems, Les Houches, 2006. 01. 9-20

10. Béla M. Somosvári, Víz-ethanol-PVC elegy habosíthatóságának vizsgálata (Foamability investigation of water-ethanol-PVC compound), presentation, ME Doktorandusz fórum, Miskolc, 2005. 11. 09.

11. Béla M. Somosvári, Martin Meier, Norbert Babcsán, Pál Bárczy, Experiments on Particle Loaded Aqueous Foams, poster, EUROMAT 2005, Prague, 2005. 09. 05-08.

12. Béla M. Somosvári, Martin Meier, Experiments on Particle Stabilized Aqueous Foams, presentation, microCAD 2005, Miskolc 2005. 03. 10-11

Consulted Master Theses

1. Huszár Márton: PUR szivacs habképző képességének összehasonlító vizsgálata. PUR csőszigeteléssel épített melegvíz távvezeték hőveszteségének meghatározása (Comparative investigation of foam generation ability of PUR sponge. Determination of heat loss of hot water line equipped with PUR insulation.), Master Thesis, Dept. of Polymer Eng., 2008, Univ. of Miskolc, consultants: Dr. Bárczy Pál, Dr. Szemmelweisz Tamásné, Somosvári Béla Márton

Professional presentations, reports

1. Pál Bárczy (speaker), János Szőke, Béla M. Somosvári, Péter Szirovicza, Tamás Bárczy, FOCUS Experiment, Joint CSA/ESA/JAXA/NASA Science Symposium, Increment 21-22, 2009. 09. 02-03.

2. Béla M. Somosvári, Investigation of Water-ethanol-PVC System, presentation, LEONARDO DA VINCI II MOBILITY PROGRAMME, TU-Berlin, 2005. 08. 18.

3. Béla M. Somosvári (speaker), Dr-Ing. Martin Meier, Experimental Study of Aqueous Suspension Foams, presentation, BTU-Cottbus, 2004. 11. 03.

Other publications

1. Szőke J., Somosvári B.: Lézeres habvizsgáló berendezés fejlesztése (Development of Laser Foam Analyser), Innováció és Tudás 2007. Miskolci Egyetem. 2007. pp.85-94

2. Somosvári Béla M., A habok világa (World of Foams), Miskolci Egyetem Felvételi Lap 2006

3. Babcsán Norbert, Somosvári Béla M., Anyagtudománnyal átívelt távolságok (Distances Conquered by Materials Science), Természet Világa, 2006/8, pp. 348

4. Béla M. Somosvári, Szilárd Csizmadia, Light Curve Analysis of the Eclipsing Binary Star System V404 Lyrae, Astrophysics of Variable Stars, ASP Conference Series Vol 349, 2006 Ed: C. Sterken, C. Aerts

Bibliography

[1] D. Weaire and S. Hutzler, "Making, modelling and measuring foams," *Europhysics News*, vol. 30, 3, pp. 73–75, 1999.

[2] M. Andersson, J. Banhart, H. Caps, D. Durian, F. Garcia-Moreno, S. Hutzler, B. Kronberg, D. Langevin, M. Saadatfar, A. Saint-Jalmes, N. Vandevalle, M. Vignes-Adler, and D. Weaire, "Foam Research in Microgravity," *J. Jpn. Soc. Microgravity Appl.*, vol. 25, no. 3, 2008.

[3] C. Monnereau, M. Vignes-Adler, and B. Kronberg, "Influence of gravity on foams," *J. Chim. Phys.*, vol. 96, pp. 958–967, 1999.

[4] P. Grassia, S. J. Neethling, C. Cervantes, and H. T. Lee, "The growth, drainage and bursting of foams," *Colloids Surf. A: Physicochem. Eng. Aspects*, vol. 274, pp. 110–124, 2006.

[5] A. Saint-Jalmes, S. Marze, M. Safouane, and D. Langevin, "Foam experiments in parabolic flights: Development of an ISS facility and capillary drainage experiments," *Microgravity Sci. Tec.*, vol. 18-1, pp. 22–30, 2006.

[6] M. Vignes-Adler and D. Weaire, "New foams: Fresh challenges and opportunities," *Curr. Opin. Colloid In.*, vol. 13, pp. 141–149, 2008.

[7] G. Kaptay, "Interfacial criteria for stabilization of foams by solid particles," *Colloids Surf. A: Physicochem. Eng. Aspects*, vol. 230, pp. 67–80, 2004.

[8] J. Banhart, F. Garcia-Moreno, S. Hutzler, D. Langevin, L. Liggieri, R. Miller, A. S. Jalmes, and D. Weaire, "Foams and emulsions in space," *Europhysics News*, vol. 39, no. 4, pp. 26–28, 2008.

[9] J. Banhart, "Manufacture, characterisation and application of cellular metals and metal foams," *Prog. Mater. Sci.*, vol. 46, pp. 559–632, 2001.

[10] N. E. Hotrum, M. A. C. Stuart, T. van Vliet, S. F. Avino, and G. A. van Aken, "Elucidating the relationship between the spreading coefficient, surface-mediated partial coalescence and the whipping time of artificial cream," *Colloids Surf. A: Physicochem. Eng. Aspects*, vol. 260, pp. 71–78, 2005.

[11] D. Weaire, "Foam Physics," *Adv. Eng. Mater.*, vol. 4, pp. 723–725, 2002.

[12] S. Hutzler, *The Physics of Foams*. PhD thesis, Department of Physics, Trinity College, University of Dublin, 1997.

[13] J. G. McDaniel, I. Akhatov, and R. G. Holt, "Inviscid dynamics of a wet foam drop with monodisperse bubble size distribution," *Phys. Fluids*, vol. 14, no. 6, pp. 1886–1894, 2002.

[14] W. Drenckhan and D. Langevin, "Monodisperse foams in one to three dimensions," *Curr. Opin. Colloid In.*, vol. 15, p. 341–358, 2010.

[15] L. J. Gibson and M. F. Ashby, *Cellular Solids: Structure & Properties*. New York: Pergamon Press, 1988.

[16] N. Babcsán, *Ceramic Particles Stabilized Aluminum Foams*. PhD thesis, Materials Science and Tehcnology PhD School Kerpely Antal, 2003.

[17] S. T. Tobin, J. D. Barry, A. J. Meagher, B. Bulfin, C. E. O'Rathaille, and S. Hutzler, "Ordered polyhedral foams in tubes with circular, triangular and square cross-section," *Colloids Surf. A: Physicochem. Eng. Aspects*, vol. 382, pp. 24–31, 2011.

[18] Dennis Weaire, "Fizz and froth: how the bubbles take the strain," *New Sci.*, vol. 1, p. 33, October 1987.

[19] Charles Kittel, *Bevezetés a szilárdtestfizikába*. Műszaki Könyvkiadó, 1981.

[20] L. Bragg and J. Nye, "A dynamical model of a crystal structure," *Proc R Soc Lond, A*, vol. 190, no. 8, pp. 474–481, 1947.

[21] Yann YIP CHEUNG SANG, *Vers des micromousses stimulables*. PhD thesis, Université Paris Diderot - Paris 7, Laboratoire Matiére et Systèmes Complexes & Université Paris Est Marne-la-Vallé Laboratoire de Physique des Matériaux Divisés et des Interfaces.

[22] "Liquide glycérique," Last accessed Aug 2011. Joseph Plateau Biography, Museum voor de Geschiedenis van de Wetenschappen, Universiteit Gent
http://mhsgent.ugent.be/engl-plat10.html.

[23] "Daguerreotype portrait depicting Joseph Plateau," Last accessed Aug 2011. Joseph Plateau collection, University of Ghent
http://users.telenet.be/thomasweynants/opticaltoys-phena.html.

[24] J. Plateau, "Statique expérimentale et théorique des liquides soumis aux seules forces moléculaires," *Senles Force Moleculaires, Ghent*, 1873.

[25] V. Gergely, R. L. Jones, and T. W. Clyne, "The effect of capillarity-driven melt flow and size of particles in cell faces on metal foam structure evolution," *Transactions of JWRI. Special Issue*, vol. 30, pp. 371–376, 2001.

[26] E. B. Matzke, "The three-dimensional shape of bubbles in foam — an analysis of the role of surface forces in three-dimensional cell shape determination," *Am. J. Bot.*, vol. 33, no. 1, p. 58, 1946.

[27] Tomase Aste and Dennis Weaire, *The pursuit of perfect packing*. IOP Publishing Ltd., 2000.

[28] D. Weaire, "Kelvin's foam structure: a commentary," *Phil. Mag. Lett.*, vol. 88, no. 2, pp. 91–102, 2008.

[29] "Plateau's Problem," Last accessed Aug 2011. Bellevue College, Science Division
http://scidiv.bellevuecollege.edu/math/Plateau.html.

[30] F. J. Almgren and J. Taylor, "The geometry of soap films and soap bubbles," *Sci.Am.*, vol. 235, no. 7, pp. 82–93, 1976.

[31] J. E. Taylor, "Soap bubbles and crystals," *Resonance*, vol. 11, no. 6, pp. 26–30, 2006.

[32] M. Aggerbeck, S. E. Kristensen, K.-O. Markussen, R. Olsen, S. Simonsen, and A. Søndergaard, "The geometry of soap films and soap bubbles," Last accessed Aug 2011.
http://www.soapbubble.dk/en/bubbles/geometry.php.

[33] T. C. Hales, "The Honeycomb conjecture," *Discr. Comput. Geom.*, vol. 25, pp. 1–22, 2001.

[34] Lord Kelvin (Sir William Thomson), "On the Division of Space with Minimum Partitional Area," *Philos. Mag.*, vol. 124, no. 151, p. 503, 1887.

[35] "Beating Kelvin's Partition of Space," Last accessed Aug 2011.
http://www.susqu.edu/brakke/kelvin/kelvin.html.

[36] K. Brakke, "The Surface Evolver," Last accessed Aug 2011.
http://www.susqu.edu/brakke/evolver/evolver.html.

[37] Ken Brakke, "The Surface Evolver," *Exp. Math.*, vol. 1, pp. 141–165, 1992.

[38] Kraynik A.M., Reinelt D.A., and van Swol F., "Structure of random monodisperse foam," *Phys. Rev. E*, vol. 67, 2003.

[39] A. Kraynik, D. Reinelt, F. van Swol, and S. Hilgenfeldt, "Foam Structure and Rheology: The shape and feel of random soap froth 'Foam Microrheology'," Last accessed Aug 2011. Sandia National Laboratories
http://www.ima.umn.edu/2009-2010/W10.12-16.09/activities/Kraynik-Andrew/IMA_Kraynik.pdf.

[40] D. Weaire and R. Phelan, "A counter-example to Kelvin's conjecture on minimal surfaces," *Phil. Mag. Lett.*, vol. 69, no. 2, pp. 107–110, 2009.

[41] R. Phelan, D. Weaire, and K. Brakke, "Computation of equilibrium foam structures using the surface evolver," *Exp. Math.*, vol. 4, no. 3, pp. 181–192, 1995.

[42] "Gas Hydrate: What is it?," Last accessed Sept 2011. U.S. Geological Survey, Woods Hole Science Center
http://woodshole.er.usgs.gov/project-pages/hydrates/what.html.

[43] M. T. Mangan and K. V. Cashman, "The structure of basaltic scoria and reticulite and inferences for vesiculation, foam formation, and fragmentation in lava fountains," *J. Volcanol. Geoth. Res.*, vol. 73, pp. 1–18, 1996.

[44] J. V. Gundy, "Reticulite," Last accessed Aug 2011. Earth Science Picture of the Day
http://epod.usra.edu/blog/2010/06/reticulite.html.

[45] R. Gabrielli, "A new counter-example to Kelvin's conjecture on minimal surfaces," *Phil. Mag. Lett.*, vol. 89, no. 8, pp. 483–491, August 2009.

[46] "Breaktrough in Bubble Research at Bath," Last accessed Aug 2011. University of Bath
http://www.bath.ac.uk/news/2009/09/02/foam/.

[47] "The Water Cube, Beijing, China," Last accessed Aug 2011. http://www.mondoarc.com/projects/Architectural/209999/the_water_cube_beijing_china.html.

[48] M. F. Ashby and R. F. M. Medalist, "The mechanical properties of cellular solids," *Metall. Mater. Trans. A*, vol. 14, no. 9, pp. 1755–1769, 1983.

[49] "Natural beehive - honeycomb structure," Last accessed Sept 2011. http://s469.photobucket.com/albums/rr56/bluegrass_photo/Bees/.

[50] A. Cooper and M. W. Kennedy, "Biofoams and natural protein surfactants," *Biophys. Chem.*, vol. 15, pp. 96–104, 2010.

[51] E. V. Benno Meyer-Rochow, "Post-embryonic photoreceptor development and dark/light adaptation in the spittle bug Philaenus spumarius (L.) (Homoptera, Cercopidae)," *Arthropod Struct. Dev.*, vol. 33, pp. 405–417, 2004.

[52] W. Jonsson, "Fry of cosby gourami under bubblenest," Last accessed Sept 2011. http://wiljo.se/images/fisksidae/trichogaster_trichopterus5.htm.

[53] "Aprónépek," Last accessed Sept 2011. Pásti Csaba http://pasticsaba.blogspot.com/2011/05/apronepek.html.

[54] A. Kirillov and D. Turaev, "Foam-like structure of the Universe," *Phys. Lett. B*, vol. 656, pp. 1–8, 2007.

[55] A.A. Kirillov and E.P. Savelova and P.S. Zolotarev, "Propagation of cosmic rays in the foam-like Universe," *Phys. Lett. B*, vol. 663, pp. 372–376, 2008.

[56] Roger Penrose, *The road to reality.* Jonathan Cape, London, 2004.

[57] J. V. Gundy, "The Foam Book," Last accessed Oct 2011. Aqueous Foam Technology References http://www.aquafoam.com/.

[58] S. Nóra, "Habzás vizsgálati módszerei," tech. rep., 2007.

[59] D. Langevin, M. Adler, N. Vandevalle, A. Saint-Jalmes, and S. Hutzler, "Hydrodynamics of wet foams," Tech. Rep. MAP AO 99-108, 2009.

[60] M. Meier, "Nonmetallic solids foams - a non-exhaustive overview," *Anyagok Világa (Materials World)*, vol. 6, no. 1, 2005.

[61] S. Guessasma and L. Chaunier and G. Della Valle and D. Lourdin, "Mechanical codeling of cereal solid foods," *Trends Food Sci. Tech.*, vol. 22, pp. 142–153, 2011.

[62] "NASA Photo Gallery," Last accessed Oct 2011. External tank images http://www.nasa.gov/returntoflight/multimedia/external_tank_images.html.

[63] "Carbon Foam from TouchStone Research Laboratory," Last accessed Oct 2011. http://www.cfoam.com/index.htm.

[64] S. Kelso and B. Goodman, "Foam core enables stiff lightweight mirrors," Last accessed Oct 2011. http://spie.org/x8709.xml.

[65] G. Griffith, "Carbon Foam: A Next-Generation Structural Material," Last accessed Oct 2011. Touchstone Research Laboratory Ltd http://www.industrialheating.com.

[66] B. Sosnick, "Process for making foamlike mass of metal," 1948. US Patent.

[67] D. Schwingel, H.-W. Seeliger, C. Vecchionacci, D. Alwes, and J. Dittrich, "Aluminium foam sandwich structures for space applications," *Acta Astronautica*, vol. 61, pp. 326–330, 2007.

[68] Hans-Peter Degischer and Brigitte Kriszt, ed., *Handbook of Cellular Metals: Production, Processing, Applications.* Wiley-VCH Verlag GmbH & Co. KGaA, 2002.

[69] Michael F. Ashby, Anthony Evans, Norman A. Fleck, Lorna J. Gibson, John W. Hutchinson, and Haydn N. G. Wadley, *Metal foams - A design guide.* Butterworth-Heinemann, Elsevier, 2000.

[70] "ADMATIS - ADvanced MAterials In Space," Last accessed Oct 2011. A kezdetek — Bealuca http://www.admatis.com.

[71] B. M. Somosvári, "30 Days Accomplishment Report on Foam Casting and Utilization in Space," Tech. Rep. FOC-REP-SCI-ACR, 2010.

[72] "AluBone - Metal Foam," Last accessed Oct 2011. http://www.alubone.com/index.html.

[73] "Metal Foam Competence," Last accessed Oct 2011. http://www.femhab.hu/index.php/en.html.

[74] "Duocel Foam Properties & Application Guide," Last accessed Oct 2011. http://www.ergaerospace.com/Material-Applications-guide.html.

[75] "MetComb - Technical Overview," Last accessed Oct 2011. http://www.metcomb.com/products.html.

[76] Z. Chen, W. Ren, L. Gao, B. Liu, S. Pei, and H.-M. Cheng, "Three-dimensional flexible and conductive interconnected graphene networks grown by chemical vapour deposition," *Nat. Mater.*, vol. 10, pp. 424–428, 2011.

[77] D. L. Sutliff, D. M. Elliott, M. G. Jones, and T. C. Hartley, "Attenuation of fj44 turbofan engine noise with a foam-metal liner installed over-the-rotor," Tech. Rep. NASA/TM—2009-215666, 2009.

[78] "Markets and applications for spray polyurethane foam," Last accessed Oct 2011. Spray Foam Insulation Community Portal and Guide http://www.sprayfoam.com/spps/ahpg.cfm?spgid=18.

[79] M. Saha, M. Kabir, and S. Jeelani, "Enhancement in thermal and mechanical properties of polyurethane foam infused with nanoparticles," *Mat. Sci. Eng. A-Struct.*, vol. 479, pp. 213–222, 2008.

[80] "Last-a-foam product features and benefits," Last accessed Oct 2011. General Plastics Mfg. Company http://www.generalplastics.com/solutions/product-lines/rigid-foams/fr-3700#details.

[81] B. M. Somosvári, "Fémhabok alkalmazási lehetőségei az űrtevékenységben," tech. rep., 2004.

[82] "Vehicle Survivability Conference," Last accessed Oct 2011. http://www.vehicle-survivability.com/.

[83] M. Stackpoole, "Refractory ceramic foams for novel applications," Last accessed Oct 2011. http://www.techbriefs.com/component/content/article/2795.

[84] J. Luyten, S. Mullens, J. Cooymans, A. D. Wilde, I. Thijs, and R. Kemps, "Different methods to synthesize ceramic foams," *J. Eur. Cer. Soc.*, vol. 29, pp. 829–832, 2009.

[85] "Foamed lightweight concrete," Last accessed Oct 2011. Allied Foam Tech http://www.alliedfoamtech.com/index.html.

[86] D. Exerowa and P. M. Kruglyakov, *Foam and Foam Films: Theory, Experiment, Application.* Elsevier Science BV, 1998.

[87] L. L. Schramm, *Emulsions, Foams and Suspensions.* WILEY-VCH Verlag GmbH & Co. KGaA, 2005.

[88] Dr. Farkas Ferenc, *Poliuretánok.* Kémszám Bt. Budapest, 2004.

[89] International conference 'ADVANCED METALLIC MATERIALS', *Metal foams - manufacture and the physics of foaming*, (Smolenice (Szomolány), Slovakia), 5-7 nov. 2003.

[90] R. J. Pugh, "Foaming, foam films, antifoaming and defoaming," *Adv. Colloid. Interfac.*, vol. 64, pp. 67–142, 1996.

[91] V. M. Gotovtsev and A. M. Korshunov, "Hydrostatic Equilibrium in a Foam Column," *Theor. Found. Chem. Eng.*, vol. 34, no. 2, p. 108–111, 2000.

[92] EUFOAM 2010 Conference, *An interactive study of the lifetime distribution of soap films*, (Borovets, Bulgaria), 14-16 July 2010.

[93] L. L. Schramm, *Surfactants: Fundamentals and Applications in the Petroleum Industry.* Cambridge Univ. Press, 2000.

[94] B. P. Binks and T. S. Horozov, "Aqueous foams stabilized loely by silica nanoparticles," *Angew. Chem. Int. Ed.*, vol. 44, pp. 3722–3725, 2005.

[95] B. P. Binks, "Particles as surfactants - similarities and differences," *Curr. Opin. Colloid In.*, vol. 7, pp. 21–41, 2002.

[96] T. N. Hunter, R. J. Pugh, G. V. Franks, and G. Jameson, "The role of particles in stabilising foams and emulsions," *Advances in Coll. Intf. Sci.*, vol. 137, pp. 57–81, 2008.

[97] U. T. Gonzenbach, A. R. Studart, E. Tervoort, and L. J. Gauckler, "Ultrastable particle-stabilized foams," *Angew Chem. Int. Ed.*, vol. 45, pp. 3526–3530, 2006.

[98] G. Kaptay, "On the equation of the maximum capillary pressure induces by solid particles to stabilize emulsions and foams and on the emulsion stability diagrams," *Colloids Surf. A: Physicochem. Eng. Aspects*, vol. 282-283, pp. 387–401, 2006.

[99] B. Somosvári and P. Bárczy, "Stabilization effect of particles in aqueous suspension foams," 2006. Presented at EUFOAM Conference 2-6 July, 2006, Potsdam.

[100] J. Banhart, B. Kronberg, D. Langevin, and S. O. et al., "microgfoam - final report," tech. rep., 2000-2003.

[101] S. Vincent-Bonnieu, "FOAM Coarsening Experiment Scientific Requirements," tech. rep., ESA, 2007.

[102] A. Saint-Jalmes and D. Langevin, "Time evolution of aqueous foams: drainage and coarsening," *J. Phys-Condens. Mat.*, vol. 14, pp. 9397–9412, 2002.

[103] A. Dutta, A. Chengara, A. D. Nikolov, D. Wasan, K. Chen, and B. Campbell, "Destabilization of aerated food products: effects of Ostwald ripening and gas diffusion," *Journal of Food Engineering*, vol. 62, p. 177–184, 2004.

[104] V. A. Thomas, N. S. Prasad, and C. A. M. Reddy, "Microgravity research platforms - a study," *Current Sci.*, vol. 79, no. 3, pp. 336–340, 2000.

[105] "ZARM Hyper-g Centrifuge," Last accessed Nov 2011. Center for Applied Space Technology and Microgravity `http://www.zarm.uni-bremen.de/menu/facilities/centrifuge.html`.

[106] G. Seibert, *A world without gravity*. ESA Publications Division, 2001.

[107] E. Ceglia, "European Users Guide to Low Gravity Platforms," Last accessed Jan 2012. `http://www.esa.int/esaMI/HSF_Research/SEMG2W4KXMF_0.html`.

[108] "Space Processing Applications Rocket project, SPAR 2," tech. rep., Nov. 1977.

[109] J. Patten and E. Greenwell, "Feasibility of producing closed-cell metal foams ina zero-gravity environment from spotter-deposited inert gasberaing metals and alloys (74-10)," tech. rep., Battelle North-West Laboratories, Materials Department, Materials and Process Engineering Section. Post-flight Technical Report, SPAR Flight 2 and Final Report.

[110] F. C. Wessling, S. P. McManus, J. Matthews, and D. Patel, "Foam formation in low gravity," *J Spacecraft Rockets*, vol. 27, no. 3, 1989.

[111] D. A. Noever, "Foam fractionation of particles in low gravity," *J Spacecraft Rockets*, vol. 31, no. 2, 1994.

[112] D. A. Noever and R. J. Cronise, "Gravitational effects on closed-cellular-foam microstructure," *J Spacecraft Rockets*, vol. 33, no. 2, 1996.

[113] R. Fuller, T. Campbell, U. S. NASA, A. A. of Physics Teachers, and S. Program, "Soap and water : film footage from nasa skylab missions. [motion picture]," 1974. Title from teacher's guide.

[114] A. G. Merzhanov, "Shs processes in microgravity activities: first experiments in space," *Adv. Space Res.*, vol. 29, no. 4, pp. 487–495, 2002.

[115] M. Anderson, B. Kronberg, C. Lockowandt, B. Prunet-Foch, and M. Vignes-Adler, "Foaming mechanisms in transient foams under microgravity," *J. Chim. Phys.*, vol. 11, pp. 227–230, 2001.

[116] H. Caps, H. Decauwer, M.-L. Chevalier, M. Ausloos, and N. Vandewalle, "Foam imbibition in microgravity," *Eur. Phys. J. B*, vol. 33, pp. 115–119, 2003.

[117] S. J. Cox and G. Verbist, "Liquid flow in foams under microgravity," *Microgravity sci. technol.*, vol. XIV/4, pp. 45–52, 2003.

[118] H. Caps, S. J. Cox, H. Decauwer, D. Weaire, and N. Vandewalle, "Capillary rise in foams under microgravity," *Colloids Surf. A: Physicochem. Eng. Aspects*, vol. 261, pp. 131–134, 2005.

[119] M. Meier, D. Hille, and G. Wallot, "Experiments on the stability of solid particle loaden aqueous foams," in *Cellular Metals: Manufacture, Properties, Applications* (J. Banhart, N. A. Fleck, and A. Mortensen, eds.), pp. 65–70, MIT Publ. ISBN 3-935538-12-X, 2003.

[120] T. Wübben and S. Odenbach, "Stabilization of metallic foams by solid particles," *Colloids and Surfaces A: Physicochem. Eng. Aspects*, vol. 266, pp. 207–213, 2005.

[121] N. Babcsán, F. Garcia-Moreno, D. Leitlmeier, and J. Banhart, "Liquid metal foams - a perspective for feasible in-situ experiments under low gravity," *Materials Science Forum*, vol. 508, pp. 275–280, 2006.

[122] F. Garcia-Moreno, M. Mukherjee, C. Jimenez, and J. Banhart, "X-ray radioscopy of liquid metal foams under microgravity," *Transactions of The Indian Institute of Metals*, vol. 62, pp. 451–454, 2009.

[123] D. J. Durian and G. A. Zimmerli, "Foam optics and mechanics," 2002.

[124] "Maxus - microgravity for up to 14 minutes," Last accessed Feb 2012. `http://www.sscspace.com/maxus`.

[125] "Foam stability," Last accessed Apr 2012. `http://www.esa.int/SPECIALS/HSF_Research/SEMSYK0YDUF_0.html`.

[126] "Space oddities to teach science," Last accessed Apr 2012. ESA `http://www.esa.int/esaHS/SEM47X1YRYG_index_0.html`.

[127] N. Vandevalle, H. Caps, G. Delon, A. Saint-Jalmes, E. Rio, L. Saulnier, M. Adler, A. L. Biance, O. Pitois, S. C. Addad, R. Hohler, D. Weaire, S. Hutzler, and D. Langevin, "Foam stability in microgravity," *J. Phys. Conf. Ser.*, vol. 327, no. 012024, pp. 1–9, 2011.

[128] "Foam coarsening," Last accessed Apr 2012. `http://www.esa.int/SPECIALS/HSF_Research/SEMGYK0YDUF_0.html`.

[129] T. P. D. Turner, B. Dlugogorski, "Factors affecting the stability of foamed concentrated emulsions," *Colloids Surf. A: Physicochem. Eng. Aspects*, vol. 150, pp. 171–184, 1999.

[130] B. M. Somosvári, P. Bárczy, P. Szirovicza, J. Szőke, and T. Bárczy, "Foam evolution and stability at elevated gravity levels," *Mat. Sci. For.*, vol. 649, pp. 391–397, 2010.

[131] B. M. Somosvári, "Részecske-stabilizált habok vizsgálata növelt gravitációban," Tech. Rep. MŰI TP/212 2006, 2007.

[132] B. M. Somosvári, N. Babcsán, P. Bárczy, and A. Berthold, "Pvc particles stabilized water–ethanol compound foams," *Colloids and Surface A: Physicochem. Eng. Aspects*, vol. 309, pp. 240–245, 2007.

[133] B. M. Somosvári, "Summary of shelf-life tests in focus experiment preparation," Tech. Rep. ESA FOCUS SURE AO-019 / PECS 98045, 2009.

[134] B. M. Somosvári, P. Bárczy, J. Szőke, P. Szirovicza, and T. Bárczy, "Focus: Foam evolution and stability in microgravity," *Colloids Surf. A: Physicochem. Eng. Aspects*, vol. 382, pp. 58–63, 2011.

[135] L. I. Nass and C. A. Heiberger, *Encyclopaedia of PVC - Volume 1: Resin Manufacture and Properties*, pp. 86–91. Dekker, New York, 1976.

[136] W. V. Titow, *PVC Technology*, pp. 15, 44–45. Elsevier, London, 1984.

[137] S. R.Röthele and W. Witt, "Laser diffraction: millenium link for particle size analysis," *Powder Handling Process* , vol. 11, no. 1, 1999.

[138] O. I. del Río and A. W. Neumann, "Axisymmetric drop shape analysis: Computational methods for the measurement of interfacial properties from the shape and dimensions of pendant and sessile drops," *J. Colloid. Interf. Sci.*, vol. 196, pp. 136–147, 1997.

[139] "Perfect toners hide a secret: HDK® pyrogenic silica," Last accessed Nov 2011. Wacker Silicones `http://www.wacker.com/cms/media/publications/downloads/6178_EN.pdf`.

[140] B. Somosvári, P. Bárczy, and J. Szőke, "Investigation of shelf-life and foaming of water-SiO_2-SDS compound," 2011. Presented at Colloids and Materials Symposium 8-11 May 2011, Amsterdam.

[141] "Certificate of pu foam (poran k 2790)," Tech. Rep. K 0270010000.

[142] H. Márton, "PUR szivacs habképző képességének összehasonlító vizsgálata. PUR csőszigeteléssel épített melegvíz távvezeték hőveszteségének meghatározása (Comparative investigation of foam generation ability of PUR sponge. Determination of heat loss of hot water line equipped with PUR insulation.)," Master's thesis, Dept. of Polymer Eng. Univ. of Miskolc, 2008.

[143] H. Márton, "Infiltrációs folyamatok vizsgálata PUR-habokban," tech. rep., 2007.

[144] S. Hilgenfeldt, S. A. Koehler, and H. A. Stone, "Dynamics of coarsening foams: Accelerated and self-limiting drainage," *PHYSICAL REVIEW LETTERS*, vol. 86, no. 20, 2001.

[145] "Full public report, hfc-245fa (2004)," tech. rep., National Industrial Chemicals Notification and Assessment Scheme (NICNAS), Last accessed nov 2011.

[146] Honeywell, "Genetron 245fa applications development guide," tech. rep., Honeywell, 2003.

[147] F. G. Moreno, M. Fromme, and J. Banhart, "Real-time x-ray radioscopy on metallic foams using a compact micro-focus source," *Adv. Eng. Mater.*, vol. 6, pp. 416–420, 2004.

[148] J. R. Dann, "Forces involved in the adhesive process : 2. nondispersion forces at solid-liquid interfaces," *J. Colloid Interf. Sci.*, vol. 32, pp. 321–331, 1970.

[149] Y. Q. Sun and T. Gao, "The Optimum Wetting Angle for the Stabilization of Liquid Metal Foams by Ceramic Particles: Experimental Simulations," *Metall. Trans.*, vol. 33A, pp. 3285–3292, 2002.

[150] A. C. Martinez, E. Rio, A. Saint-Jalmes, D. Langevin, and B. P. Binks, "On the origin of the remarkable stability of aqueous foam stabilised by nanoparticles: link with microscopic surface properties," *Soft Matter*, vol. 4, pp. 1531–1535, 2008.

[151] F. Krauss, U. T. Gonzenbach, A. R. Studart, and L. J. Gauckler, "Self-setting particle-stabilized foams with hierarchical pore structures," *Materials Letters*, vol. 64, pp. 1468–1470, 2010.